



**FOREIGN
BROADCAST
INFORMATION
SERVICE**

JPRS Report

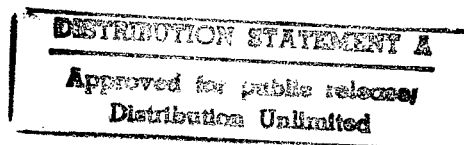
Science & Technology

Japan
SOR TECHNOLOGY UPDATE

DTIC QUALITY INSPECTED 3

REPRODUCED BY
U.S. DEPARTMENT OF COMMERCE
NATIONAL TECHNICAL INFORMATION SERVICE
SPRINGFIELD, VA. 22161

19980203 327



SCIENCE & TECHNOLOGY

JAPAN

SOR TECHNOLOGY UPDATE

916C3800 Tokyo NTT R&D in Japanese Vol 39 No 4, 10 Apr 90 pp 543-618

CONTENTS

Superconducting Compact Storage Ring, Super-ALIS [Teruo Hosokawa, Joji Nakata, et al.].....	1
Normal-Conducting Accelerating Ring (NAR) [Toa Hayasaka, Yasumichi Uno, et al.].....	14
Structure, Manufacture, and Performance of Multilayers in Synchrotron Radiation [Yoshikazu Ishii, Hisataka Takenaka, et al.].....	26
SOR Lithography Beamline [Takashi Kaneko, Yasunao Saito, et al.].....	43
SOR X-Ray Stepper [Sunao Ishihara, Atsunobu Une, et al.].....	54
X-Ray Mask [Hideo Yoshihara, Shigehisa Oki, et al.].....	68
Resist Process for SOR Lithography [Kimiyoishi Deguchi, Toshiyuki Horiuchi, et al.].....	81
Deep Submicrometer MOSICs Fabricated Using SOR Lithography for All Levels [Masayasu Miyake, Yukio Okazaki, et al.].....	93

Superconducting Compact Storage Ring, Super-ALIS

916C3800A Tokyo NTT R&D in Japanese Vol 39 No 4, 10 Apr 90 pp 543-552

[Paper by Teruo Hosokawa, Joji Nakata, Masayuki Nakajima, and Koji Yamada of the NTT LSI Laboratories, and Satoshi Ido of NTT Affiliated Companies Headquarters]

[Text] Preface

We have developed a small superconducting storage ring, Super-ALIS (Superconducting Atsugi Lithographic SOR), that is SOR (synchrotron orbit radiation) generating equipment used for X-ray lithography. Super-ALIS is the world's first equipment to attain SOR luminescence in a small superconducting ring, and now stores greater than 100 mA beams. The magnetic arrangement is a racetrack type, realizing optimum beam characteristics for lithography with two superconducting bending (180°) magnets and two quadrupole magnets arranged in the linear region. Super-ALIS uses a low-energy one-pulse injection scheme, thereby simplifying the injection system greatly. The injection energy is 15 MeV, and the storage energy is 600 MeV. To store large current beams with this injection scheme, we have developed a linac system involving small amounts of energy diffusion and space emittance. To expand the SOR irradiation region, a new beam-wobbling system is added; this achieves ideal expansion of the region.

[English abstract reprinted from original] This paper presents a superconducting electron storage ring, Super-ALIS. It is the first superconducting compact ring to generate SOR at the final energy, and now stores more than 100 mA-beams. The lattice has a racetrack form; 2 bending and 6 quadrupole magnets achieve the optimum beam characteristics for lithography. Super-ALIS uses a low-energy-one-pulse injection scheme; the injection energy is 15 MeV and the final energy is 600 MeV. A linac system has been developed for storing large current beams using this scheme. A novel beam wobbling system achieves ideal SOR vertical expansion.

1. Introduction

To put SOR lithography into practical use, an economical SOR source is necessary. Conventional SOR equipment consists of a linac, a synchrotron, and a normal conducting electron storage ring. The approximately 15 MeV

electrons from the linac are further accelerated by the synchrotron until they become the final electrons, which are slowly stacked in the storage ring. The structure thus formed makes operation secure, but it is so large in scale that using it as industrial equipment as it is involves many problems from the viewpoint of economic feasibility.

SOR equipment for X-ray lithography needs to be made small in size and economical. To meet such needs, Super-ALIS adopts (a) a low-energy incidence scheme, and (b) superconductive bending magnets. The low-energy incidence scheme lowers the energy of electrons to be incident upon the ring, gives the storage ring the function of a conventional synchrotron, and simplifies the accelerator for the incidence. In addition, it is possible to reduce power consumption by making the bending magnet superconductive, and to reduce the equipment size and the extent of emittance by a strong magnetic field. However, because electron beams tend to become unstable when energy is lower and electric currents are larger, it has been regarded as difficult to realize the storage of large currents when incident energy is lower. On the other hand, the bending magnet for accelerators requires the magnetic field to be uniform on a 10^{-4} level. In addition, although high-angle bending is indispensable for small rings, it has been impossible for the superconducting type to realize a high-angle bending magnet having a highly uniform magnetic field. The Fermi Laboratories' linear magnet for TEVATRON, having a low bending angle, is the only superconducting bending magnet so far realized.¹

In this paper, we will give an outline of Super-ALIS and of the design policy adopted to resolve these problems. In addition, we will describe the current status of the equipment and the problems involved.

2. Outline of Super-ALIS

The purposes for developing Super-ALIS are (a) to verify that the superconducting ring is a potential SOR illuminant, and (b) to comprehensively promote research on SOR lithography by providing SOR rays at an early stage. To make these purposes compatible, machinery and equipment involving not only research factors but also insurance factors have been introduced.

The structure of Super-ALIS is shown in Figure 1. The arrangement of bending magnets is a racetrack form. For a small ring, the magnets can be arranged in a circle, a racetrack, or a rectangle, each of which has its merits and demerits.² However, we adopted the racetrack form in consideration of throughput, resolvability, and so forth. In making a lattice design (design for the arrangement of magnets and so forth), we took into consideration (a) the beam properties necessary for lithography, (b) reduction of the effects of geomagnetism, (c) reduction of the effects of errors in the arrangement of magnets, (d) simplification of adjustment, (e) stability of beams, (f) reduction of the uniform region of the necessary magnetic field, and so forth. We established two incidence systems, based on a 15 MeV incidence. However, to reduce the development risks of the low-energy incidence scheme, 200-600 MeV incidence systems were also set up. During high-energy incidence, a normal conducting storage ring (NAR)³ developed simultaneously is used as an accelerator for incidence. The main ring parameters are listed in Table 1.

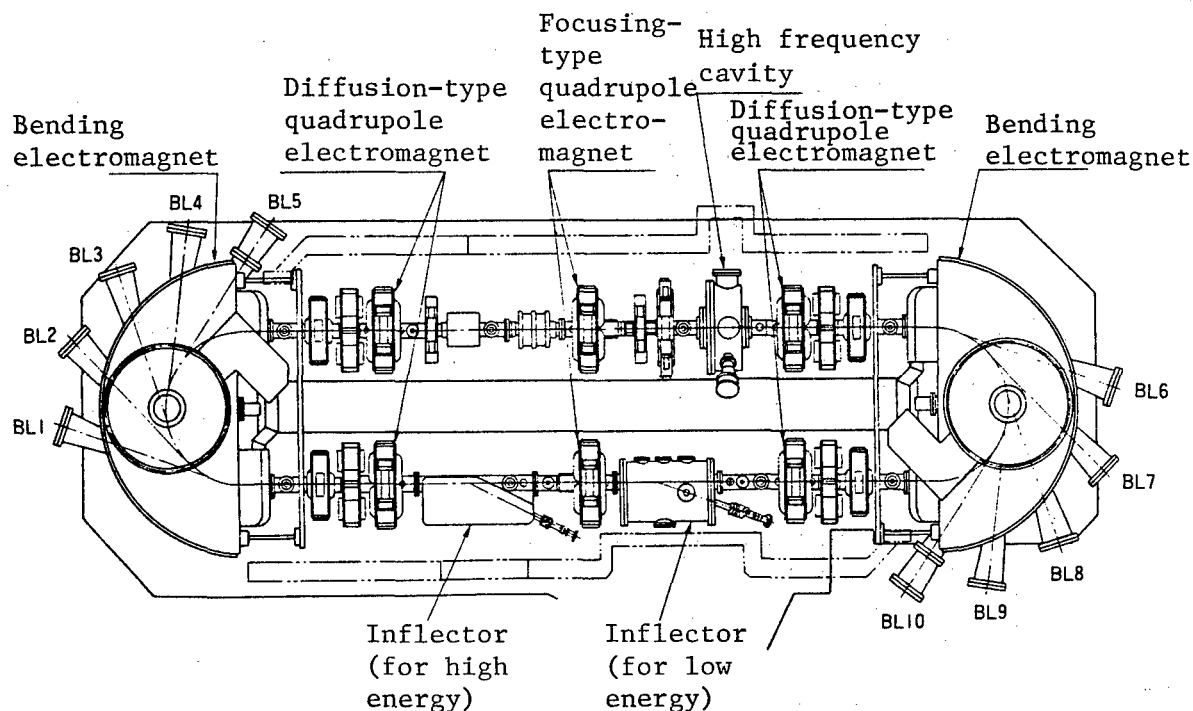


Figure 1. Brief Sketch of Super-ALIS

Table 1. Ring Parameters for Super-ALIS

	Design value	Measurement value
Energy	600 MeV	600 MeV
Incidence energy	15 MeV	15 MeV
Maximum bending magnetic field	3 T	3 T
Maximum magnetic field rise time	0.23 T/s	0.23 T/s
Number of betatrons vx	1.55-1.70	1.565
vy	0.2-0.7	0.530
Beam size σ_x	<1 mm	1.26 mm
σ_y	-	0.19 mm
Acceleration frequency	125 MHz	124.855 MHz
Peak wavelength	5.8 Å	-
Degree of vacuum (when there is no load)	5×10^{-10} Torr	2×10^{-10} Torr
Number of SOR ports	10	-
Circumference	16.8 m	-
Floor space	$2.5 \times 8.8 \text{ m}^2$	-

The peak wavelength (5.8 Å) was determined from a lithographic point of view. Six quadrupole magnets, two inflectors, and one high-frequency acceleration cavity were arranged in the region represented by long straight lines, thereby realizing beam stability and producing the necessary beam characteristics. A beam profile monitor, a beam current monitor, a beam position monitor, an rf pickup, and a SOR monitor are set up as beam monitors. The

10 ports (BL1 through BL10) to extract SOR are large enough (maximum horizontal angle: 10°) for efficient SOR use. A beam orbit wobbling system is also established to expand the region for vertical SOR irradiation. Under the method⁴ so far proposed, the extent of expansion varies with each beam port, which has the defect of bringing about run-out errors (errors in the position of replication) involved in the expansion of the radiation region. However, the new wobbling system⁵ wobbles the vertical orbit position in a state in which the orbit plane in a bending magnet is kept horizontal, as shown in Figure 2. Therefore, this system can eliminate the defects so far pointed out. The maximum degree of wobbling is ± 15 mm.

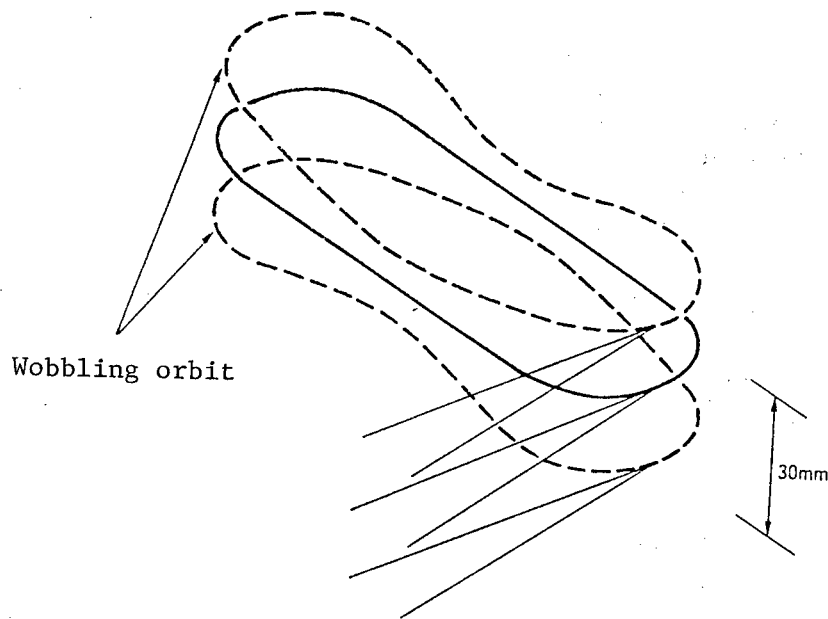


Figure 2. Wobbling Orbit of Super-ALIS

2.1. Incidence Energy

The lower the incidence energy is, the more simplified the incidence accelerator and radiation shield and the greater its economic merit. On the other hand, the lower the energy is, the more unstable the beams and the more difficult the storage of large electric currents. For example, the following relationship is known to exist between a threshold beam current I_{th} based on the instability of vertical beams and electron energy E :

$$I_{th} \propto E / |Z/n|_0$$

Where $|Z/n|_0$ is an amount called coupling impedance,⁶ which is determined by the shape and quality of the vacuum duct. Also, when the energy is low, the closed orbit distortion due to geomagnetism or residual magnetization narrows the beam aperture, making the incidence of large currents difficult. Thus, determination of incidence energy is important. However, the theory of beam instability involves many uncertainty factors, and the determination cannot

be based on theory alone. Therefore, we carried out incidence experiments using the synchrotron of the Molecular Science Research Institute⁷ and determined incidence energy with reference to the results of the experiments. The incidence energy in this synchrotron was 15 MeV, the accelerated currents were 20 mA, the degree of vacuum was 5×10^{-8} Torr, and the duration of acceleration was approximately 350 ms. The beam life during the incidence was governed by the degree of vacuum, and the influence of the closed orbit distortion was also observed. In addition, the beams were stable, without revealing any unstable phenomena. That the beams at the time of incidence were comparatively stable was conceivably due to the large beam size and to an increase in the number of betatron vibrations. This experimental result and the above-mentioned formula suggest that if the coupling impedance is lowered by about one digit, it will be possible to accelerate electric currents to about 200 mA, 10 times the amount in the case of using the synchrotron of the Molecular Science Research Institute. In addition, that the beam life during the incidence was governed by the degree of vacuum means that the aforesaid current value can be obtained even when the duration of acceleration is lengthened to tens of seconds, because the beam life becomes two digits longer when the degree of vacuum is fixed at less than 5×10^{-10} Torr. This point is very important because it is difficult to rapidly change a superconducting magnetic field. On the basis of the aforesaid result, we carried out designs for vacuum ducts in order to secure a necessary degree of vacuum for Super-ALIS, fixing the incidence energy at 15 MeV and giving importance to reducing the coupling impedance. The influence of geomagnetism and residual magnetization were coped with through a lattice design and the selection of an appropriate magnetic pole material.

Because this energy is not enough to produce the effect of stacking incidence, we adopted the method of one-pulse incidence. For incidence beams, it is essential that electric currents be large and that space emittance and energy diffusion be small if the incidence coefficient is to be raised. In addition, the reliability of equipment is important. Taking these points into consideration, we adopted a linear accelerator for incidence purposes, involving large currents and having many actual records of medical and industrial uses. One-pulse incidence imposes a technical burden on accelerators for incidence use, but this incidence method has a great advantage in further simplifying radiation shielding.

With acceleration of beams, the beam size becomes small because of adiabatic and radiative attenuation. It becomes the smallest at about 100 MeV, and the electric current density becomes the highest at this point. The interaction in the vacuum between ionized residual gas and electrons (ion trapping) and the interaction of electrons with the acceleration cavity and the vacuum duct tend to bring about instability; this restricts the upper limit of stored beams. To avoid this instability, we set up ion-clear electrodes, knockout electrodes, multipolar magnets, and so forth.

2.2. Superconductive Bending Magnet

A superconductive bending magnet is equipped with a ferromagnetic pole, and the magnet pole and the vacuum duct in the magnet are kept at normal

temperature. We are working to simplify the structure by the aforesaid scheme and to reduce the risks in manufacture of superconducting magnets by lessening the force applied to the cooling volume and the coils. The wire is NbTi. For the magnetic pole material, we chose a laminate steel plate having a small degree of residual magnetization. The maximum intensity of the bending magnetic field was 3 T, the orbital radius was 0.66 m, and the maximum velocity of the magnetic field rise was 0.23 T/s. Two bending magnets, connected in series, were driven with one power source. For the magnet design, we used a three-dimensional magnetic field analyzing program on a supercomputer.⁸ The essential point of the design is the uniformity of the magnetic field, but the uniformity is achieved by the form of a magnetic field when the field is low, and by optimizing the coil form when the magnetic field is high. The degree of uniformity is low near the saturation point of a magnetic pole, but the beam size at this point is small. During acceleration, the beams stay at this field value for only a short time, so it is all right for the area of a uniform magnetic field to be small. The field distribution changes around the saturation point, but we designed for the form of a magnetic pole so that the change would be the smallest.

2.3. Control System

In constructing a control system, we paid attention to meeting the following conditions: (a) ease of adjustment at the time of an equipment rise, (b) expansion involved as the research progressed, and (c) automatization for ordinary operation. The control system structure is shown in Figure 3. The computer for man-machine interface and the one for control purposes are connected by communication circuits for exclusive use; various machines and apparatuses for Super-ALIS are connected under the control computer. The computer for man-machine interface is connected with other kinds of computers (work stations and large computers) through GPIB and ETHERNET so as to have expansivity and flexibility. For operation of Super-ALIS, a CRT, a keyboard, a mouse, and a console panel are used. The console panel, provided to facilitate adjustment, is directly connected with the control computer to quicken responses and to enhance operability. This panel performs the functions of indicating and controlling the conditions of various machines and apparatuses (change of excited currents, and so forth). With these functions of the panel included, the input-output operations by the control computer can be controlled from the man-machine interface computer. Measurement data obtained from a current monitor, a position monitor, and so forth, are collected even during acceleration, and they can be input to the computer for man-machine interface. Therefore, all operations can be automatized if operational processes (algorithms) are determined. For example, this system can be widely applied to regular operations, automatic correction of beam closed-orbit-distortions (COD), automatic formation of exciting patterns, and so forth.

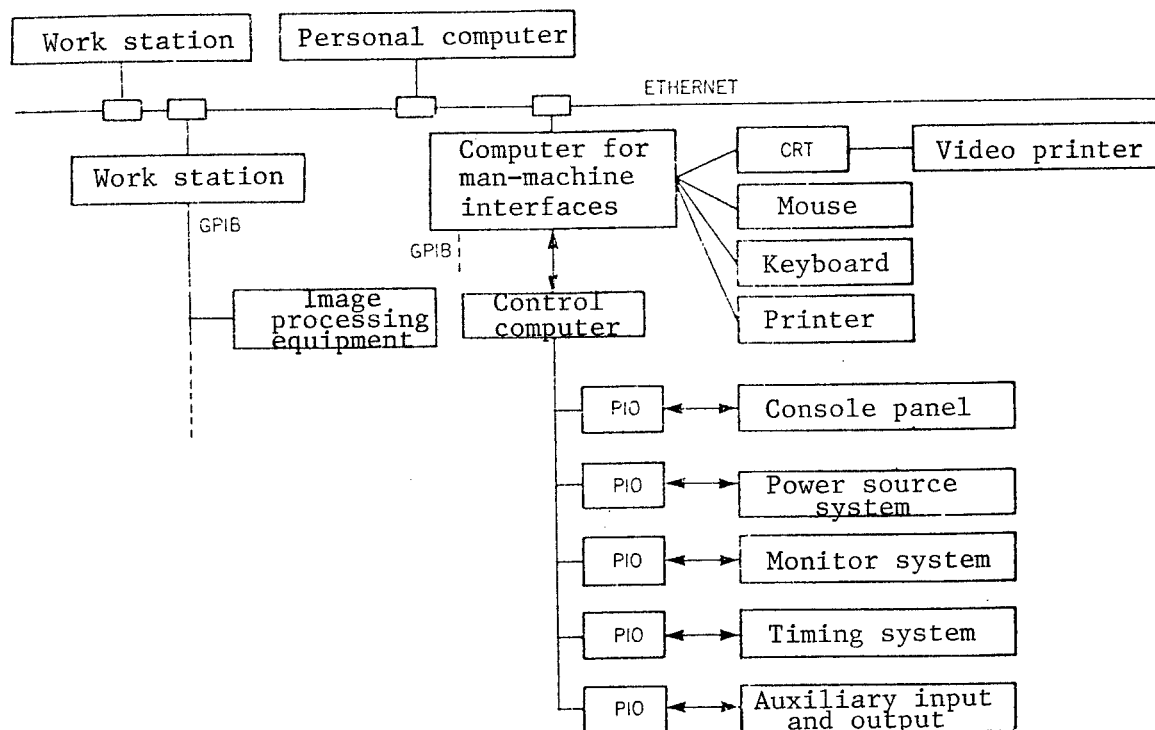


Figure 3. Structure of Super-ALIS Control System

3. Incidence Accelerators

For incidence of large current beams upon the ring, the incidence beams need to meet such requirements as large currents, low space emittance, and low energy dispersion. From analyzing the incidence beam orbit, the performance of a conventional linear accelerator was found to be unable to meet the specifications required for Super-ALIS; therefore, we developed a new linear incidence accelerator.⁹ Figure 4 shows the linear incidence accelerator system structure. This equipment consists of an electron gun region, an acceleration tube region, an energy compression region (ECS), an energy analysis region, and a high frequency region. We adopted an electron gun having high brightness, and carried out designs that considered both the space (distance) and time characteristics of two pre-bunchers and the main acceleration tube, thereby realizing a target specification. The electrons emitted from the electron gun at 90 kV undergo bunching action by the pre-bunchers, and they are accelerated in the main acceleration tube up to about 15 MeV. The energy dispersion is reduced in the ECS region, and the emitted energy is also stabilized. Properties of the electron beams emitted from the linear acceleration system are measured in the energy analysis region. The high frequency system transmits the output of a frequency synthesizer (2856.65 MHz) with coaxial cable, and amplifies it with a progressing wave tube. Thereafter it is amplified with a klystron up to a maximum 10 MW (pulse). The output of the klystron branches off in four parts and is supplied to the pre-buncher, the main acceleration tube, and the ECS-acceleration tube through a phase shifter and a variable attenuator. The beam monitors, including a high-speed current monitor, a Faraday cup, and a

The diagram is a schematic of a particle accelerator system, divided into three main sections: Energy analysis system, Energy compression system (ECS), and Acceleration system.

- Energy analysis system:** Includes components like GV_2 , IG , IP_2 , STC , AM , Q , FCM_1 , SL_1 , TR_1 , IP_1 , TMP , W_3 , and DC .
- Energy compression system (ECS):** Includes EM_1 , EM_2 , SL_2 , QT_1 , STC_1 , STC_2 , FCM_2 , CM_1 , TR_2 , IP_2 , TMP , W_2 , and DC .
- Acceleration system:** Includes HL_1 , HL_2 , ACC , PB_1 , PB_2 , CM_2 , SL_2 , GUN , IP_1 , W_1 , DC , and ΦA_2 .

The diagram shows the flow of particles from the Energy analysis system through the ECS and Acceleration system. Key components include FCMs, SLs, TRs, STCs, QTs, EMs, ACC, PBs, CMs, and GUN. Power supplies like W_1 , W_2 , and DC are also indicated.

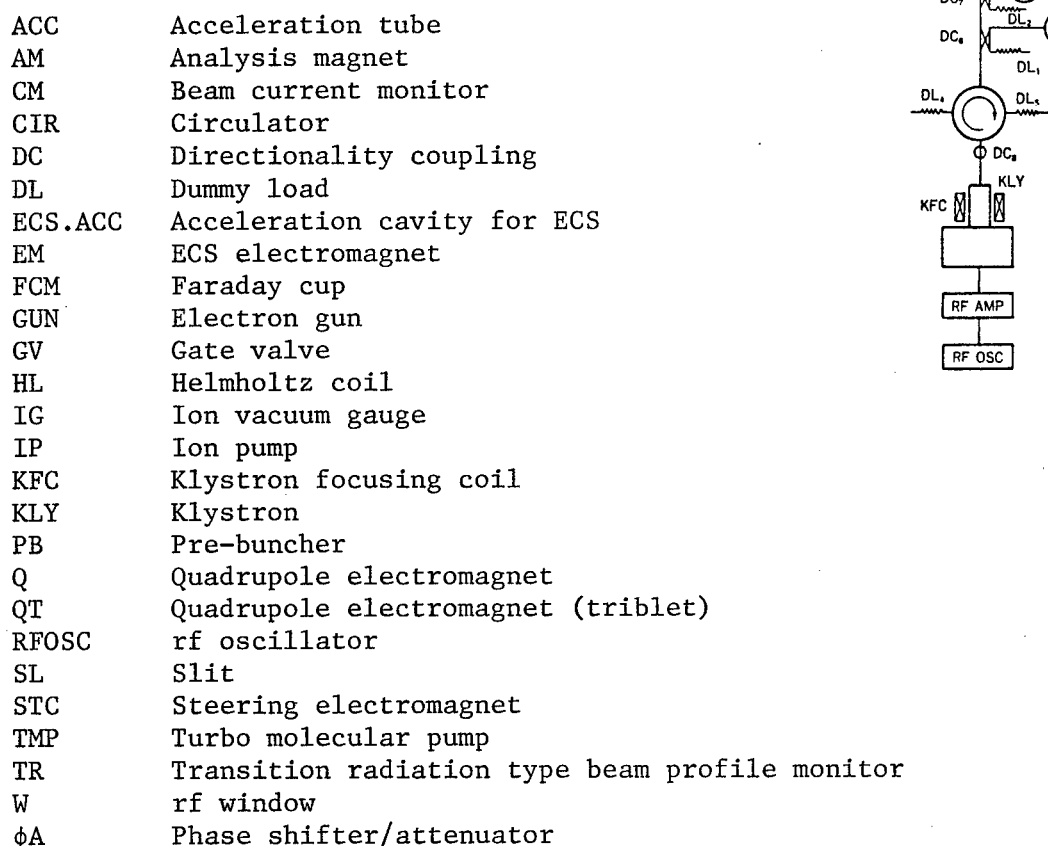


Figure 4. Structure of Linear Incidence Accelerator

Table 2. Performance of Linear Accelerator

	Design value	Measurement value
Energy	>13 MeV	15 MeV
Pulse width	>2.0 μ S	2.0 μ S
Beam current	>250 mA	270 mA
Energy fraction	<1% (FW)	1% (FW)
Beam size	<4.0 mm ϕ	3.0 mm ϕ
Beam emanation angle	<0.5 mrad	1.4 mrad
Space emittance	<1x10 ⁻⁶ π mmrad	<2.1x10 ⁻⁶ π mmrad
Repeat frequency	3 Hz max.	3 Hz max.

4. Development and Current Status

The installation and separate inspections of Super-ALIS were completed in April 1988, and adjustment was started in May, including the beam transport system. Acceleration and storage up to 600 MeV were achieved in February 1989. The initially stored electric currents amounted to 1.3 mA. Thereafter, adjustment was continued for the primary purpose of increasing beam currents, and the currents exceeded 100 mA. Storage of these beam currents was achieved by a 15 MeV one-pulse incidence scheme. The beam currents several ms after the incidence amounted to about 150 mA. The greater part of a beam loss occurs at the initial stage of acceleration. The main causes of this loss are the life span of beams and a tracking error. The life span is short because the beams spread all over the aperture because of low energy and the incidence. Figure 5 shows the SOR rays at the time of 600 MeV storage, observed from BL8 [beam port 8] by a TV camera. In this illustration, the beam size appears to have changed through its dependence on electric currents, but the beam size defined by 1/e the strength of the central rays is stable at $\sigma_x = 1.26$ mm and $\sigma_y = 0.19$ mm, without any connection with the beam currents. However, the life span of the beams is still as short as about 7,000 seconds (100 mA). The average degree of vacuum at this time is 1×10^{-8} Torr. With the decline of the beam currents, the degree of vacuum becomes higher, and the life span of the beams becomes longer. The relationship between the beam life and the degree of vacuum is shown in Figure 6. Because life span is generally in inverse proportion to the degree of vacuum, it can be thought that the short life span at this time is caused by the scattering of electrons and the residual gas in the vacuum duct. The decline in the degree of vacuum is due to the light-stimulated release of residual gas. With an increase in the duration of SOR irradiation of the inner surface of the vacuum duct because of continued operation of the equipment, the disconnection coefficient drops and the life span improves.

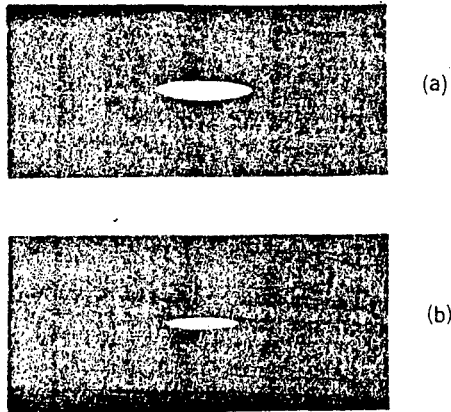


Figure 5. SOR Profile. Beam energy: 600 MeV, beam current: 80 mA (a) and 20 mA (b)

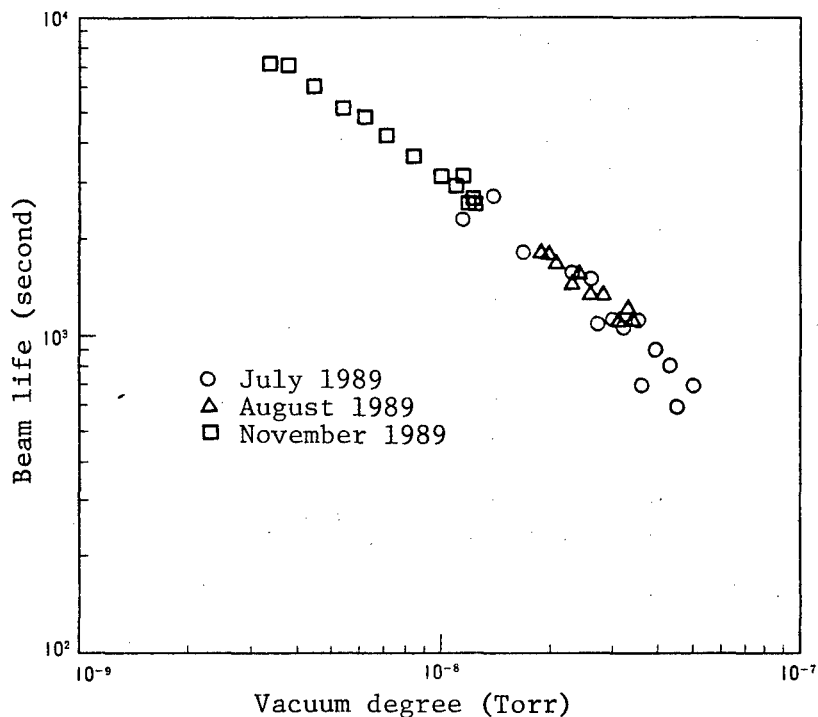


Figure 6. Beam Life and Average Degree of Vacuum

5. Conclusion

We have developed a small superconducting storage ring to be exclusively used for X-ray lithography, and have successfully extracted SOR rays for the first time in the world. We have also achieved the storage of large electric currents exceeding 100 mA, even under a 15 MeV pulse incidence scheme. Stored currents are currently restricted by (a) incidence currents, (b) tracking errors, and (c) the life span originating in the degree of vacuum. However, all these factors leave room for improvement. The point

that time is required for improving the degree of vacuum is one of the problems involved in this storage ring being used for industrial equipment. Anticipating this point from the design stage, we adopted a policy of avoiding this problem by employing materials showing low light-stimulated detachment coefficients, and have been studying materials in parallel with this. We have at this stage finished our property evaluation, and as a detachment coefficient we have obtained a value about one digit lower than the current coefficient.¹⁰ We are scheduled to carry out lithographic experiments by setting up an aligner to each beam line and to promote the completion of semiconductor manufacturing equipment, while confirming its performance and working to improve its reliability.

Acknowledgements

We express our deep thanks to Dr. H. Mukai, former director of the LSI Laboratories, and Dr. T. Kitayama, former chief researcher of the Laboratories, for giving us guidance in our development of Super-ALIS. In addition, we thank the researchers of the Molecular Science Research Institute, including Professor H. Iguchi, director of the UVSOR facility (currently director of the Molecular Science Research Institute), and Assistant Professor T. Kasuga (currently serving at Hiroshima University), for giving us an opportunity to carry out experiments at the Molecular Science Institute UVSOR and instructing us on accelerator techniques. We also express our thanks to the researchers and engineers of the High Energy Physics Research Institute and the Nuclear Research Laboratory of Tokyo University's Physical Property Research Institute for their instructions concerning accelerator physics in general.

Profiles of the Authors

Teruo Hosokawa, chief researcher of the NTT LSI Laboratories, joined NTT in 1972 and engaged in research on electron beam technology. He is currently engaged in the study of superconducting storage rings.

In 1973 he finished the electronic engineering course of Osaka University's engineering department, and in 1978 finished the second-term course (specializing in electronic engineering) of the graduate school of the same university. He received a doctorate in engineering (Osaka University) in the same year.

In 1978 he was awarded a prize for the encouragement of science from the Society of Electronic Communications of Japan, and was commended by the NTT president in 1989.

Satoshi Ido, manager of NTT Affiliated Companies Headquarters, joined NTT in 1972, and engaged in research mainly on the sample stage for electron beam exposure equipment and on the SOR vacuum system.

In 1970 he finished the precision engineering course of Osaka University's department of engineering, and in 1972 finished the master's course in precision engineering in the graduate school of the same university.

He was commended by the NTT president in 1989.

Joji Nakata, chief researcher of the NTT LSI Laboratories, joined NTT in 1976 and engaged mainly in research on high energy ion injection methods. In 1982 he engaged in business operations to prepare for the establishment of an Atsugi telecommunications research laboratories, and in 1983 in promotion of the laboratories' planning and management office. In 1985 he started research on superconducting deflection of small superconducting SOR equipment, as well as designs for electromagnet and radiation shields. He was also engaged in business operations connected with the Science and Technology Agency.

In 1976 he finished the master's course in physics in the Department of Science, Tokyo University, and obtained a doctorate in science (Tokyo University) in 1990.

He is a member of the Society of Physics and the Society of Applied Physics.

He was commended by the NTT president in 1989.

Masayuki Nakajima, chief researcher of the NTT LSI Laboratories, joined NTT in 1985 and engaged chiefly in the study and practical use of SOR light generation equipment.

In 1983 he finished the physics course of the department of science, Tokyo University. In 1985 he majored in physics in the scientific study course of the graduate school of the same university, and finished the master's course in physics.

He is a member of the Society of Physics of Japan.

He was commended by the NTT president in 1990.

Koji Yamada, member of the NTT LSI Laboratories, joined NTT in 1988 and engaged mainly in the research and development of superconducting electron storage rings.

In 1986 he finished the applied nuclear engineering course of the department of engineering, Kyushu University. In 1988 he majored in applied nuclear engineering in the engineering study course of the same university, and finished the master's course in applied nuclear engineering.

He is a member of the Physical Society of Japan.

References

1. P. S. Martin, Proceedings of 1989 IEEE Particle Accelerator Conference, 1379 (1987).
2. T. Hosokawa, T. Kitayama, T. Hayasaka, S. Ido, Y. Uno, A. Shibayama, J. Nakata, K. Nishimura, and M. Nakajima, Rev. Sci. Instrum., 60, 1783 (1989).

3. A. Shibayama, T. Kitayama, T. Hayasaka, S. Ido, Y. Uno, T. Hosokawa, J. Nakata, K. Nishimura, and M. Nakajima, Rev. Sci. Instrum., 60, 1779 (1989).
4. T. Tomimasu, Jpn. J. Appl. Phys., 26, 741 (1987).
5. Hosokawa and Anai, patent application 1985-180427.
6. A. Hofmann, BNL-25465 (1978).
7. M. Watanabe et al., Proceedings of the 5th Symp. on Accelerator Science and Technology, 15 (1984).
8. J. Nakata, M. Nakajima, T. Hosokawa, and T. Kitayama, Proceedings of Conference on Computation of Electromagnetic Fields, COMPUMAG-TOKYO (1989).
9. T. Hosokawa, T. Kitayama, T. Hayasaka, S. Ido, Y. Uno, A. Shibayama, J. Nakata, K. Nishimura, and M. Nakajima, Proceedings of 1989 Particle Accelerator Conference, 1459 (1989).
10. T. Murashita, T. Kaneko, H. Yoshihara, and T. Kitayama, Proceedings of the 11th International Vacuum Congress (expected to be carried in 1990).

Normal-Conducting Accelerating Ring (NAR)

916C3800B Tokyo NTT R&D in Japanese Vol 39 No 4, 10 Apr 90 pp 553-560

[Paper by Toa Hayasaka, Yasumichi Uno, Akinori Shibayama, and Kazuyoshi Nishimura, NTT LSI Laboratories]

[Text] Preface

We have developed a storage ring that uses a low-energy injection scheme by which electrons are injected at 15 MeV and stored after being accelerated to 800 MeV. The development was targeted as (1) a high energy injector for the superconducting storage ring, and (2) a storage ring for various SOR [synchrotron orbit radiation] applications and research on the ring itself. To make the functions of the injector compatible with those of the storage ring, we formed a polygonal ring using a normal-conducting magnet and elaborated many contrivances for the vacuum system, the rf system, and so forth. We also developed a linear accelerator, a superconducting storage ring, and an electron transport system to connect the ring. Synchrotron orbit radiation has been successfully extracted from this ring, and research is now being pursued to improve the performance of the equipment while using the ring for the study of X-ray lithography and so forth.

[English abstract reprinted from original] This paper presents a normal-conducting storage ring using a low energy injection scheme by which electron energy is boosted from 15 MeV (injection energy) to 800 MeV (final energy). The design goals are a high energy injector for the Super-ALIS, and a multi-purpose storage ring. To combine these functions, the ring has an octagonal configuration with 8 normal-conducting bending magnets. To achieve a high beam current, [a] newly developed injection system, rf system, vacuum system have been installed. A beam transport system has also been developed to connect a linear accelerator, Super-ALIS and this ring. Synchrotron radiation has been successfully extracted from this ring. The ring has been used in the study of X-ray lithography, and the investigation of the ring.

1. Introduction

In developing a superconducting storage ring (Super-ALIS)¹ as a SOR illuminant for X-ray lithography, a low-energy injection scheme was adopted

from the standpoint of size reduction and economization. This scheme, if successful, would produce significant effects, but would involve development risks as well. To reduce these risks, a high-energy injection system was needed. SOR is a powerful and very bright radiation, covering an extremely wide band of wavelengths from X-rays to infrared rays. Because of this, SOR has come to be widely used for studies on physical properties, living things, medical science, and so forth. The conventional SOR generator stores high-energy electrons, amounting to several hundred to several thousand MeV, that are to be injected into a ring. It needs large, expensive injectors, such as high-energy linear accelerators and synchrotrons, for acceleration use. Therefore, efforts have been made to reduce the size and price in order to expand the use of SOR. The storage ring Aladdin² of the University of Wisconsin, for example, injects 100 MeV electrons from a small injector and, after accelerating them in the ring to the final energy level, stores them.

Because of the aforesaid background, we developed a normal conducting storage ring to effect acceleration and storage from a low energy level; the aim was to create an economical SOR generator for SOR-use research and to achieve a high-energy injector for a superconducting storage ring.

In this paper we will mainly describe the normal conducting storage ring, and will outline a beam transport system to carry electrons among various electron accelerators in the NTT SOR facility.

2. Normal Conducting Storage Ring³

2.1. Design Concept

We considered the following items in designing a ring having the functions of both an injector and an illuminant SOR:

(1) Fundamental Parameter of a Ring

The most fundamental parameter of a SOR illuminant ring is a critical wavelength (λ_c). This determines the wavelength range of the SOR to be generated. On the other hand, there is a relationship in terms of $\lambda_c = 18.64 / (BE^2)$, where B represents the magnetic field (T) of a bending magnet, and E is an electronic energy (GeV). On the basis of this formula, λ_c , the bending magnetic field, and energy are determined. Thinking that this ring will have a wide range of SOR use, including lithography, we fixed the SOR spectrum peak at about 10 Å.

To make it a high-energy injector, electrons need to be accelerated and emitted with a quick repeat cycle, and we therefore used a normal conducting magnet. A superconducting magnet is very effective in such economic aspects as power consumption for operation under normal conditions, as in the case of a luminous source for lithography. However, a superconducting magnet is considered disadvantageous when it must operate in a variety of conditions as an injector or a luminous source for research purposes, as mentioned above. We fixed the maximum magnetic field of the normal conducting magnet at 1.44 T, taking the saturation of the ferromagnetic electrode into

consideration. The radius $p(m)$ of the electron orbit in the bending part is fixed in terms of $p = 10E/3B$. Giving comprehensive thought to the size of the entire equipment, the relative difficulty of beam line installation, and so forth, we fixed the final energy at 800 MeV and λ_c at 20.2 Å.

(2) Ring Form

With a view to expanding SOR applications, it must be possible in the future to establish an insertion light source for undulators and wigglers. For this purpose, the ring is polygonal, making it easy to secure a long, straight line for the installation of the insertion light source.

(3) Electro-Optical Design for a Ring

(a) Orbital deflection due to the dispersion of electron energy has to be reduced to zero in the bending equipment for injection, in the bending equipment for emission of accelerated electrons, and in the region where a high frequency accelerated cavity is to be created, in order to capture as many electrons as possible as well as to make this reduction advantageous for a high-frequency acceleration system.

(b) To facilitate injection and emission, the lead of the betatron vibration phase between the pulse magnet for injection and the bending equipment for injection and between the pulse magnet for emission and the bending equipment for emission has to be fixed between 90 degrees and the vicinity of a degree that is integral times as high.

(c) To cause attenuation of radiation and to give a variety to operational conditions, the inclination (n) of the magnetic field of a bending magnet has to be fixed at zero, and the magnet layout must be a separated type.

(d) To correctly effect the tracking at the time of acceleration, the number of control (power source) items has to be as small as possible.

(e) The point of ring operation has to be established so as to avoid dangerous sector resonance.

(f) With consideration given to SOR applications except for lithography, such as analyses, the ring has to have the lowest possible emittance in order to obtain beams with a small diameter in the bending region.

(g) In consideration of lengthening the life span of stored currents and installation of a luminous source of the insertion type, the β function in the region of long, straight lines must be as large as possible.

The configuration of a normal conducting storage ring designed in consideration of these items is shown in Figure 1, and a photo thereof is given in Figure 2. In addition, the main parameters are listed in Table 1.

To reduce the size of the entire ring, we set up sections of long, straight lines at four places, and allotted two places (S3, S5) for insertion luminous sources and one place each for injection/emission (S1) and the high-frequency acceleration cavity (S7). The length of the line was fixed at 5 m, making it possible to set up an insertion luminous source measuring about 3 m. For the electro-optical system, the simplest Double Focus Achromat system was adopted to improve the tracking accuracy necessary under the low-energy injection scheme. Thus, we formed a four-symmetry ring using eight bending magnets, as shown in Figure 1. The orbit circumference was 52.78 m. From this ring, a spectrum having a peak at about 7 Å can be obtained, as shown in Figure 3. We designed for the ring to be operable with a low emittance as well as with an ordinary emittance.

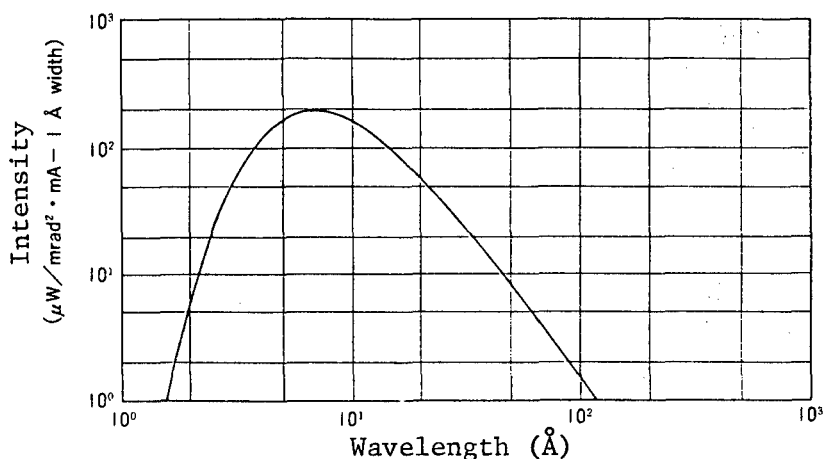


Figure 3. Photon Radiation Spectrum of Normal Conducting Storage Ring NAR

2.2. Structural Characteristics

As a luminous source ring adopting the low-energy injection scheme, and also as a high-energy injector, the ring has the following characteristics:

(1) Magnet and Its Power Source

The electromagnet used for the ring fulfills the function of an injector, so it needs to be excited at high speed. When the magnetic pole is made of an iron block, eddy currents arise during excitation and disturb the magnetic field. Therefore, we formed a magnetic pole with laminate steel plate.

The magnetic power source⁴ must be able to increase the coil currents moment by moment during acceleration and must be able to keep the coil currents constant during storage operation. Therefore, we developed a highly accurate dc amplifier with a wide dynamic range. It is capable of excitation with a desired pattern on the basis of the tracking data from a computer. When it is to be operated as a high-energy injector for the

superconducting storage ring, it is necessary to repeat high-speed excitation for a short time. To shorten the time until making the next acceleration after finishing the preceding acceleration, an inverter circuit is attached.

(2) Vacuum System

The problem with a vacuum system is electron loss due to a collision between wheeling electrons and residual gas molecules or to an interaction between ionized gas molecules and electrons during acceleration, particularly in the low-energy region. For a storage mode, a sufficient life span is also necessary. Therefore, the vacuum exhaust capacity was fixed at 24,000 l/s. An ion pump, a titanium getter pump, and a distribution-type ion pump were arranged appropriately. Because the injection energy is very low, ion trapping (a phenomenon of ionized gas being captured by a group of electrons) was thought to be a problem. Therefore, we placed an electrode to remove these ions. Also, eddy currents arising in the beam duct during the rise of the magnetic field give rise to six-pole magnetic field components and disturb the movement of electrons. Therefore, the thickness of the duct was made smaller than that for an ordinary high-energy injection storage ring. In consideration of the coupling impedance of the beam duct, we took care to smooth the duct all around the ring.

The ports to extract SOR are set up for both the rays from the bending magnet and those that are expected to come from a future insertion luminous source.

(3) rf Acceleration System⁵

Taking into consideration the energy of electrons, acceleration, and beam stability during storage, we fixed the acceleration frequency at 125 MHz.

The conditions for operation of an rf acceleration system have great effects on beam currents. Immediately after injection, rf voltage needs to be fixed at a low level to restrain the spread of energy dispersion. The resonant frequency in the rf cavity must also be changed (detuned) in a wide range. In the high-energy region, an rf voltage as high as about 60 kV is necessary to lengthen the life span of electrons through Coulomb scattering. Also, to minimize the reflection power, detuned frequency must be controlled by a feedback system. To meet these requirements, we developed an rf power source having a 26 dB voltage control region, and a cavity that allows a wide range of detuning.

(4) Injection System

Ordinary rings exclusively used for luminous sources adopt a scheme for injecting high-energy electrons many times and increasing the density of storage currents through stacking. In the case of the ring we developed, however, the energy of injected electrons is as low as 15 MeV, and therefore its life span in the ring is so short that the aforesaid scheme cannot be adopted. Therefore, we looked for the most appropriate arrangement of four pulse magnets for injection (perturbators), and made it possible to establish

optimum conditions for injection even in the case of a change in the condition for ring operation. Thus we have developed a scheme making it possible to inject large currents in one injection operation.

(5) Injection System

This ring is equipped to emit accelerated electrons to a superconducting storage ring. Because this is a storage ring needing super-high vacuum, the emission system is different from that of a ring exclusively used for acceleration. The degree of vacuum is maintained by placing a kicker electromagnet for emission use outside the vacuum duct, thereby making possible its operation as a luminous source ring. A perturbator for emission use is set up to increase the emission energy to 200-600 MeV in coordination with the superconducting storage ring. Electrons can also be emitted from a 30 MeV level by adding a pulse power source for emission use.

3. Beam Transport System

The structure of a beam transport system to carry electrons among a linear accelerator,⁶ a normal conducting storage ring, and a superconducting storage ring, is shown in Figure 4; the various characteristics of the system are given in Table 2. Because the energy range of the electrons transported is as wide as 15 to 600 MeV, the entire system will have to be formed with a specification for high energy, if it is to be formed in one unit. Therefore, we formed two units--one for high energy and the other for low energy--with an eye on economization by such means as joint use of a magnet power source. The units (BT-1 and BT-3) to transport low-energy (15 MeV) beams switch the beams with an upstream bending magnet, and lead them to the normal conducting and superconducting storage rings. The BT-2, a unit to transport high-energy electrons from the normal conducting storage ring to the superconducting storage ring, can transport these electrons in an energy range of 30 to about 600 MeV. This beam transport system, carrying low-energy electrons for a long distance, restrains the electronic orbit deflection due to geomagnetism, and therefore we provided the vacuum duct with as many geomagnetic shields as possible.

The electro-optical system was basically achromatic, and a design was made so that the beam size at the entrance to the beam transport system and the angle of divergence would reappear at the exit.

4. Current Status of the Normal Conducting Storage Ring

This ring successfully achieved electron storage at 800 MeV in June 1988. Since then we have been pursuing research on the ring while using it for SOR-use experiments and so forth. The initial current stands at about 20 mA and the $1/e$ life is about three hours.

By setting up a photon radiation absorber⁷ (shown in Figure 5) in a part of the beam duct in the bending region, we are carrying out experiments on the reduction of light stimulation released gas. Single Si crystals are arranged in an area wherein SOR is applied. Because Si contains only a

small amount of light stimulation released gas, a remarkable improvement in the degree of vacuum is expected.

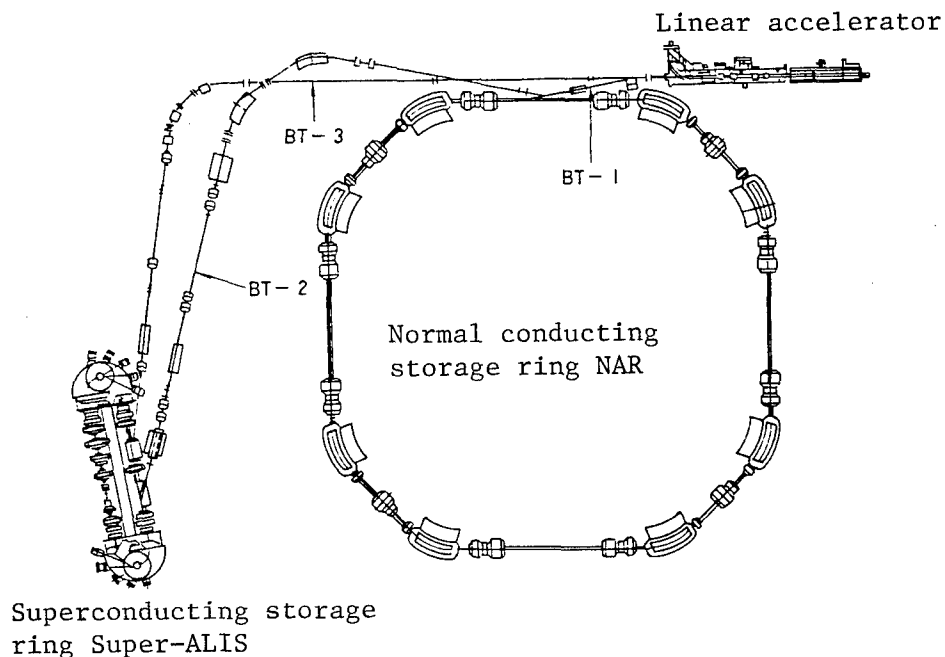


Figure 4. Structure of a Beam Transport System

Table 2. Various Characteristics of the Beam Transport System

Items	BT-1	BT-2	BT-3
Energy	15 MeV	30-600 MeV	15 MeV
Total length	4 m	25 m	30 m
Number of bending magnets	1	4	4
Magnetic field intensity	0.03 T	Max. 1.2 T	0.09 T
Number of quadrupole magnets	7	14	18
Degree of vacuum	10^{-8} Torr	10^{-6} Torr	10^{-6}

Figure 6 shows changes in the degree of vacuum when storage is started, standardized by the initial value of the stored currents. The standardized degree of vacuum is improved with an increase in the integral storage duration, at a point where an integral current value exceeds 10 mA/s. The electric current at the initial stage of storage shows little change, standing at about 20 mA, and the degree of vacuum is improved. During the operation, there was a vacuum break due to repair, but the degree of vacuum was quickly restored on resumption of the operation. It is conceivable that the degree of vacuum will show a further improvement if baking to remove the aforesaid gas by SOR rays makes progress.

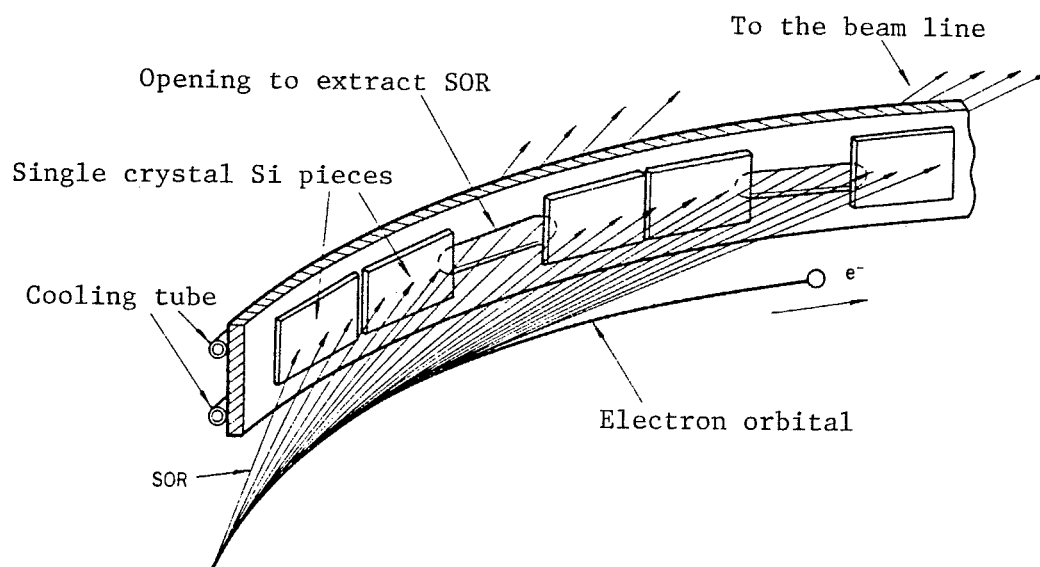


Figure 5. SOR Absorber

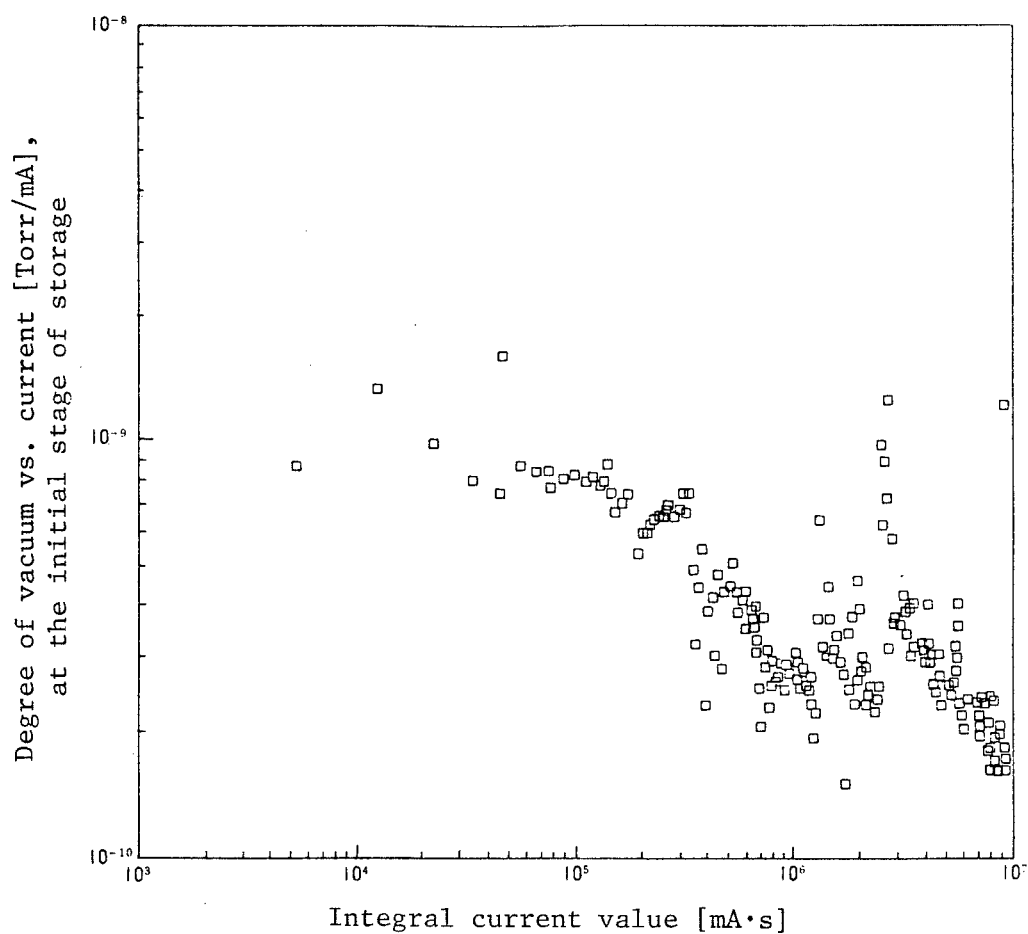


Figure 6. Changes in the Degree of Vacuum

This ring is equipped with a beam line⁸ and exposure equipment⁹ for conducting evaluations. In addition, research on MOS devices,¹⁰ DFB laser,¹¹ and so forth is being pursued by using this experimental exposure system.

5. Conclusion

We have outlined the normal conducting ring and the beam transport beam, and have described the current status of the ring. A low-energy injection scheme was adopted for the design, with the functions of high-energy injection and a storage ring combined; many contrivances were elaborated to attain our goal. They are capable of storage through acceleration up to 800 MeV with 15 MeV injection, and they are being used for SOR-use experiments. In the future, we will pursue research with a view to improving the performance of such equipment, including an increase of storage currents, while using the ring as a luminous source.

Acknowledgement

We would like to express our deep thanks to the people of the High-Energy Physical Research Laboratory, Molecular Science Research Laboratory, and the Tokyo University Physical Property Research Laboratory for giving us various instructions in the pursuit of our research. We also appreciate the guidance of Dr. Hisakazu Mukai, former director of the NTT LSI Laboratories, and Dr. Toyoki Kitayama, former chief director of the same Laboratories.

Profiles of the Authors

Toa Hayasaka, chief researcher of the NTT LSI Laboratories, joined NTT in 1969 and engaged chiefly in research on X-ray exposure systems. Currently he is working on development of SOR equipment.

In 1967 he graduated from the department of precision engineering of Hokkaido University, and in 1969 finished the master's course in the precision engineering department of the graduate school of the same university.

He is a member of the Society of Electronic Information and Communications, the Institute of Electrical Engineers, the Society of Applied Physics, the Society of Precision Engineering, and the Society of Radiation Optics.

In 1989 he was commended by the NTT president.

Yasumichi Uno, chief researcher of the process automation laboratory of the NTT LSI Laboratories, joined NTT in 1968 and engaged chiefly in the development of pattern generation equipment using light and electrons, and in designing for an electron synchrotron for SOR luminous sources. Now he is working on the development of electron beam exposure equipment.

In 1965 he finished the electronic engineering course in the engineering department of Tohoku University, and in 1968 finished the master's course in electronic engineering at the graduate school of the same university.

He is a member of the Society of Electronic Information and Communications and the Society of Applied Physics.

Akinori Shibayama, chief researcher of the LSI Research Laboratories, joined NTT in 1975 and engaged in research on electron beam exposure equipment, D/A converters, and accelerators for SOR lithography. Now he is engaged in the study of X-ray mask technology.

In 1973 he finished the electronic engineering course of the engineering department at Tokyo Institute of Technology, and in 1975 finished the master's course in electronic engineering at the graduate school of the same institute.

He is a member of the Society of Electronic Information and Communications.

He was commended by the NTT president in 1989.

Kazuyoshi Nishimura, chief researcher of the circuit technology research division, NTT LSI Laboratories, joined NTT in 1983 and engaged in research on designs for injection and emission systems for SOR equipment. He is currently studying LSI designing methods.

In 1981 he finished the electronic engineering course of the engineering department, Gunma University, and in 1983 finished the master's course in electronic engineering at the same university's graduate school.

He is a member of the Society of Physics.

He was commended by the NTT president in 1989.

References

1. T. Hosokawa, T. Kitayama, T. Hayasaka, S. Ido, Y. Uno, A. Shibayama, J. Nakata, K. Nishimura, and M. Nakajima, NTT Superconducting Storage Ring Super-ALIS, Rev. Sci. Instrum., 60, No 7, p 1783, 1989 (Part IIA).
2. E. M. Rowe, Update on Aladdin, Proc. 1987 IEEE Particle Accelerator Conference, p 391.
3. A. Shibayama, T. Kitayama, T. Hayasaka, S. Ido, Y. Uno, T. Hosokawa, J. Nakata, K. Nishimura, and M. Nakajima, NTT Normal-Conducting Accelerating Ring, Rev. Sci. Instrum., 60, No 7, p 1779, 1989 (Part IIA).
4. T. Kitayama, A. Shibayama, Y. Uno, N. Kawakami, Y. Watanabe, and Y. Sato, High-Speed, High-Accuracy Magnet Power Supply Using FET Chopper for Synchrotron Facility, Proc. 1989 IEEE Particle Accelerator Conference, p 1145, 1989.
5. A. Shibayama, 125 MHz Cavity for NAR, Proc. 1989 IEEE Particle Accelerator Conference, p 240, 1989.

6. T. Hosokawa, T. Kitayama, T. Hayasaka, S. Ido, Y. Uno, A. Shibayama, J. Nakata, K. Nishimura, and M. Nakajima, Injector Linac for Super-ALIS, Proc. 1989 IEEE Particle Accelerator Conference, p 1459, 1989.
7. T. Murashita, T. Kaneko, H. Yoshihara, and T. Kitayama, A Si Single-Crystal Photon-Absorber for a Compact SR Ring, to be published in Proc. of the 11th International Vacuum Congress.
8. T. Kaneko, S. Itabashi, Y. Saito, H. Yoshihara, and T. Kitayama, A Beam Line and Its Components for SR Lithography, Jap. J. Appl. Phys., Part 2, 28, No 10, p 2080, 1989.
9. S. Ishihara, M. Kanai, A. Une, and M. Suzuki, Proc. of the 33rd Int. Sym. on Electron, Ion and Photon Beams 1989, to be published in J. Vac. Sci. Technol.
10. T. Kobayashi, M. Miyake, Y. Okazaki, T. Matsuda, M. Sato, K. Deguchi, S. Ohki, and M. Oda, IEDM Technical Digest, p 881, 1988.
11. T. Nishida, M. Nakao, T. Tamamura, A. Ozawa, Y. Saito, K. Nishimura, and H. Yoshihara, Synchrotron Radiation Lithography for DFB Laser Gratings, Jap. J. Appl. Phys, Part 2, 28, No 11, p 2333, 1989.

Structure, Manufacture, and Performance of Multilayers in Synchrotron Radiation

916C3800C Tokyo NTT R&D in Japanese Vol 39 No 4, 10 Apr 90 pp 561-572

[Paper by Yoshikazu Ishii and Hisataka Takenaka of the NTT Applied Electronics Laboratories, and Hiroo Kinoshita and Kenji Kurihara of the NTT LSI Laboratories]

[Text] Preface

SOR in the soft X-ray region is essential for research on the structural analysis of materials, including light elements, and for the study of X-ray reduction lithography aimed at developing VLSIs for the next generation. To use this SOR, spectral diffraction of the wavelength of soft X-rays and optical elements for focusing and reflection purposes are necessary. We conducted studies on the formation and evaluation of artificial multilayer films that are attracting attention as such optical elements for soft X-rays. By using magnetron rf sputtering equipment, newly developed for the manufacture of artificial multilayer films, we have established a technique to fabricate artificial multilayer films that are uniform over a large area and that have a high-precision periodic structure. From evaluation of the reflecting and condensing properties of the X-ray and soft X-ray regions of the fabricated artificial multilayer films, we found uniformity to be within 1 percent over a 100 mm diameter, an X-ray reflectivity close to the value of theoretical calculation, a condensing property generally agreeing with the result of ray-tracing calculations, and so forth. In particular, for 13 nm soft X-rays, we found a high reflectivity of 46 percent; we also anticipate using it for a reflecting mirror for reduction lithography.

[English abstract reprinted from original] Multilayers can be used as dispersion elements and focusing mirrors for soft X-ray synchrotron radiation. New reflective optical elements can be developed using the multilayer. Newly-developed magnetron rf sputtering equipment is used to make large flat and curved multilayers. The multilayers are uniform in layer period within about 1 percent. Their reflectivity agrees well with theoretical calculations. The focusing properties of the curved multilayers agree with ray-tracing calculations. The excellent reflectivity of 46 percent at 13-nm wavelength is sufficient for use as the focusing mirror for soft X-rays.

1. Introduction

If it is possible to develop an optical system to use soft X-rays measuring 1 nm to tens of nm in wavelength for spectral diffraction, focusing, and image formation in the same way as in the case of visible light, it will become possible to carry out soft X-ray reduction exposure aimed at the structural analysis of materials including light elements, high-sensitivity analysis of light elements, and development of a VLSI for the next generation. Moreover, this would pave the way for realizing an X-ray microscope suitable for non-destructive observations of bio-samples, an X-ray telescope for astronomical observations, and so forth. At present, when it is becoming possible to directly use photon radiation that is a superior soft X-ray source, it has become extremely significant to establish techniques to extract or focus soft X-rays of a desired wavelength from the photon radiation. To date, single crystals have been used for spectral diffraction in wavelength areas below 1 nm, and diffraction lattices have been used for the spectral diffraction of soft X-rays, vacuum ultraviolet rays, and visible light measuring more than tens of nm in wavelength, as shown in Figure 1. The reason is that in the case of single crystals, the periodic length of atomic arrangement is equivalent to the wavelength that makes spectral diffraction possible, and that, in the case of diffraction lattices, the periodic interval of the lattice slit is equivalent to such a wavelength. Between these wavelengths--that is, in the region of wavelengths ranging from 1 nm to several nm--a diffraction grating is used, but its reflectance is as low as less than 1 percent. Therefore, an artificial multilayer film, formed by alternately stacking a heavy element layer and a light element layer, with a thickness of several nm to tens of nm, has come to attract attention as the most promising spectroscopic element of condensing element covering this region. If a spectroscopic device using this artificial multilayer film is produced, it will become possible to develop spectroscopic, light condensing, and image forming optical systems covering this wavelength region. For more than 10 years, therefore, full-dress research on an artificial multilayer film has been under way in the United States.¹ For 5 years, the NTT Laboratories have also been tackling the development of an artificial multilayer film as a device suitable for the spectral diffraction and condensation of photon radiation that is a superior soft X-ray source. Currently it has established a technique to fabricate high-quality artificial multilayer films on the most advanced level.² Here we will report chiefly on the technique to fabricate this kind of film and the X-ray optical properties of the artificial multilayer films fabricated.

2. Artificial Multilayer Film

The artificial multilayer film has a structure with two kinds of materials, largely varying in scattering factors, piled up periodically and alternately, as shown in Figure 2. Plainly speaking, a heavy element layer (consisting of tungsten (W) or molybdenum (Mo), for example) that readily reflects soft X-rays, and a light element layer (consisting of carbon (C) or silicon (Si), for example) playing the role of a spacer readily passing soft X-rays through, are piled up alternately in the form of a thin layer, thereby forming an artificial, high-precision periodic structure like that of a

crystal lattice. There are several to hundreds of paired layers according to uses. When the thickness of each layer is represented by d_A, d_B , the thickness of one pair (d) is $d_A + d_B$. When the wavelength of an incident X-ray is represented by λ , it is possible to obtain a wavelength satisfying Bragg's formula:

$$\lambda = 2d \sin\theta$$

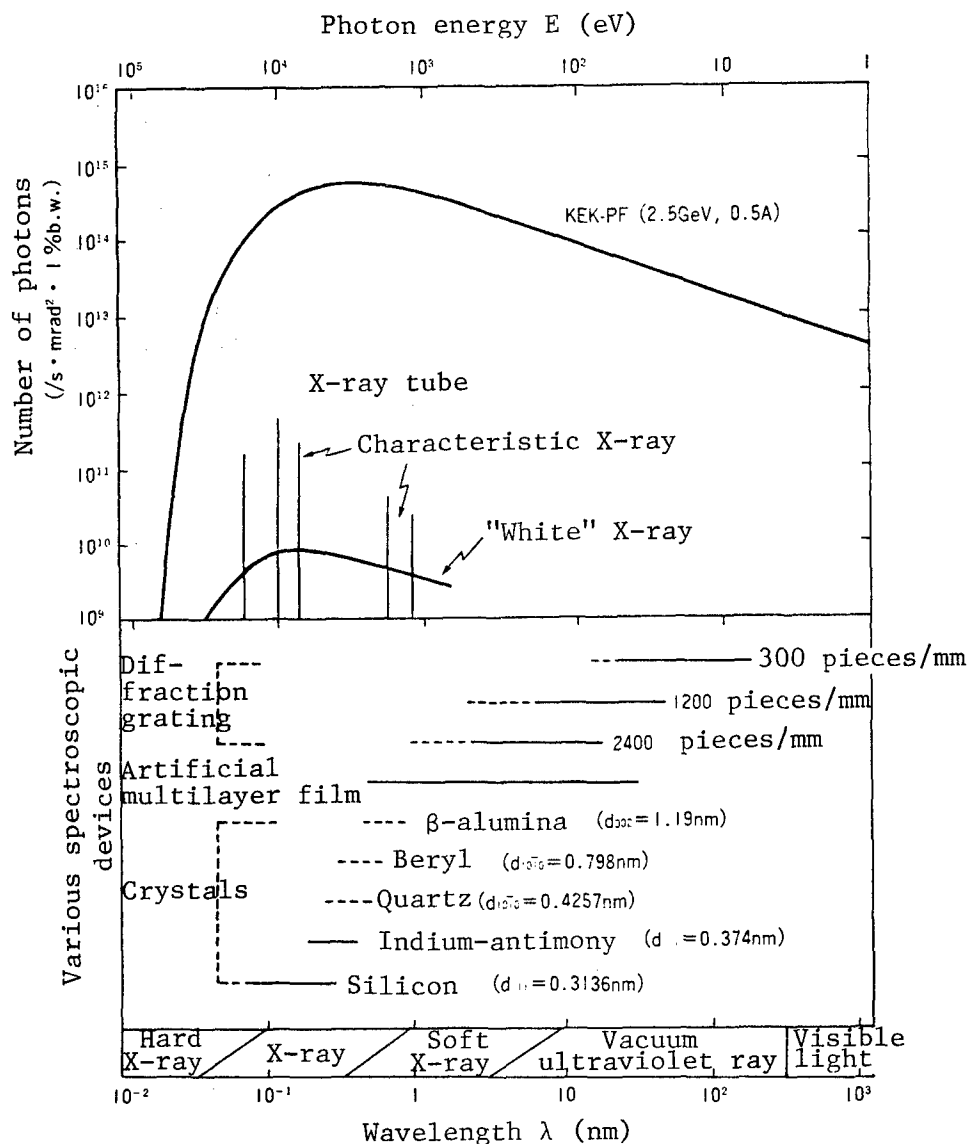


Figure 1. Scope of Applications of Photon Radiation Intensity and Various Spectroscopic Devices With Regard to Wavelength

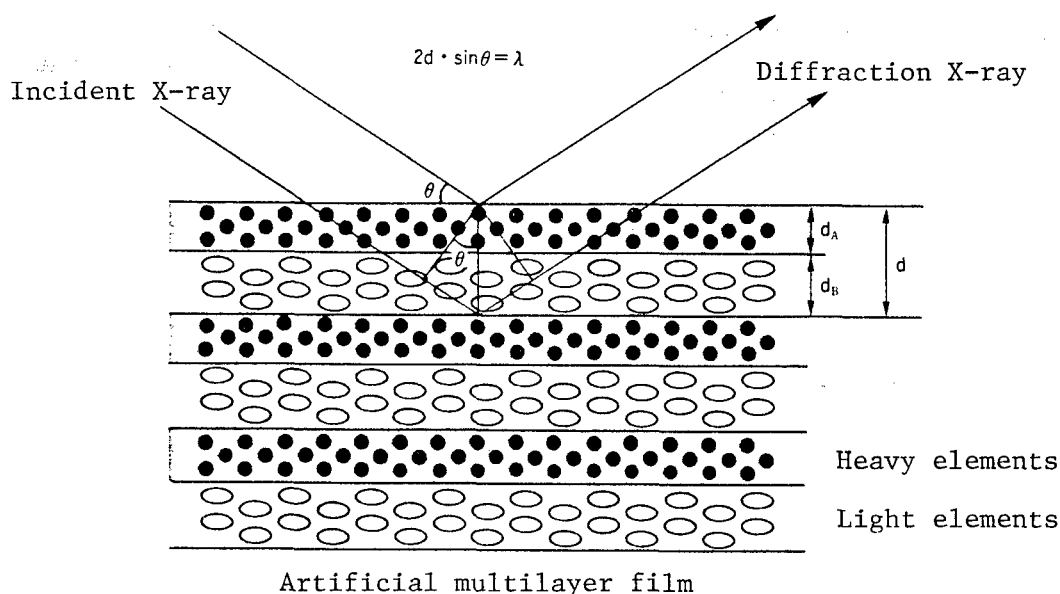


Figure 2. Classification of Various Spectroscopic Elements

When the periodic length (d) of the artificial multilayer film is changed within the limit of 2 to 10 nm, a wavelength less than 4 to 20 nm can be obtained. Because this multilayer film is used like a spectroscopic crystal having a lattice constant (d), it is also called an artificial lattice film. As mentioned later, the charm of the artificial multilayer film is that its reflectance in the soft X-ray region is tens of percent, one to two digits higher than the 1 percent or lower in the case of a diffraction grating.

3. Uses of Artificial Multilayer Film and Demand Conditions

In 1984, NTT Laboratories undertook construction of a beam line for exclusive use in the photon radiation experimental facility (KEK-PF) of the High-Energy Physical Research Laboratory. The NTT beam line (BL-1) is an ultra-high vacuum beam line using the photon radiation of vacuum ultraviolet rays from soft X-rays. It is used by being divided into three diverged beam lines (A, B, and C). As an example, an NTT photon radiation beam line (BL-1A)³ for the analysis of materials is outlined in Figure 3. The A line is a materials analyzing beam line having an extensive wavelength, ranging from soft X-rays to vacuum ultraviolet rays. It uses a GCM spectroscope (grating/crystal monochrometer) capable of spectral diffraction of the photon radiation of vacuum ultraviolet rays from soft X-rays by the use of one spectroscope. This monochrometer is characterized by its ability to use three spectral elements--crystals, artificial multilayer film, and diffraction grating--for X-rays, soft X-rays, and vacuum ultraviolet rays. This beam line makes it possible to obtain information about the composition of materials and the state of chemical bond through photoelectron spectroscopic analyses. It is also expected to make it possible to carry out X-ray local structural analyses of materials containing small amounts of such light elements as oxygen, carbon, or silicon. With regard to the soft X-ray

region, we are studying the use of artificial multilayer film double monochrometers. The size of a photon radiation beam is 70 mm (horizontal direction) x 8 mm (vertical direction); therefore, a spectral element receiving this beam needs an area of about 70 mm x 60 mm. In other words, an artificial multilayer film that is uniform over a large area becomes necessary. It is also necessary to make the periodic structure of the artificial multilayer film highly accurate, because the spectrum width of a monochromatic light undergoing spectral diffraction to raise the accuracy of material analysis should be as small as possible.

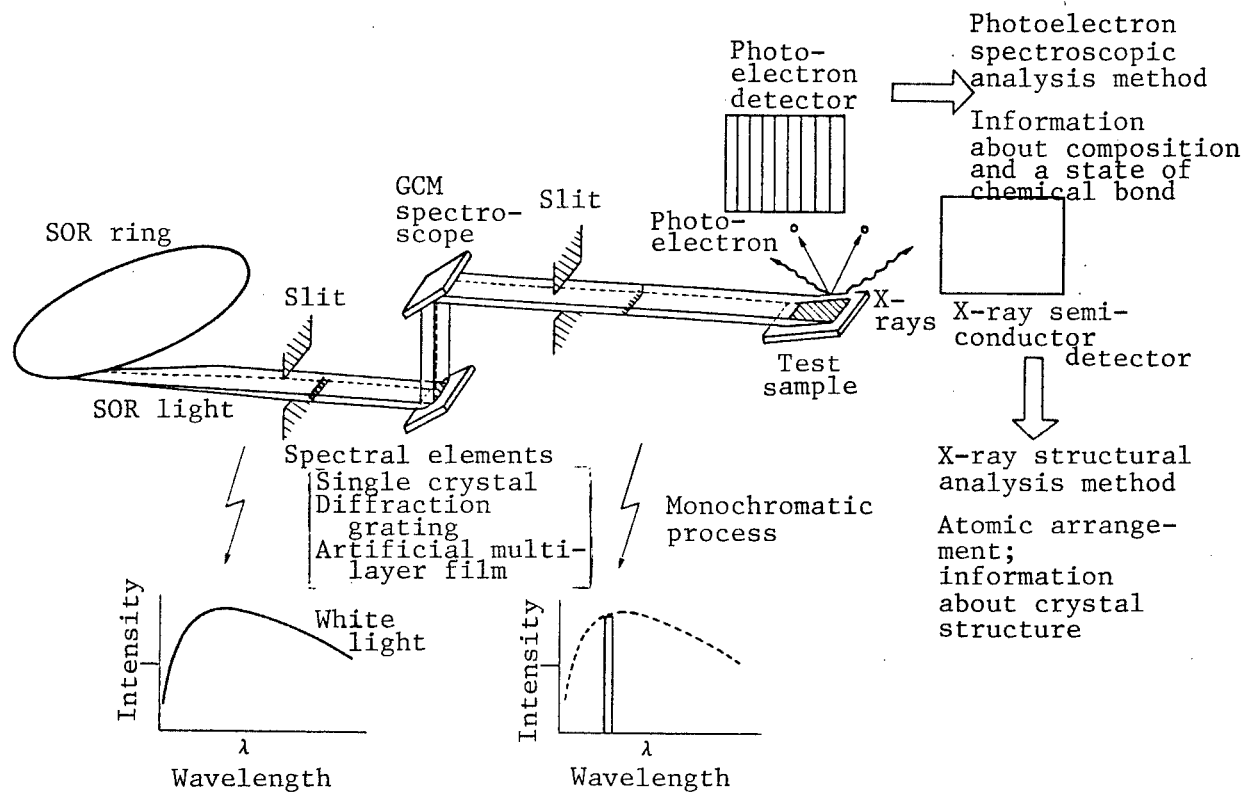


Figure 3. NTT Photon Radiation Beam Line (BL-1A) for the Analysis of Materials

The B line is to be used for X-ray lithography that is indispensable for development of VLSIs for the next generation. In addition to conducting basic studies on pattern replication characteristics and the evaluation of process adaptability, we have recently been studying⁴ techniques for mask-reduced pattern-projected exposure using photon radiation soft X-rays for the next-generation VLSIs. For the reduction optical system using soft X-rays, a reflecting mirror using artificial multilayer film is used. Figure 4 shows a photon radiation-used, mask-reduced pattern-projected exposure optical system using multilayer film. This reduction optical system, combined with a concave-convex mirror, is called a Schwarzschild optical system. A multilayer film is formed on the concave-convex surface, and this is used as a mirror upon which soft X-rays are incident and

reflected almost vertically. Ordinary masks are of a transmission type, but use of a multilayer film makes it possible to produce a mask of a reflection type and a large mask with little strain. For the concave-convex mirror, a uniform, artificial multilayer film needs to be formed along the curved surface. For the reflection-type mask, too, it is necessary to form a uniform artificial multilayer film in a large area to the extent of about 4 inches square. When we began this research, such an artificial multilayer film was not generally available, but was at the research and trial manufacture stage. Therefore, we started studying the manufacture of this kind of film. Recently, such films have been placed on the market as test samples by some foreign enterprises. However, it is difficult to obtain high-reflectance artificial multilayer films at an early date through freely-determined desired materials, size, or structure. They are also extremely expensive.

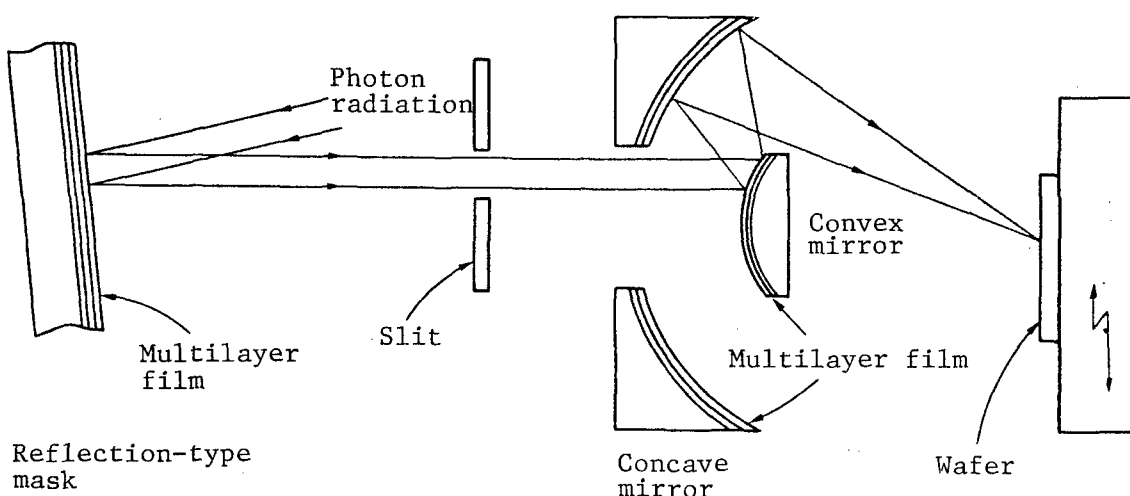


Figure 4. Photon Radiation-Used, Mask-Reduced Pattern-Projected Exposure Optical System Using Multilayer Film

4. Guidelines for Artificial Multilayer Film Designs and Calculation of Reflectance

The fundamental requisites for design of an artificial multilayer film are (1) selecting the component materials of heavy and light elements, (2) the thickness of a heavy element layer and a light element layer, (3) the ratio between the thickness of the heavy element layer and that of the light element layer, and (4) determining the number of layers. The peak reflectance of an X-ray reflection profile, the peak wavelength, and the width of the wavelength zone are basically determined by these requisites. The maximum reflectance theoretically obtainable and the wavelength zone to be used are generally determined by the selection of materials, in particular. To obtain a high reflectance, therefore, it is generally necessary to select component materials satisfying the conditions that the difference in optical constants (n , k) between two kinds of materials--heavy and light

elements--is large, and that the absorption coefficient of the light element is lower. The peak reflectance can be obtained by a method¹ based on the Fresnel formula.

When a monochromatic plane wave with a length of λ is incident from a vacuum at an angle of α upon an m-layer film consisting of plane films with a complex refractive index (n_j) of $(\lambda) = 1 - \sigma_j(\lambda) - i\beta_j(\lambda)$ and a thickness of t_j , that are piled up on a substrate from $j = 1$ to m , the amplitude reflectance (R'_j) in the interface from the $(j + 1)$ layer to the j layer is:

$$R'_j = \frac{r'_j + R_{j+1}' \cdot e^{-\Delta_j}}{1 + r'_j R_{j+1}' \cdot e^{-\Delta_j}} \quad (1)$$

Here r'_j is the complex amplitude reflectance in the interface between the medium of n_{j+1} and that of n_j , and it can be obtained from the following Fresnel formula:

$$r'_j = \frac{n_{j+1} \cos \alpha_{j+1} - n_j \cos \alpha_j}{n_{j+1} \cos \alpha_{j+1} + n_j \cos \alpha_j} \quad (\text{s component})$$

However, Δ_j is a phase difference and is expressed by

$$\Delta_j = 4 \pi n_j t_j \cos \alpha_j / \lambda$$

The α_j can be obtained from Snell's law-- $\sin \alpha = \sin \alpha_0 / n_j$.

Therefore, the complex amplitude reflectance (R_m) of a multilayer film reflection mirror can be obtained by making successive calculations from the first layer to the m layer by using equation (1).

5. Fabrication of Artificial Multilayer Films

Such methods as electron beam deposition,^{1,5} ion beam sputtering,⁶ and magnetron sputtering⁷ are used for fabricating artificial multilayer films. We designed and manufactured rf magnetron sputtering equipment by an independent scheme in order to fabricate multilayer films for soft X-ray photon radiation spectroscopic elements, aimed at analyzing the high-sensitivity local structure of light elements, and to fabricate multilayers for optical systems or masks to be used for X-ray mask-reduced pattern-projected exposure, aimed at lithography using photon radiation. This is an rf sputtering apparatus⁸ by a shutter opening and closing arrangement linked with substrate rotation, characterized by producing--with high reproducibility and productivity--a very precise and fine, uniform and homogeneous multilayer on a large substrate having a diameter of about 100 mm. The basic structure of this apparatus is shown in Figure 5. It fabricates multilayers by alternate lamination with a stated periodic length and a stated ratio of layer thickness, using two targets (150 mm in diameter) and rotating a substrate holder electrode. This equipment consists of a high-precision substrate rotation system, a substrate rotation

linkage type shutter opening and closing control system, a high-speed shutter opening-closing driving system, a sputtering chamber of bulkhead structure, and so forth. We made it possible to arbitrarily establish the speed of substrate rotation and the frequency of shutter opening and closing on each target. Therefore, it is possible to fabricate films with an arbitrary layer thickness ratio and periodic length without changing the film quality of each layer, that is, without changing the optimum sputtering conditions. Mixing of sputtered particles from the two targets can also be prevented by making the structure of the bulkhead in the sputtering chamber most appropriate and by optimizing the opening form of the shield mask. It is also possible to equalize the film thickness in the direction of a radius vector, and to form a uniform multilayer film on a large substrate measuring more than 100 mm in diameter, two-thirds the target diameter. In addition, multiple substrates can be placed on the substrate holder, making it possible to form many multilayer films of the same structure at the same time.

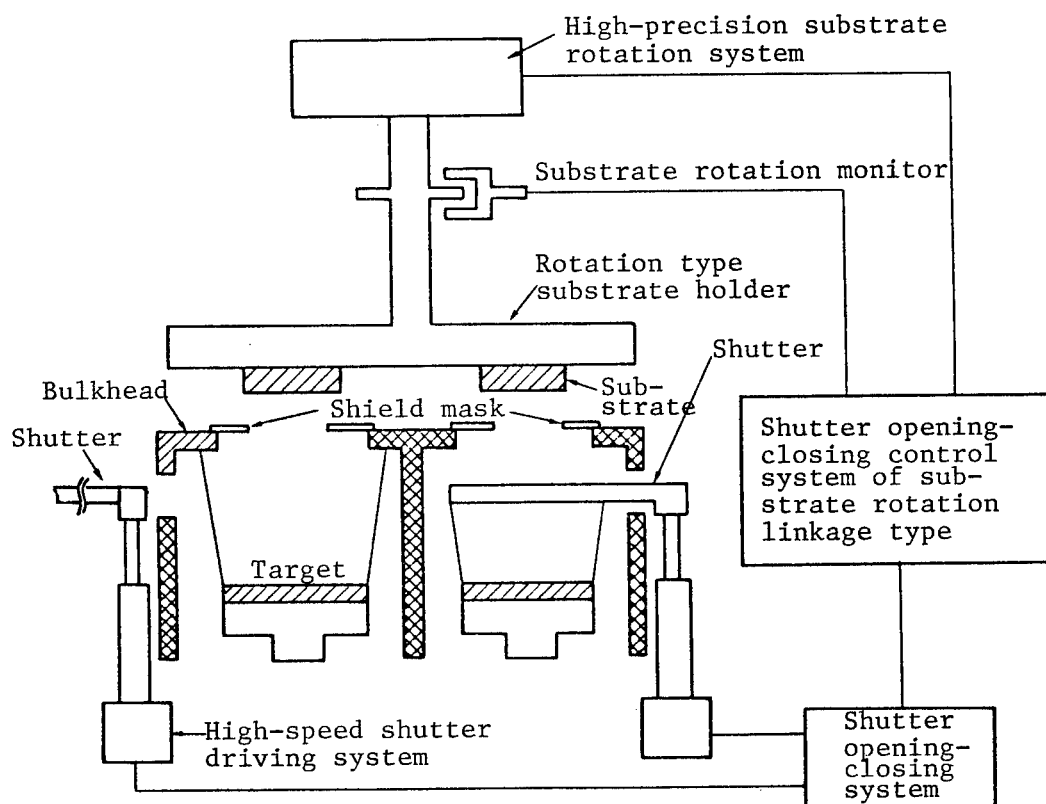


Figure 5. Substrate Rotation Linkage Type Magnetron Sputtering Equipment With a Shutter Opening and Closing Scheme

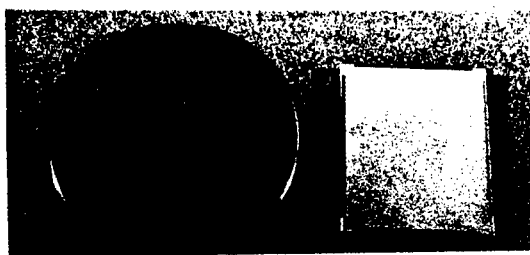
6. Various Properties of Artificial Multilayer Film

6.1. Homogeneity

Figure 6 shows the external appearance of multilayer film spectroscopic devices produced, with a tungsten-carbon artificial multilayer film as an

example. This is a multilayer film produced by alternately piling up 40 pairs of tungsten layers, each measuring 1.6 nm in thickness, and carbon layers, each measuring 2.4 nm. We evaluated artificial multilayer films measuring 2 to 20 nm in periodic length, produced with the sputtering equipment developed this time, using a probe-type thickness gauge and precision X-ray diffraction equipment. As a result, it has become clear that an unprecedentedly superior uniformity can be secured, with the degree of fluctuation in film thickness and in X-ray reflectance accounting for about 1 percent within a 100 mm diameter.

W/C artificial multilayer film.
(W: 1.6 nm; C: 2.4 nm, 40 pairs)



Si wafer Quartz substrate
(4 inches across) (70 x 80 mm)

Figure 6. External Appearance of a Reflection-Type Multilayer Film Mask (left) and a Multilayer Film Spectroscopic Device (right)

6.2. Periodic Structure of Multilayer Film

An electron microscope mirror image of the cross section of a W/Si multilayer film, as shown in Figure 7, is an example of the cross-section image of an artificial multilayer film. This is a cross-section photo of a part of a multilayer film consisting of 200 pairs of layers with a periodic length of 4.2 nm. The black lines represent W layers and the white lines show Si layers. To quantitatively grasp the disorder of the periodic length of such a periodic structure, we developed a precision photon radiation topographic apparatus and evaluated a W/C artificial multilayer film with a periodic length of 4 nm. As a result it became clear that the disorder of the periodic length was within a range of about 0.1 nm.⁹

6.3. Characteristics of X-Ray Reflection⁹

Figure 8 shows examples of measurement and calculation of the X-ray reflectance of an artificial multilayer film. The W/C artificial multilayer film we used has a periodic length of 3.84 nm and consists of 40 pairs of layers. The incident X-rays are characteristic of copper, having a wavelength of 0.154 nm. First, total reflection occurs near the incidence angle of 0°, and drops to about 0.5° together with the incidence angle. However, a diffractive reflection occurs at an angle satisfying Bragg's formula. The ratio between the peak intensity of this reflection and the maximum value of the total reflection reveals a high reflectance of 70 percent. When the

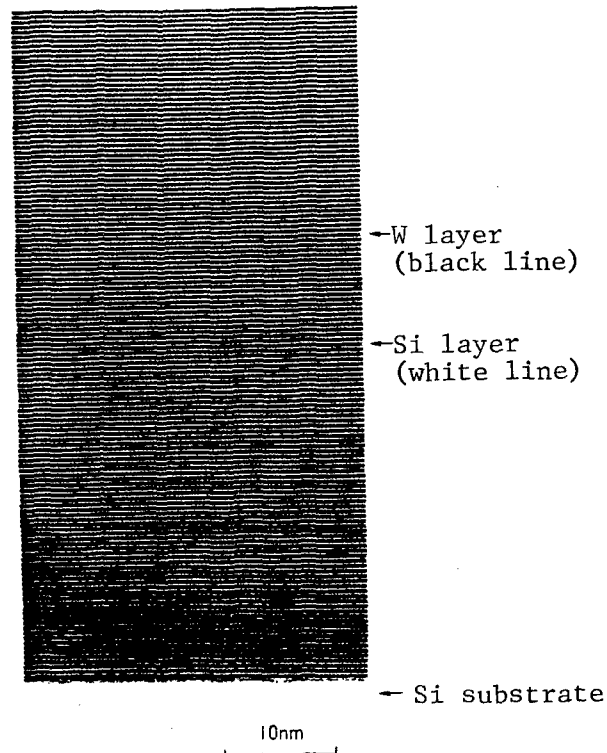


Figure 7. Electron Microscope Mirror Image of the Cross Section of a W/Si Multilayer Film ($d = 4.2$ nm)

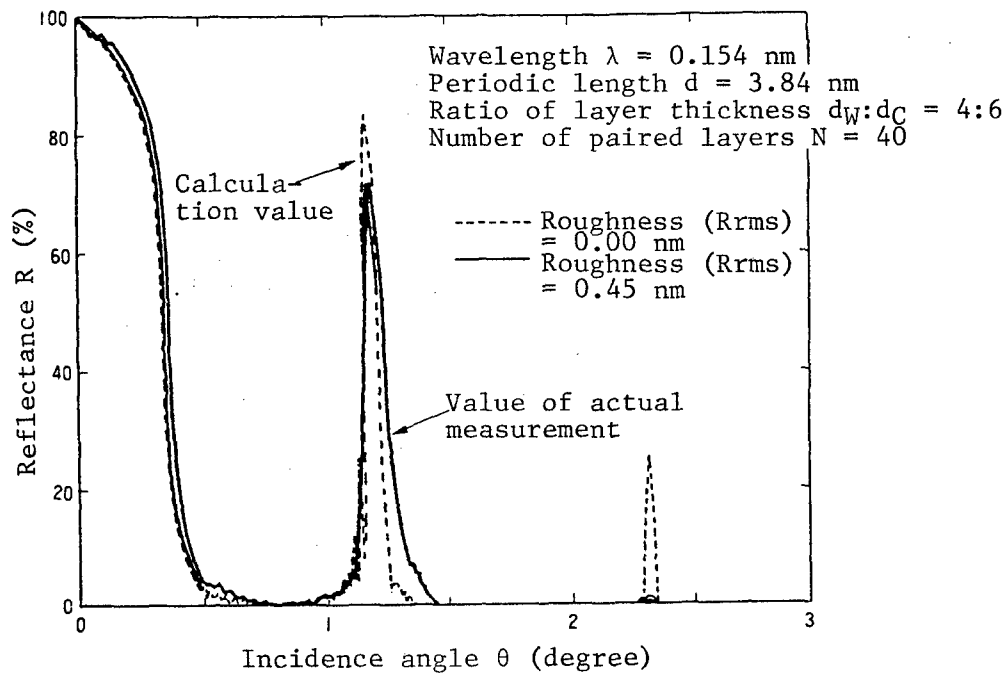


Figure 8. Examples of Measurement and Calculation of the X-Ray Reflectance of an Artificial Multilayer Film

surface of an artificial multilayer film is like a perfect mirror surface, that is, when it is not rough, the ideal calculation value of the reflectance is 84 percent. When a calculation is made by estimating the roughness (R_{rms}) of the surface and the interface of each layer is 0.45 nm, the calculation value is equal to a reflectance close to the value of actual measurement. From this it can be presumed that approximately 0.45 nm roughness of the surface of this artificial multilayer film, or of the interface of each layer, influences the X-ray reflectance. The relationship between the periodic length and the X-ray reflectance is shown in Figure 9, with a W/Si artificial multilayer film as an example. When the periodic length is 10 nm or more, the X-ray reflectance is constant at about 86 percent; this reflectance generally agrees with the calculation value in an ideal state. The substrate used this time was a silicon crystal finished to a mirror-like surface, with its roughness standing at 0.3 to 0.5 nm. In other words, when the periodic length is as large as 10 nm, the roughness of the surface has little effect on reflectance. X-ray reflectance drops with a decrease in periodic length, but a high reflectance of about 53 percent is currently obtained at a periodic length of 2.35 nm. When the periodic length is smaller than 2 nm, the roughness of the surface or the interface has greater effects. Thus, the formation of smoother substrates or films is important.

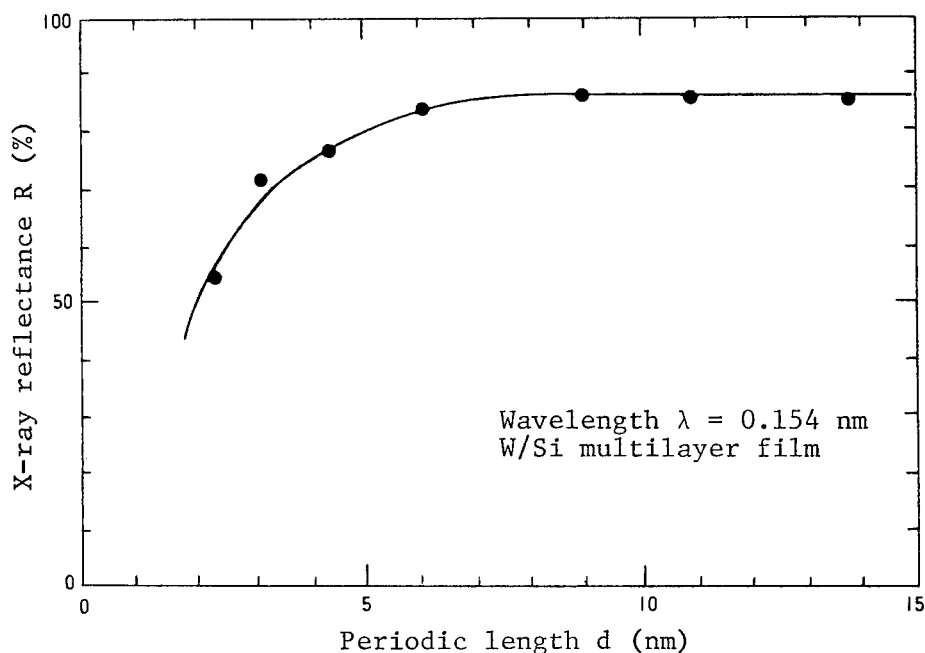
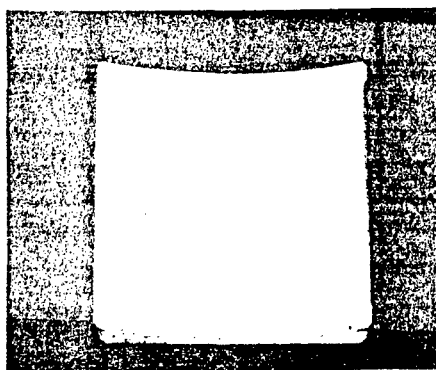


Figure 9. Relationship Between the Periodic Length of an Artificial Multilayer Film and X-Ray Reflectance

6.4. Focusing Property of X-Rays

When an artificial multilayer film is formed on a curved surface and used for an X-ray reflex mirror, it can focus X-rays the way it does visible light. The external appearance of a reflex mirror, with an artificial

multilayer film formed on a cylindrical surface, is shown in Figure 10. This cylindrical surface multilayer film mirror measures 46 mm in the radius of curvature and has a 50 mm square external form. Even on the curved surface, the uniformity of the film thickness is within ± 1 percent. We will show an example of focusing experiments we carried out with 54 mm x 6 mm photon radiation beams, using this reflex mirror. We carried out the experiments basically by the method shown in Figure 11. The photon radiation beams incident upon the cylindrical multilayer film reflex mirror are divided into beams reflected by Bragg's diffraction and some direct beams that are not incident upon the multilayer film reflex mirror. We photographed the sectional images of these beams after changing the position of the film, and examined their condensibility. The result is shown in Figure 12. The photon radiation beams were narrowed down to about one-sixth at a point 1 to 1.1 m away from the reflex mirror. In other words, the intensity of photon radiation beams can be increased six-fold. This result of condensation also generally agrees with the result of ray tracing calculations. Therefore, it is conceivable that a uniform artificial multilayer film is formed on the curved surface.



W/C multilayer film on a cylindrical surface
(Form: 50 mm square)
(Radius of curvature: 46 mm)

Figure 10. External Appearance of a Cylindrical Surface Multilayer Film Reflex Mirror

6.5. Soft X-Ray Reflectance

Using this method, we produced a Mo/Si artificial multilayer film that is expected to show a high reflectance in the soft X-ray region with a wavelength of about 13 nm and that is hoped to be applied to mask-reduced optical elements for soft X-ray lithography in particular; we also evaluated its soft X-ray reflection properties. The Mo/Si film produced had a periodic length of 6.5 nm, and the thickness ratio between the Mo layer and the Si layer was 2 to 3. There were 30 layers. We combined an optical system for evaluation of soft-X-ray reflectance with the B1-1B of the High Energy Physical Research Laboratory, and evaluated its reflective properties.

The reflective profile in the neighborhood of 13 nm in wavelength is shown in Figure 13. It has become clear that there is a high reflectance of 16 percent in a wavelength position beyond the L absorption terminal of Si. Reflex mirrors for light X-rays need to show a reflectance of more than 10 to 30 percent, although this depends on their use. This result indicates that the Mo/Si artificial multilayer film produced this time can be fully applied to reflex mirrors for soft X-ray condensation, including soft X-ray lithography.

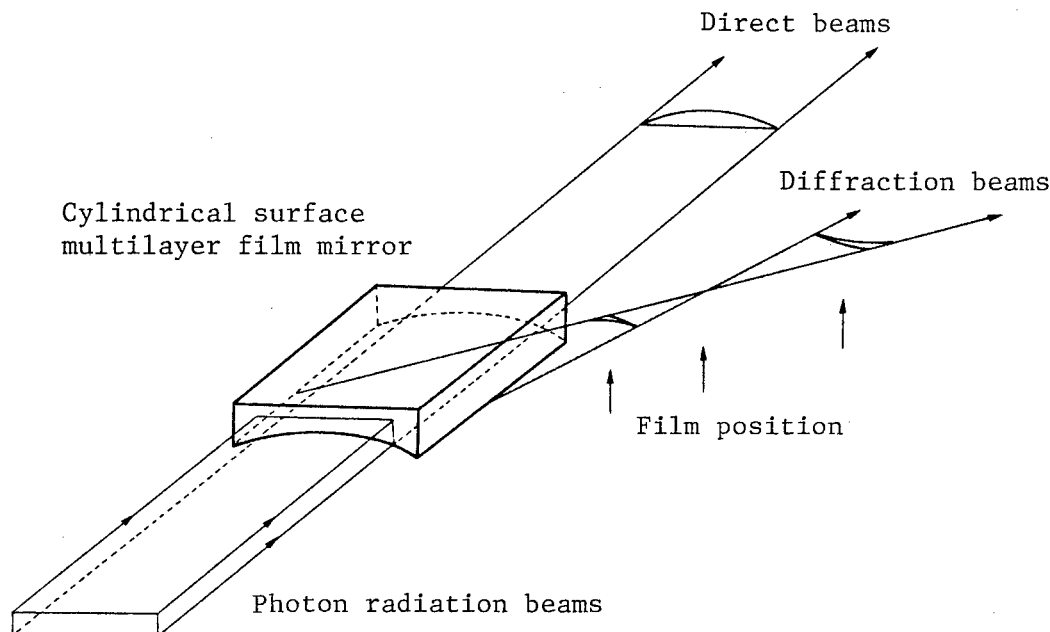


Figure 11. Experimental Method for the Condensation of X-Ray Photon Radiation by Means of a Reflex Mirror Involving a Multilayer Film on a Cylindrical Surface

7. Conclusion

We studied methods to produce and evaluate artificial multilayer films that are noted for spectral diffraction and condensation in the soft X-ray region of photon radiation, and have established a technology that makes it possible to simultaneously produce many artificial multilayer films having an arbitrary periodic length, ratio of film thickness, and number of layers, and to form uniform films for large substrates with curved surfaces as well. This technology is effective in producing devices for optical systems using multiple multilayer films of the same structure, such as double monochromatic spectral multilayer optical systems and soft X-ray multilayer film optical systems for multi-reflection. However, the present artificial multilayer films involve disorder in periodic structure and in interface, although slight, and they have not reached the point of having a perfect structure like that of a crystal. Therefore, X-ray reflectance drops rapidly, particularly in the case of an artificial multilayer film with a small periodic length of 2 μm or less. To achieve a higher reflectance in this region, there are many tasks for improvement, such as raising the accuracy

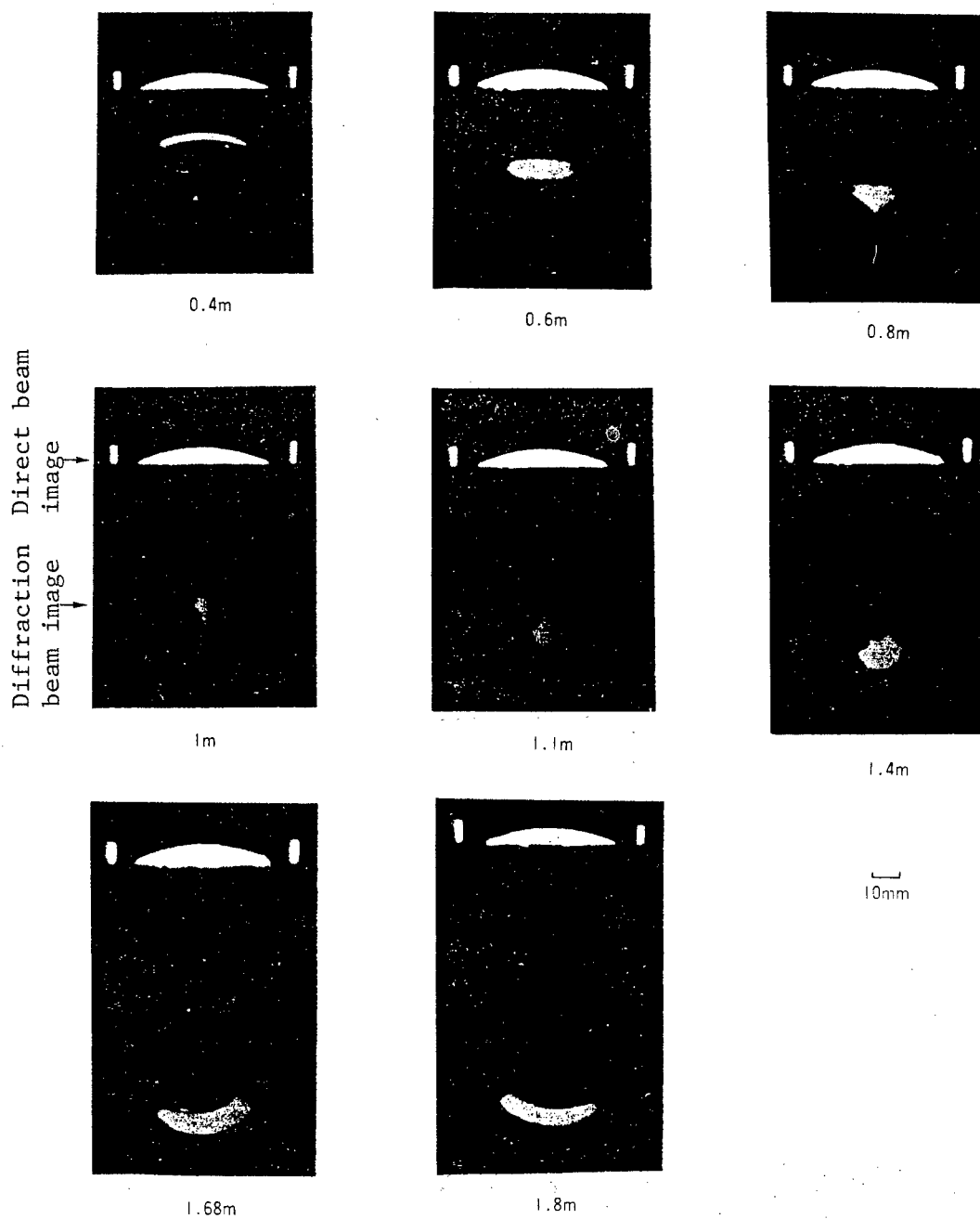


Figure 12. Condensing Properties of X-Ray Photon Radiation by Using a Cylindrical Surface Multilayer Film Reflex Mirror

of the periodic structure of artificial multilayer films, reducing the roughness of the surfaces and interfaces, and making the film quality of each layer homogeneous. At any rate, we expect the artificial multilayer film will be noted as one of the influential optical devices for spectral diffraction and condensation in the soft X-ray region.

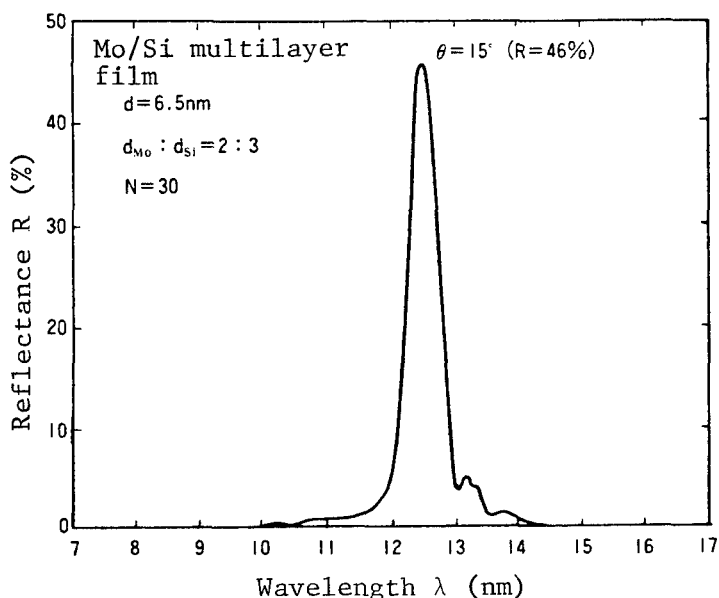


Figure 13. An Example of Soft X-Ray Reflection Profiles

Profiles of the Authors

Yoshikazu Ishii, manager of the Functional Materials Research Department of the Electronic Applications Research Laboratory, joined NTT in 1971 and engaged in research on oxide magnetic thin film disks by the sputtering method, on the analysis of materials using photon radiation, and on techniques for the analysis of semiconductive materials. He was appointed director of a materials analysis research office in 1986, and assumed his present post in 1990. He is engaged mainly in research on the manufacture and evaluation of multilayer films.

In 1969 he finished the metal processing course of the department of engineering, Tohoku University, and in 1971 finished the master's course in metal engineering at that university's graduate school. He received a doctorate in engineering (Tohoku University) in 1982.

He is a member of the Society of Applied Physics and the Society of Radiation Optics.

In 1983 he was awarded a prize on technological development from the Japan Institute of Metals.

Hisataka Takenaka, chief researcher of the Functional Materials Research Department of the Electronic Application Research Laboratory, joined NTT in 1979 and engaged in research on development of electric contact materials and Josephson junction devices. Thereafter he carried out research mainly on methods to produce and evaluate multilayer films.

In 1974 he finished the physics course of the department of science, Kansai Gakuin University, and in 1976 finished the master's course in physical study at the graduate school of the same university. In 1979 he finished the doctor's course in physics in the same department, and received a doctorate in science (Kansai Gakuin University) in the same year.

He is a member of the Physical Society of Japan and the Japan Society of Applied Physics.

Hiroo Kinoshita, chief researcher of the Process Automation Research Division of the LSI Laboratories, joined NTT in 1974 and engaged mainly in development of semiconductor manufacturing equipment. At present he is carrying out research on stepper technology in the soft X-ray region.

In 1974 he finished the machine engineering course of the department of engineering, Keio University, and in 1974 finished the master's course in machine engineering at the same university's graduate school.

He is a member of the Society of Applied Physics and the Society of Precision Machinery.

In 1982 he was awarded a technological prize from the Association for the Promotion of Machinery, and in 1988 received a thesis prize from the Society of Precision Engineering.

Kenji Kurihara, chief researcher of the Process Automation Research Division of the LSI Laboratories, joined NTT in 1977 and engaged chiefly in research on the inspection of LSI pattern defects, on electron beam and ion beam optical systems, and on ECR etching. He is now engaged in the study of X-ray reduction and projection.

In 1975 he finished the applied physics course of the department of science, the Tokyo Institute of Technology, and in 1977 finished the master's course in applied physics in the science and engineering department of the same institute's graduate school.

He is a member of the Society of Electronic Information and Communications and the Society of Applied Physics.

References

1. E. Spiller, Evaporated Multilayer Dispersion Elements for Soft X-Rays, Low Energy X-Ray Diagnostics-1981, ed. D. T. Attwood and B. L. Henke (AIP, New York, 1981) 124.

2. T. Namioka, Current Research Activities in the Field of Multilayers for Soft X-Rays in Japan, *Revue Phys. Appl.*, 23 (1988) 1711.
3. T. Kawamura, S. Maeyama, M. Oshima, Y. Ishii, and T. Miyahara, Solid Surface Analysis Beamline BL-1A at the Photon Factory, *Rev. Sci. Instrum.* 60 (1989) 1928.
4. H. Kinoshita, K. Kurihara, Y. Ishii, and Y. Torii, Soft X-Ray Reduction Lithography Using Multilayer Mirrors, 33rd Int'l. Symp. on E.I.P. Beams (1989).
5. E. Spiller, Experience With the in situ Monitor System for the Fabrication of X-Ray Mirrors, *Proc. SPIE*, 563 (1985) 367.
6. M. Yamamoto, A. Arai, H. Shibata, and T. Namioka, Thickness Monitoring of Ultra-Thin Films of Multi-Layered Coatings for VUV Mirrors by Ellipsometry, *Conf. Dig. ICO-13 Sapporo* (1984) 626.
7. T. W. Barbee, Jr., Sputtered Layered Synthetic Microstructure (LSM) Dispersion Elements, *Low Energy X-Ray Diagnostics-1981*, ed. D. T. Attwood and B. L. Henke (AIP, New York, 1981) 131.
8. Y. Ishii, H. Takenaka, and H. Takaoka, Preparation and Characterization of Sputtered W/C Multilayer Films, *MRS Int'l. Mtg. on Adv. Mats.*, 10 (1989) M231.
9. H. Takenaka, H. Takaoka, Y. Ishii, and H. Hashizume, Structural Uniformity of Multilayered Tungsten-Carbon Bragg Reflectors Prepared by rf Magnetron Sputtering, *Rev. Sci. Instrum.* 60 (1989) 2021.
10. H. Takenaka, Y. Muramatsu, H. Takaoka, Y. Ishii, and H. Hashizume, Focusing of Synchrotron Radiation by a Multilayer-Cylindrical Tungsten-Carbon Bragg Reflector, *Rev. Sci. Instrum.* 60 (1989) 2018.

SOR Lithography Beamline

916C3800D Tokyo NTT R&D in Japanese Vol 39 No 4, 10 Apr 90 pp 573-580

[Paper by Takashi Kaneko, Yasunao Saito, Seiichi Itabashi, and Hideo Yoshihara, NTT LSI Laboratories]

[Text] Preface

We have developed a beamline designed for research on X-ray lithography. This beamline, aimed at improving X-ray intensity and expanding the area of exposure, is formed basically by an obliquely incident X-ray mirror optical system with two toroidal mirrors combined with each other. In this system, parallel X-ray beams are formed with a condensing angle of 1.7 degrees and a beam width of 20 mm. The second mirror is rotated and vibrated through computer control, thereby exposing a 20 x 20 mm area by vertical scanning without losing the parallelism of the X-ray beams (variation of the beam direction: 5.6 mrad or less). Furthermore, windows to extract X-rays are formed in two stages, one consisting of Be film and the other of SiN film, making exposure in air possible through joint use of helium replacement.

[English abstract reprinted from original] This paper presents an efficient beamline for synchrotron radiation (SOR) lithography. It uses two X-ray mirrors to achieve the strong-intensity exposure and the vertical expansion of the exposure area. The first mirror converges SOR beams with a divergence angle of 1.7°. The second mirror, controlled by a microcomputer, collimates the beams and vibrates to produce an exposure area of 20 x 20 mm. Two X-ray windows of Be and SiN achieve the exposure in an atmospheric environment.

1. Introduction

Active research has been carried out on X-ray lithography using synchrotron orbit radiation (SOR) as a technology indispensable for development of next-generation LSIs, through the installation of a lithographic beamline for a large, general-purpose storage ring. Recently, development of a small storage ring to be exclusively used for X-ray lithography has been promoted, and exposure in an atmospheric environment has become the mainstream. With this development, the conventional beamline structure presents a problem with respect to the efficiency of SOR use, the occupied space, and so forth. Therefore, a small beamline suitable for small storage rings has begun to be explored, and a small beamline for exposure in air has been reported by IMT.¹

We have developed a beamline, ABL-5C, consisting of a two-X-ray-mirror optical system and two X-ray extraction windows, directed toward realizing a small beamline that will increase SOR utilization efficiency and make exposure in air possible.

In this paper we will describe our design policy for small beamlines for lithography, and will outline the beamline ABL-5C.

2. Basic Concept of Development

We developed a small beamline for X-ray lithography having the following functions:

- (1) X-rays emitted from a storage ring are efficiently condensed and led to exposure equipment.
- (2) The parallelism of SOR rays (variation of the beam direction: 10 mrad or less) can be maintained to lessen the run-out errors during exposure.
- (3) A desired area can be exposed.
- (4) X-rays with a wavelength band (7 to 12 Å) suitable for exposure can be extracted from SOR.
- (5) Exposure in air can be effected.

To design a beamline meeting these conditions, we followed the following structural fundamentals:

- (1) The beamline optical system is formed by combining two obliquely incident X-ray mirrors. The intensity of X-rays is improved by condensing them with the first mirror, and they are formed into parallel rays with the second mirror. In addition, the area of exposure is expanded by vertically scanning the exposure region.
- (2) The exposure wavelength is extracted by combining the reflective property (low pass property) of the obliquely incident X-ray mirror and the transmission property (high pass property) of the X-ray extracting system.
- (3) The X-ray extracting system is provided by two X-ray windows, and helium replacement² is effected between them. This system is applicable to exposure in air.

In the next section we will describe the beamline optical system we investigated under these basic policies, and the obliquely incident X-ray mirror that is a key device.

3. Study of the Beamline Optical System

3.1. Improvement of the Reflectance of an Oblique Incidence X-Ray Mirror³

X-ray optical devices that condense X-rays or turn them into parallel rays, are used extensively for such reasons as their wide effective areas and superior reflective properties in comparison with other devices. Also, as a beamline for lithography, the oblique incidence X-ray mirror is an indispensable constituent because of the X-ray transport efficiency and wavelength selecting function that are required of optical systems.

For this reason we sought to increase the reflectance of the oblique incidence X-ray mirror. We took a platinum-deposited film generally used for X-ray reflex mirrors, and experimentally looked into the difference that is observed in the roughness of a surface according to deposition methods, and into the effect on reflectance made by surface roughness and angle of oblique incidence. Figure 1 shows the X-ray reflective characteristics of the platinum-deposited film of the oblique incidence X-ray mirrors so far used and of the platinum film produced by a newly developed deposition method. The X-rays measured are characteristic of the Al-K spectra (6.34 \AA). The conventional platinum film measures 10 \AA in surface roughness, and the reflectance is about 10 percent at the oblique incidence angle of two degrees. Under the new deposition method with a low deposition speed, the surface roughness of the platinum film is 4.5 \AA , showing that reflectance has improved about four-fold in comparison with the conventional method. When the spectroscopic reflectance in the wavelength band (7 to 12 \AA) suitable for X-ray lithography was estimated by calculations made in light of this X-ray reflective property, it was found that a reflectance of 40 percent could be expected at an oblique incidence angle of less than two degrees.

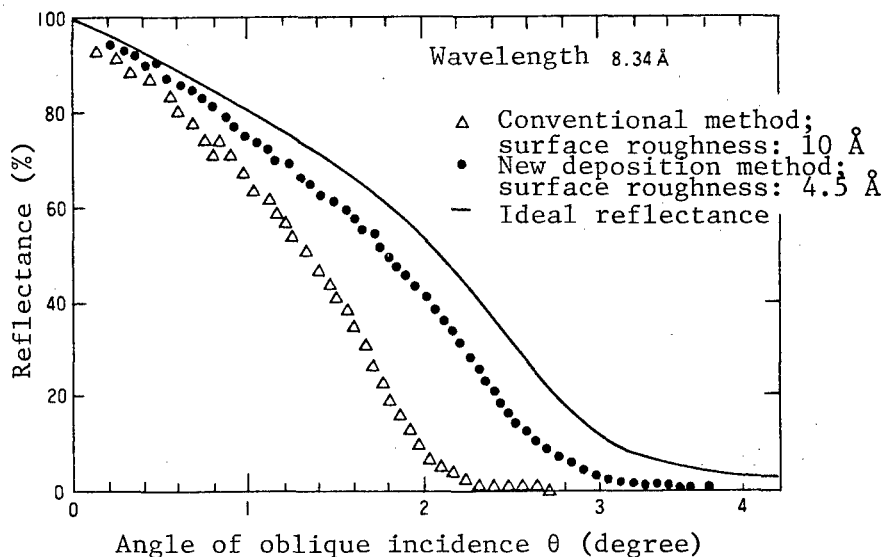


Figure 1. Reflectance Properties of a Platinum Film Coated X-Ray Mirror

3.2. Optical System With Two X-Ray Mirrors⁴

The optical system with two X-ray mirrors, which condenses X-rays and turns them into parallel rays, consists of a combination of two concave mirrors and that of a concave and a convex mirror, as shown in Figure 2. With this mirror arrangement, four kinds of structures are also conceivable. From among these structures, we sought the most appropriate one by using a ray tracing simulation. The obliquely incident X-ray mirror we used took a toroidal form. The toroidal surface can approximately reveal such curved surfaces as cylindrical, oval, and paraboloidal surfaces, so it is easy to process this surface compared with other curved surfaces.

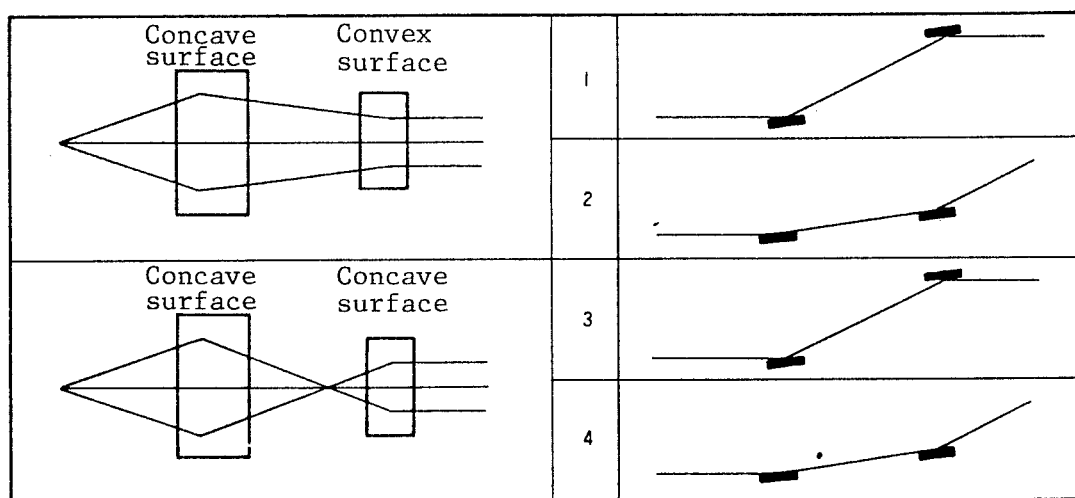


Figure 2. Structure of a Two-Mirror Optical System

An example of simulation results, shown in Figure 3, shows a ray tracing diagram of the upper and side faces in each optical system and a spot diagram on the exposed surface; the first mirror was placed 3.4 m away from the luminous source with two-degree oblique incidence, the second mirror was placed 4.6 m away from the first mirror with 1.5-degree oblique incidence, and the exposed surface was placed 2 m away from the second mirror. In the first, second, and fourth optical systems, the parallelism declines as the condensing angle becomes higher, and the beam form on the exposed surface curves. In the third optical system, wherein two concave mirrors are arranged symmetrically, parallel rays of a straight beam form can be irradiated on the exposed surface even with a condensing angle of 1.7 degrees.

Figure 4 shows the result of simulation when the second mirror in the third optical system is vibrated and X-ray beams are scanned on the exposed surfaces. The curves (a) and (c) show the X-ray beams on the exposed surfaces when the mirrors are vibrated by -0.16° and $+0.16^\circ$, respectively. The curve (b) shows the X-ray beams in the vibration center. The beams can be made flat in a horizontal direction by adjusting the first and second mirrors. A $20 \times 20 \text{ mm}^2$ exposure area can also be obtained by vibrating the

second mirror by ± 0.16 . As for the parallelism of X-ray beams, there is a difference of 1.1 mrad in the horizontal direction and 5.6 mrad in the vertical direction. The run-out errors can be ignored.

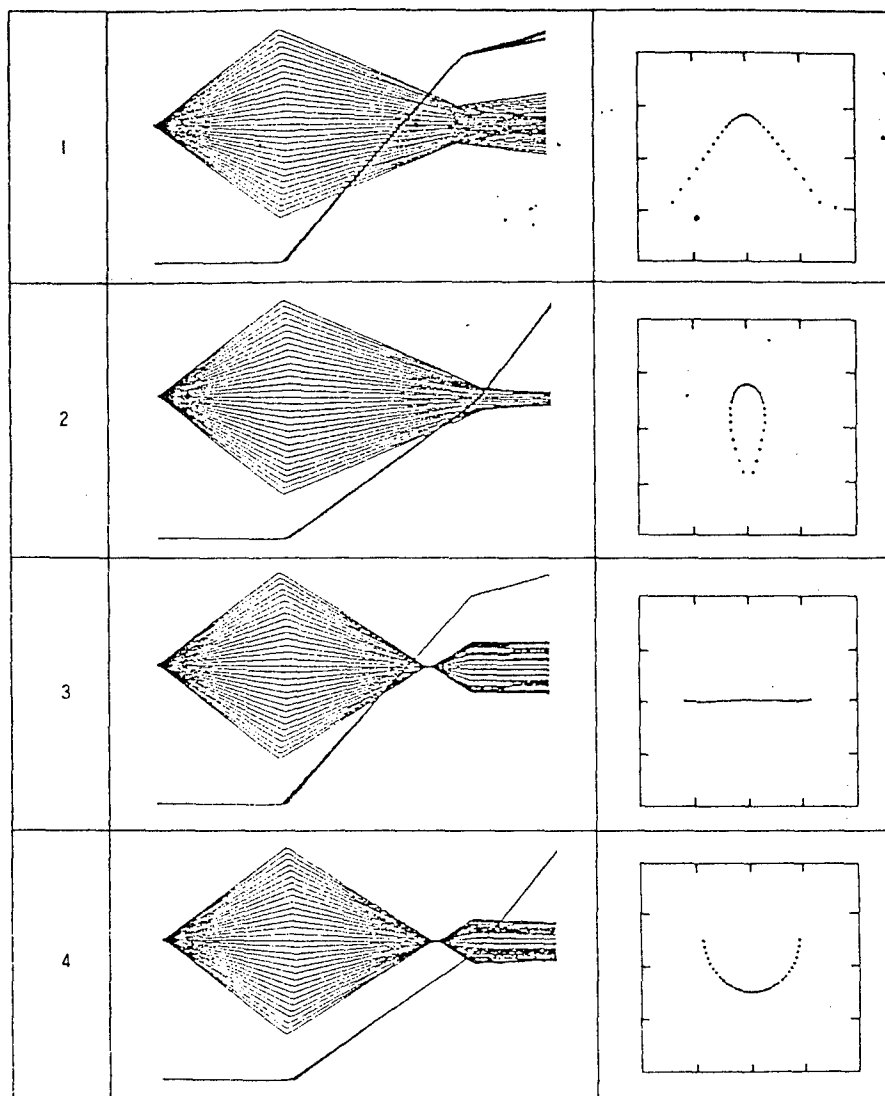


Figure 3. Comparison of Two-Mirror Optical System by Ray Tracing Simulation

When the number of rays in the exposure area in Figure 4 are compared, the number in the upper part is about 40 percent smaller than that in the lower part. When the mirror reflectance is compared, however, the reflectance in the upper part is estimated to be about 1.2 times higher than that in the lower part because the oblique incidence angle is lower in the upper part. Thus the uniformity of X-ray intensity is improved.

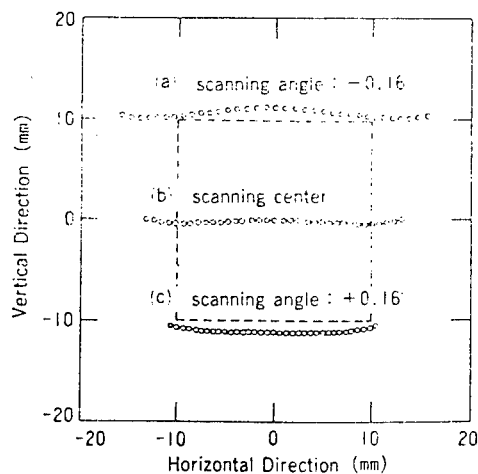


Figure 4. Expansion of Exposure Area Due to Mirror Vibration

4. Outline of Beamline ABL-5C

4.1. Basic Configuration

On the basis of the study mentioned above, we developed a beamline (ABL-5C) for lithographic use, and installed it in a normal conducting storage ring. Its configuration is shown in Figure 5 and the specifications in Table 1.

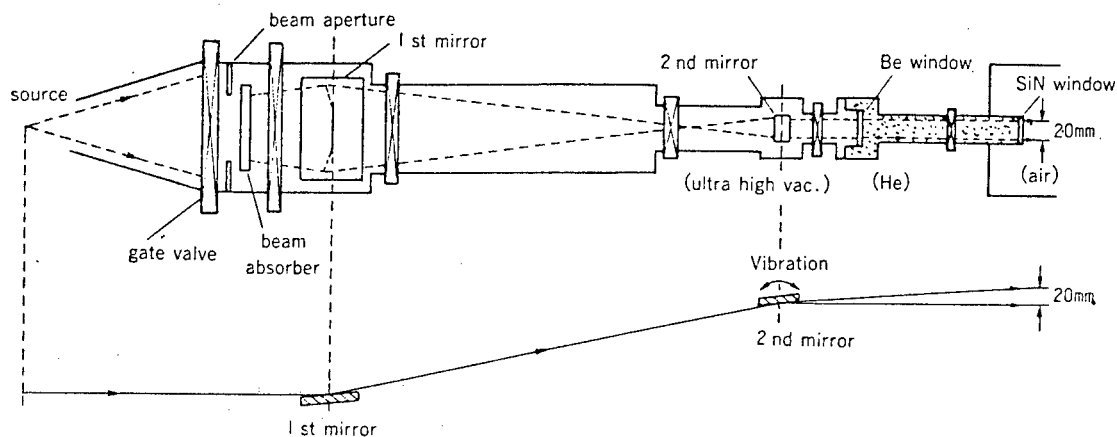


Figure 5. Configuration of Beamline ABL-5C

The SOR rays emitted fanwise from the luminous source can be obtained to the extent of a desired condensing angle through a beam aperture made of water-cooled oxygen-free copper plate. The SOR rays thus extracted fall upon the oblique incidence X-ray mirror when the beam absorber is open.

The optical system with two X-ray mirrors is set up to achieve 2.1-degree oblique incidence on the first mirror and 1.5 ± 0.16 -degree oblique incidence on the second mirror. Thus, SOR rays with a divergence angle of 1.7 degrees are condensed and irradiated on a 20 x 20 mm square exposure area.

Table 1. Specifications of Beamline ABL-5C

Total length	10 m
1st mirror	Concave toroidal mirror; 2.1° oblique incidence; 1.7 condensation
2nd mirror	Concave toroidal mirror; 1.5° ± 0.16° oblique incidence; driven by a computer-controlled vacuum pulse motor
1st bulkhead	Be film: 25 μm; vacuum/He: 1 atm; width: 30 mm, height: 8 mm; to be set up close to the 2nd mirror
2nd bulkhead	SiN film: 1 μm; He: 1 atmospheric pressure/atmosphere
Vacuum exhaust system	Four ion pumps and two turbo molecular pumps
Exposure area	Maximum 20 mm square

4.2. Mirror Attitude Adjustment Mechanism

The oblique incidence X-ray mirror is stored in a six-shaft shifter so that its attitude can be adjusted in a super-high vacuum. It is possible to set up X-ray beams in a stated position and form by adjusting the mirror attitude while observing the beams with a beam position monitor.

With regard to the mirror vibration to expand the exposure area, a method^{5,6} of driving the mirror in the vacuum chamber from outside has been reported. We adopted a method of providing a vacuum pulse motor in the mirror chamber and directly vibrating the mirror by computer control so as to facilitate a high-speed X-ray mirror vibration and a change of the vibration pattern. This makes it possible to generate an arbitrary vibration pattern with a computer, and thus to rectify various factors to maintain the uniformity of the X-ray intensity on the exposed surface.

4.3. X-Ray Extraction System

To ensure the degree of vacuum in the storage ring and to prevent pollution of the X-ray mirror due to residual gas, we maintained the upper part of the second mirror in a state of a superhigh vacuum (2×10^{-9} Torr or less) and provided a two-stage X-ray extraction window to make exposure in air possible. Thus we separated the super-high vacuum from the He gas and the He gas from the atmosphere, respectively.

In the first-stage window, the super-high vacuum in the beamline upstream was separated from the 1 atm He in the beamline downstream by means of a beryllium leaf 25 μm thick. X-ray transmittance of He gas is extremely high--260 times that of the atmosphere--and therefore we used He replacement. To secure the area of exposure and to improve the pressure resistivity of the extraction window with the smallest possible area, we placed it directly behind the second mirror. The window is 30 x 8 m square, and can be vibrated to eliminate the exposure irregularity due to the uneven thickness of the Be leaf.

The second window was set up directly in front of the X-ray mask by using a SiN film 1 μm thick, and the He replacement region of the beamline was separated from the atmosphere in the exposure equipment. SiN film is superior in radiation resistance and visible light transmissibility.

4.4. Vacuum Interlock

The main exhaust apparatuses, which are ion pumps, are placed in the chambers for the beam absorber, the first and second mirrors, and so forth, maintaining a vacuum of 2×10^{-9} Torr or less. Each chamber is partitioned with a gate valve that is interlocked with vacuum gauges placed before and after the valve. Thus, opening and closing of the chambers is controlled.

In the He replacement region, an oxygen densimeter is placed to monitor the degree of replacement. An inflow valve is also provided and is interlocked with a pressure gauge to control the He gas pressure so it will not exceed 1 atm.

4.5. Beamline Characteristics

Figure 6 shows the result of measuring the wavelength distribution of exposure X-rays in the beamline ABL-5C. For this measurement we used a Si (Li) semiconductor detector that was calibrated by such characteristic X-rays as Mo-L, Al-K, and Cu-L rays. The short-wavelength components of SOR rays are removed by the entire reflective properties of the two oblique incidence X-ray mirrors, and the long-wavelength components are removed by the transmissibility of the X-ray extraction windows. The peak wavelength is about 8.5 \AA , showing that the wavelength band suitable for X-ray lithography is extracted.

The X-ray intensity is 0.08 mW/mA/cm^2 , which can expose FBM-G resist (sensitivity: 80 mJ/cm^2) with $1000 \text{ mA}\cdot\text{S}$. However, the unevenness of about ± 20 percent for the X-ray intensity in the exposure region seems to be due to the reflective property of X-ray mirrors and mirror vibration.

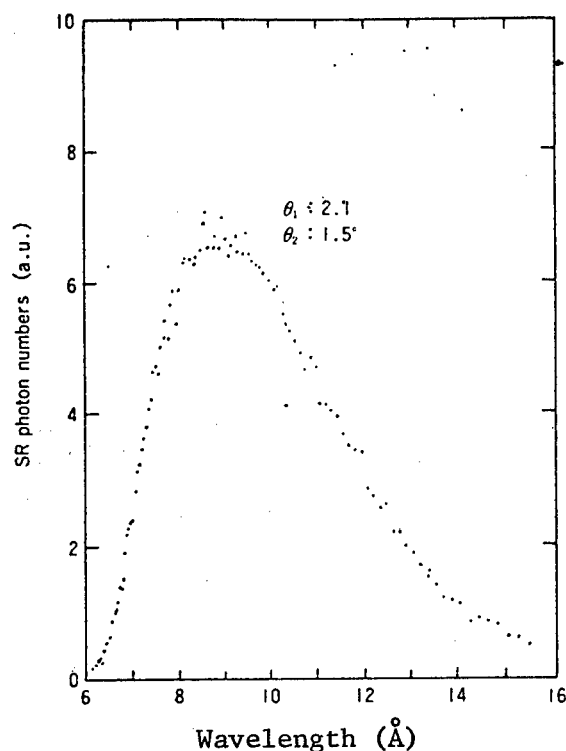
5. Conclusion

Aiming at realizing a highly efficient, small beamline for lithographic use that would be adaptable to a small storage ring, we pursued the research and development of a beamline with a condensing, exposure-in-air scheme using an optical system consisting of two oblique incidence mirrors and a two-stage X-ray extraction window. As a result, we clarified the following points:

- (1) For an oblique incidence mirror optical system for condensation and for expansion of an exposure area, a two-concave-mirror structure is most appropriate, making it possible to expose a 20 mm square area to parallel rays.
- (2) The two-stage X-ray extraction window, consisting of Be and SiN, makes it possible to ensure the vacuum degree of the storage ring and to effect exposure in the atmosphere.

(3) The uniformity of the X-ray intensity in an exposure area is about 20 percent, and efforts are being made to improve the vibration pattern of the second mirror in order to improve the uniformity.

(4) We promoted the improvement of a platinum reflection film for oblique incidence X-ray mirrors, and have increased the conventional reflectance four-fold.



1st mirror: 2.1° incidence angle

2nd mirror: 1.5° incidence angle

Figure 6. Result of Measurement of Exposure X-Ray Spectra

We plan to increase the intensity of exposure X-rays by expanding the condensing angle (two degrees or higher) and adopting high-reflectance mirrors to enhance the performance and reliability of beamlines for lithographic use.

Acknowledgement

We deeply thank Dr. Hisakazu Mukai, former director of the LSI Laboratories, and Dr. Toyoki Kitayama, former chief researcher of the same laboratories, for giving us guidance in carrying out this research. We also thank chief researcher Okada of the LSI Laboratories for allowing us to use the mirror reflectance measuring equipment.

Profiles of the Authors

Takashi Kaneko, chief researcher of the LSI Laboratories, joined NTT in 1972 and engaged in research mainly on optical information processing technology and underground object detection technology. He is now carrying out research on SOR exposure technology.

In 1970 he finished the course of applied physics of the Department of Science and Engineering, Tokyo Institute of Technology, and in 1972 finished the master's course in applied physics at that same institute's graduate school.

He is a member of the Society of Applied Physics, the Japan Society of Optics, and the Japan Society of Radiation Optics.

Yasunao Saito, chief researcher of the LSI Laboratories, joined NTT in 1963 and engaged in research mainly on X-ray exposure methods. He is now carrying out research on SOR exposure.

In 1968 he finished the course of physics of the Department of Science, Science University of Tokyo.

He is a member of the Society of Applied Physics.

Seiichi Itabashi, chief researcher of the LSI Laboratories, joined NTT in 1984, and engaged in research mainly on X-ray sources and XUV luminous sources. He is currently engaged in the study of X-ray optical parts.

In 1982 he finished the course of physics of the Department of Science, Tohoku University, and in 1984 finished the master's course in physics at that same university's graduate school.

He is a member of the Society of Applied Physics.

Hideo Yoshihara, chief researcher of the LSI Laboratories, joined NTT in 1968 and engaged in research on surface processing and on thin film fabrication using plasma. Since 1976 he has been studying X-ray exposure.

In 1966 he finished the course of metal engineering of the Department of Engineering, Yokohama National University, and in 1968 finished the master's course in metal engineering at that same department. He received a doctorate in engineering at Hokkaido University in 1983.

He is a member of the Society of Applied Physics and the Society of Electronic Information and Communications. He was awarded the 17th prize from the Association for the Promotion of Machinery in fiscal 1982.

References

1. H. Oertel, H. L. Huber, and M. Schmidt, Exposure Instrumentation for the Application of X-Ray Lithography Using Synchrotron Radiation, Rev. Sci. Instrum., 60, No 7, p 2140, 1989.
2. Kaneko, Suzuki, Ozawa, and Ohkubo, "Change in the Temperature of X-Ray Masks Due to Exposure Atmosphere," reported at a study meeting of the Laser Society, RTM-86-35, p 49, 1986.
3. Itabashi, Okada, Matsuo, and Yoshihara, "Investigation of High-Reflectance Pt Thin Film," pre-prints for the 37th spring joint speech meeting concerning applied physics, 1990.
4. T. Kaneko, S. Itabashi, Y. Saitoh, H. Yoshihara, and T. Kitayama, A Beamline and Its Components for SR Lithography, Jpn. J. Appl. Phys., 28, No 10, p 2080, 1989.
5. K. Fujii, K. Okada, M. Nagano, and H. Kuroda, Precisely Controlled Oscillating Mirror System for Highly Uniform Exposure in Synchrotron Radiation Lithography, J. Vac. Sci. Technol., B6, No 6, p 2128, 1988.
6. M. Bieber, H. Betz, and A. Heuberger, Investigation of X-Ray Exposure Using Plane Scanning Mirrors, Nucl. Instrum. Methods, 208, p 281, 1983.

SOR X-Ray Stepper

916C3800E Tokyo NTT R&D in Japanese Vol 39 No 4, 10 Apr 90 pp 581-590

[Paper by Sunao Ishihara, Atsunobu Une, Munenori Kanai, and Masanori Suzuki, NTT LSI Laboratories]

[Text] Preface

We have developed exposure equipment using SOR as a luminous source. This equipment is called an X-ray stepper because it successively replicates the microscopic pattern on a mask by an X-ray exposure process, while causing wafers to make a step movement. It is used to expose wafers in the atmosphere to SOR rays that are scanned in a vertical direction, while giving alignment support all the way through the exposure.

The key technology in making this equipment involves a vertical XY stage and an optical-heterodyne interference alignment system. In the XY stage, guiding and driving parts including lead screws all use air bearings, and it has a 5 nm motion resolving power. The optical-heterodyne detection system detects the positions of diffraction lattice marks on masks and wafers with an accuracy of 10 nm, and thus achieves high-precision position alignment. Through exposure experiments, we evaluated the performance of an X-ray stepper that had been trial-manufactured by using these techniques, and obtained an alignment precision of $\pm 0.1 \mu\text{m}$.

[English abstract reprinted from original] This paper presents a vertical stepper for synchrotron X-ray lithography. The stepper exposes wafers in a normal atmosphere to vertically-scanned SOR with continuous alignment control during exposure. The key devices of the stepper are a vertical x-y stage and an optical-heterodyne alignment system. The x-y stage uses air-lubricated components, including air bearing lead screws, and achieves 5 nm motion precision. The optical-heterodyne alignment system detects the displacement between the mask and wafer gratings with an accuracy of 10 nm. Several exposure experiments show the alignment capability to be better than $\pm 0.1 \mu\text{m}$ as a 3σ value.

1. Introduction

In the case of lithography below the quarter-micron level, which is regarded as an effective region for application of SOR-use X-ray exposure, an extremely severe precision--tens of nanometers--is required for pattern position alignment. Therefore, it is necessary to use exposure equipment capable of super-high-precision mask alignment, as well as to improve the accuracy of X-ray masks. X-ray exposure is an equimultiple proximity exposure method that places a mask and a wafer at a narrow interval of tens of μm and throws X-rays upon them. Therefore, the accuracy of position alignment for replication patterns is basically governed by the accuracy of mechanical position alignment for the mask and the wafer. For this reason, the exposure equipment needs to be ultra-precise in position determination.¹ This equipment successively replicates the mask pattern on a wafer, while causing the wafer to make a step movement. Therefore, it is called an X-ray stepper. When SOR is used as a luminous source, the mask and the wafer are arranged along a perpendicular plane, and the structure to hold them and determine their positions is vertical. Such vertical X-ray steppers are trial-manufactured for experiment purposes by research organizations both at home and abroad.²⁻⁴ However, no such equipment usable in the quarter-micron region has yet been made.

Therefore, we pursued research on a vertical, high-speed and high-precision XY stage, a multishaft fine movement mechanism, a method for the high-precision detection of mask-wafer relative positions, and so forth, and have developed SOR-use exposure equipment.⁵

This paper deals with the structure of SOR-use exposure equipment, a newly developed key technology supporting this structure, and the result of evaluating the performance of a trial-manufactured X-ray stepper.

2. Target Performance and Basic Formula

The basic performance of exposure equipment involves resolving power, super-position accuracy, and throughput. In an exposure system using SOR as the luminous source, the main factors determining these kinds of performance are the wavelength to be used, the exposure gap, and the field size. In addition, the functions peculiar to a SOR exposure system are vertical expansion of the exposure region and selection of the exposure atmosphere. Table 1 shows a target specification for SOR-use exposure equipment, determined with a view to creating an exposure system capable of application to a $0.2\ \mu\text{m}$ region in the future.

Table 1. Specification for SOR-Use X-Ray Stepper

Resolving power	$0.2\ \mu\text{m}$
Position alignment accuracy	$\pm 0.1\ \mu\text{m}$
Wavelength to be used	$0.7\text{--}1\ \text{nm}$
Exposure gap	$30\text{--}50\ \mu\text{m}$
Field size	$30 \times 30\ \text{mm}$
Exposure atmosphere	in the atmosphere
Wafer size	4-, 6-inch diameter

The characteristics are as follows:

(1) The resolving power governed by Fresnel diffraction at the X-ray absorber pattern edge is determined by the wavelength of X-rays contributing to exposure and by the gap between the mask and the wafer.⁶ To obtain 0.2 μm resolving power when a 0.7-1 nm wavelength is used, the exposure gap must be about 30 μm .

(2) Because of the trend toward expanding the semiconductor chip size and obtaining a high throughput, it is desirable to obtain a large field size. But this is a severe task when accuracy is considered. For exposure equipment, therefore, we made the field size variable so that exposure could be made up to a maximum size of 30 mm square.

(3) For expansion of an exposure region in a vertical direction, there is a method of scanning SOR rays and a process of unified mask-wafer scanning. In this system, however, we chose a method of SOR ray scanning by a beam line vibrating mirror. With this method, the mask and the wafer are exposed in a stationary state, and the accuracy of position alignment can be expected to improve.

(4) For the exposure atmosphere, we chose an exposure-in-air method to avoid a rise⁷ in the temperature of an X-ray mask due to SOR irradiation. Compared with exposure in pressure-reduced helium, this method increases the degree of X-ray attenuation. But it has an advantage in improving the operability of the equipment and raising the degree of freedom in system design.

3. Makeup of Equipment

The basic functions of SOR exposure equipment are the step movement of wafers and position alignment, including creation of a mask-wafer gap. In realizing high-performance exposure equipment, a technique for position determination is fundamental. Therefore, as fundamental factors for the makeup of the equipment, we developed a high-precision position determination stage and a system for high-precision detection of the mask-wafer relative position. Thus we trial-manufactured a SOR-using X-ray stepper by combining these factors.

3.1. Position Determination Stage Using Air Bearing Lead Screws

For the position determination stage, which needs to be highly accurate, efforts are being exerted to enhance the accuracy of movement, typically by using air bearings for the guidance and support regions, and to enhance the accuracy of position determination by mounting a fine movement mechanism having high motion-resolving power on a coarse adjustment driven by a ball screw or the like.

If an air bearing can be placed between the nut and the screw shaft in the lead screw region for driving use, it will be possible to realize a super-high precision lead system with high motion resolving power covering a long

stroke, by a non-contact screw lead involving no friction at all. However, it is difficult to form a narrow-gap air bearing in the screw of a complex form, and it has been regarded as difficult to create a practical air bearing lead screw. This time we carried out research from fundamental viewpoints involving the basic structure, materials, and processing methods, and have realized an air bearing lead screw having high degrees of hardness and accuracy, covering a 200 mm stroke.⁸ This has been applied to the vertical XY stage. The air bearing lead screw we have developed is described below.

The structure of the air bearing lead screw is shown in Figure 1. The nut flank face (where the male screw gears with the female screw) is partially porous and, when high-pressure air is supplied from outside through an air inlet, the porous region works as a restrictor and an air bearing is formed in the gearing part. By using ceramic materials and a square screw form, a narrow floating gap is created by high-precision form processing of the screw, and a static hardness of 3 kg/ μ m or more is obtained in the shaft direction, coupled with an increase in the performance of the porous restrictor. Figure 2 shows the result of measuring the minute lead property as the representative characteristic of this air bearing lead screw. A slight revolution of the screw shaft due to a piezoelectric device is changed into a straight movement of the nut (because the lead of the screw measures 6 mm, 1/1,000,000th revolution is equivalent to 60 nm linear displacement). Thus, a movement property with satisfactory linearity is obtained even in a very small region. In addition, from the step displacement of the nut at the time step-like voltage is applied to the piezoelectric device, it is found that this system has a motion resolving power of 5 nm or less.

3.2. Optical Heterodyne Interference Type Position Detection Method

Mask-wafer position alignment is accomplished by placing alignment marks on the mask and the wafer, detecting the relative displacement between the marks, and correcting their positions. It is important that the position detection resolving power is extremely high, and that the accuracy of detection is not influenced by such factors as the state of the wafer surface, which changes on each exposed layer, and the fluctuation of the gap between the mask and the wafer. Therefore, we developed an optical-heterodyne interference position-detection method; it uses optical diffraction and interference that can be expected to have high detection resolving power in comparison with the conventional method of using an image edge, and makes it possible to achieve the displacement as phase information.⁹

The theory of this type of position detection method is shown in Figure 3. Laser rays slightly varying in frequency are thrown symmetrically from two directions to diffraction lattices on a mask and a wafer. The rays diffracted upward at the diffraction lattices interfere with each other, which gives rise to beat signals. The phases of the beat signals are proportional to the horizontal displacement of the diffraction lattices, and the speed of the signals becomes a frequency that can be detected electronically. Therefore, position divergence can be detected by detecting the beat signal phases from the diffraction lattices of the mask and the wafer,

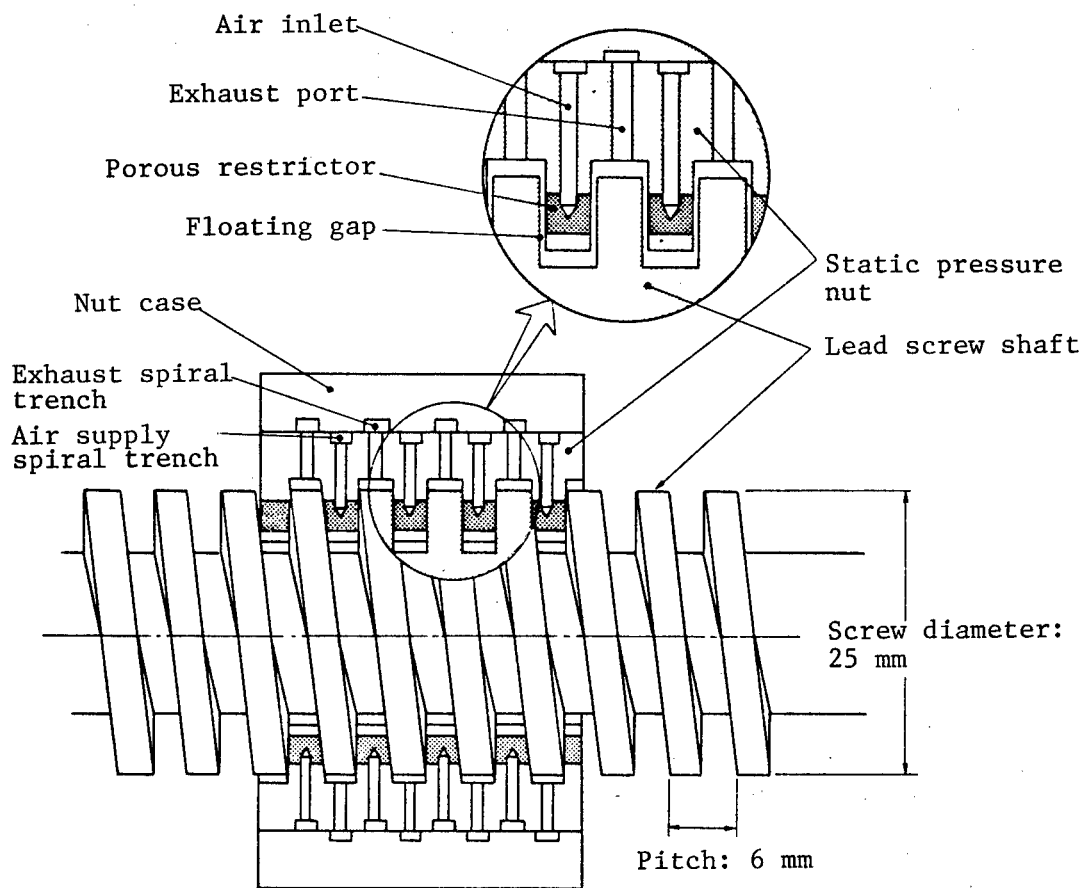


Figure 1. Structure of Air Bearing Lead Screw

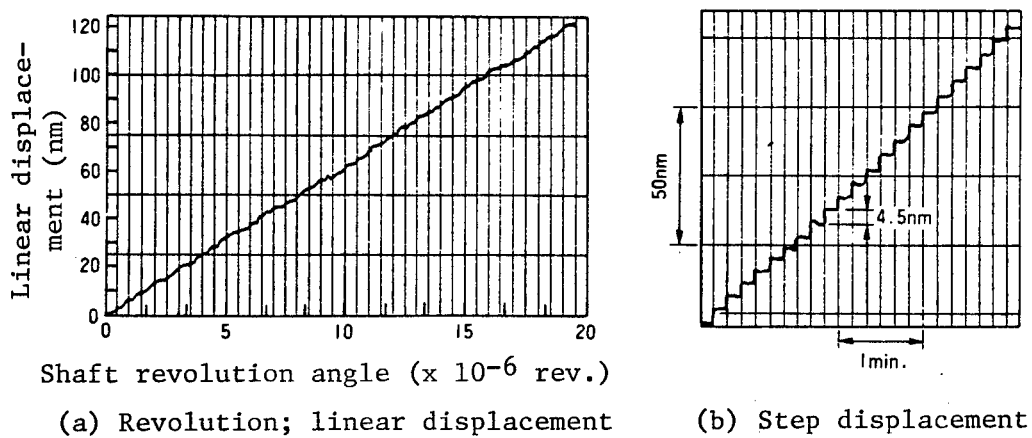


Figure 2. Minute Lead Properties of Air Bearing Lead Screw

and seeking the difference between the two. In other words, when the pitch of the diffraction lattice is represented by p and each position divergence by x , the phase difference $\Delta\phi$ is given by:

$$\Delta\phi = 2\pi \cdot x / (p/2)$$

Thus, periodic, linear signals for position detection can be obtained.

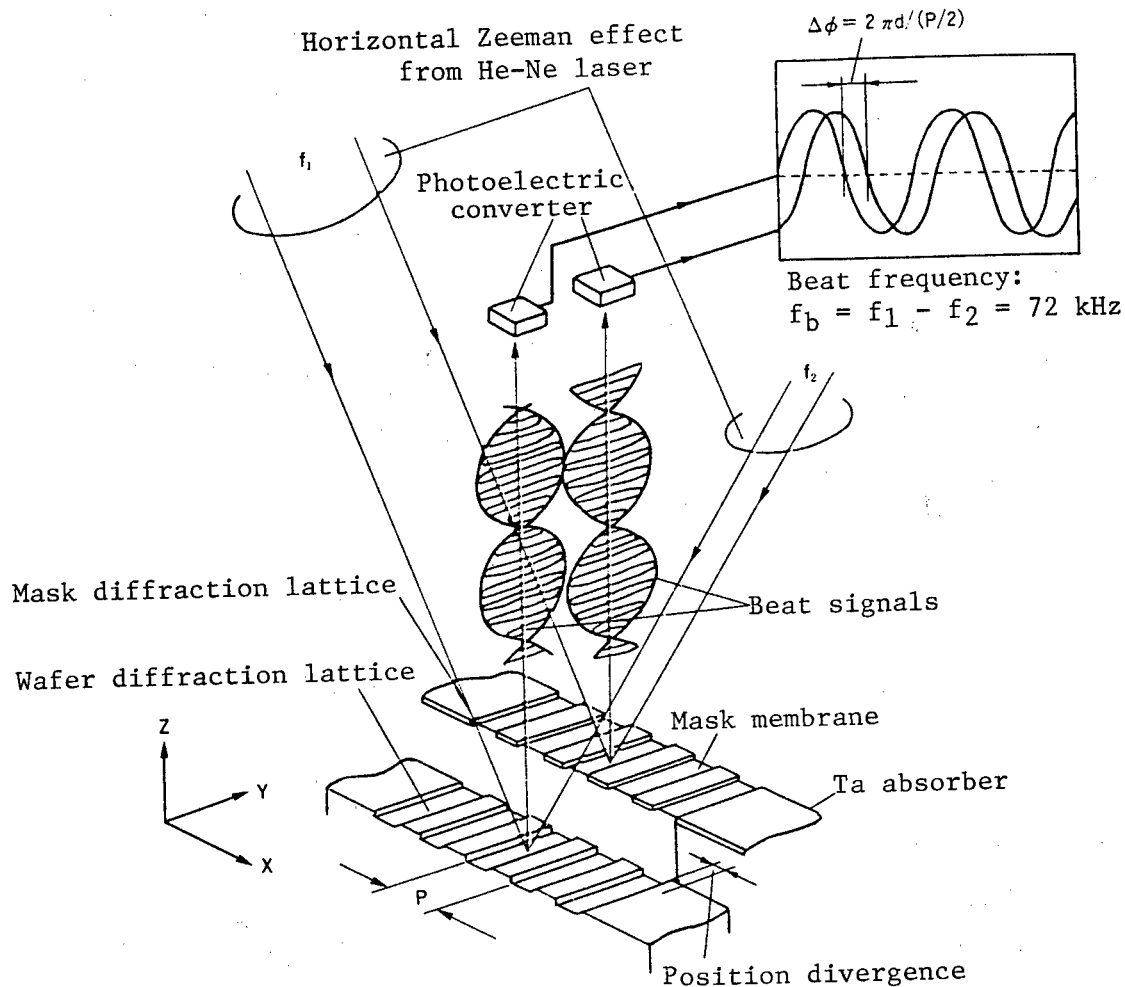


Figure 3. Theory of an Optical-Heterodyne Interference Position Detection Method

Figure 4 shows the result of experiments in the position detection of a diffraction lattice by the optical-heterodyne interference system, together with the result of a simulation of detection characteristics. As can be seen from this illustration, the greatest characteristic of this system is that its resolving power for position detection is extremely high. When, for example, a one-degree phase difference is to be detected by using a diffraction lattice with a pitch of $4 \mu\text{m}$, the system can easily achieve the resolving power to detect a displacement of about 5 nm . In addition, it is

characterized by not being influenced by a gap change, because it is a symmetrical optical system, and by the influence exerted on it by a change in wafer surface reflectance being slight, because it is designed for phase detection.

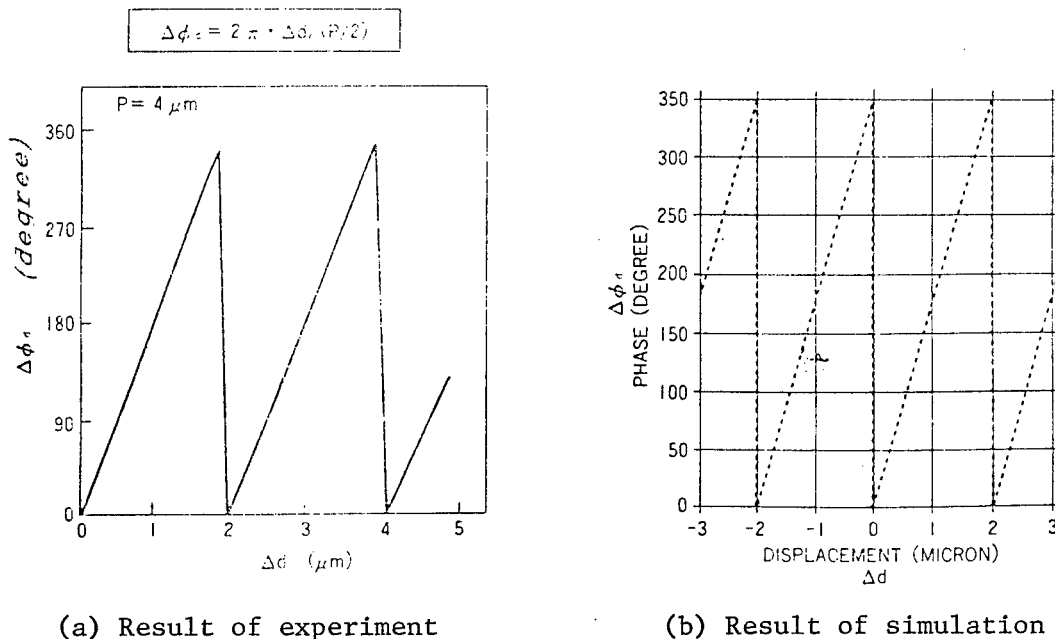


Figure 4. Position Detection Properties of the Optical-Heterodyne System

3.3. Structure of an X-Ray Stepper

The structure of a SOR-use X-ray stepper, trial-manufactured by using the aforesaid basic factors, is shown in Figure 5. It is divided broadly into a wafer unit to determine the wafer position, a mask unit to adjust the mask position and detect the mark position, and a wafer autoloader.

(1) The wafer unit is a vertical XY stage using the aforesaid air lead screw. It consists of a linear guide, a rotary guide, and a lead screw using an air bearing; it makes high-speed, high-precision position determinations by laser-used length measurements ($\lambda/128 = 5$ nm). It is also equipped with a gravity compensation system using a fixed tension spring, because it is a vertical stage.

(2) The mask unit consists of a multishaft fine motion mechanism for the mask, a prealignment scope, and a fine alignment optical system. The mask fine motion mechanism, driven by a piezoelectric device, prevents mask flapping due to the creation of an exposure gap or corrects the position of revolution. The prealignment scope is an optical detection system to automatically determine the position of an automatically supplied wafer within a scope, enabling high-precision position alignment. The fine alignment optical system uses four channels of the optical-heterodyne interference

optical system, corresponding to four sets of position alignment marks (diffraction lattices with a $6\text{ }\mu\text{m}$ pitch) arranged around the exposure region. To reduce attenuation of SOR rays in extracting them in the air, the optical systems are placed in an He atmosphere. In addition, a position alignment servomechanism is available during exposure as an optical arrangement not intercepting SOR rays.

(3) Wafers are automatically supplied through the movement of the entire XY stage to the front of the wafer loader. The wafer loader is equipped with an orientation mechanism to determine the wafer position in a rough way, a crosswise conversion mechanism to supply wafers to the vertical wafer holder, and so forth.

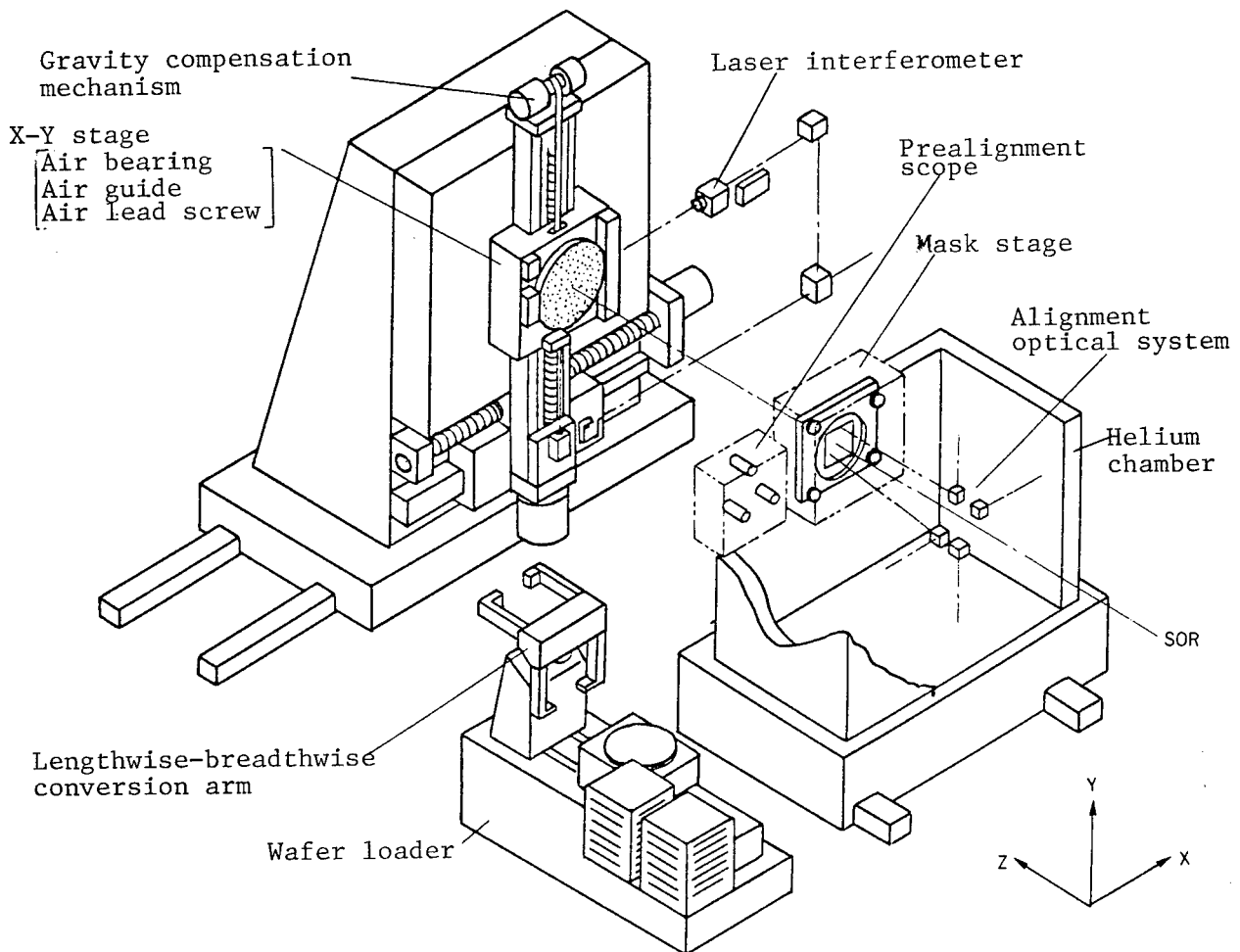


Figure 5. Structure of a SOR-Use X-Ray Stepper

4. Performance Evaluation

4.1. Operational Properties of the Equipment

Operation of the equipment is computer controlled after mask loading and plane leveling, in the order of wafer supply, prealignment, wafer step movement, fine alignment, and exposure. The wafer position is determined from the millimeter region to the nanometer region in the order of mechanical press with the loader, control of position determination with a laser interferometer after chucking the wafer to the holder, and control of position alignment with optical-heterodyne detection signals right under the mask.

Figure 6 (a) shows the step movement characteristics of the XY stage. Highly precise position determination to the extent of a 20 mm step has been achieved in a short time, about 0.5 second, through the ordinary control of feedback position determination that is to be exercised to switch the speed signal from a tacho generator and the position signal from a laser interferometer 10 μm in front of the target position.

Figure 6 (b) shows the operational wave form at the time of switching the control, after the step movement, from the laser interferometer to a servo-alignment mode by optical-heterodyne detection signals. Efforts are being made to stabilize the switch by providing an approximately 100 ms duration for the simultaneous feedback of both signals during the switch. However, a wave-form disorder due to an imbalance of gravity compensation is observed in the vertical Y axis. As is seen in the illustration, a fine alignment of XY axes is completed about 0.5 second after the control switch, even in the case of a large-scale supplementary operation close to 1 μm .

4.2. Accuracy of Position Alignment

Position alignment performance of the exposure equipment was evaluated through exposure experiments, and the position of pattern replication by this equipment was measured by using a light wave interference type coordinate measurement apparatus on the wafer.

Figure 7 (a) shows the accuracy of position alignment of the upper layer pattern with the lower layer pattern, through the SOR exposure of a wafer on which the lower layer pattern is previously printed with a photostepper, after making position alignment for the upper layer pattern with this equipment by using alignment marks. The errors of position alignment in this case involve all the error factors, including mask errors and photostepper errors. Therefore, we seek the dispersion of position divergence data centered on the average value of position divergence at each point of measurement in the exposure field, and regard it as the position alignment accuracy (reproducibility) of the equipment. As shown in the illustration, this position alignment reproducibility is about $\pm 0.1 \mu\text{m}$ (3σ value).

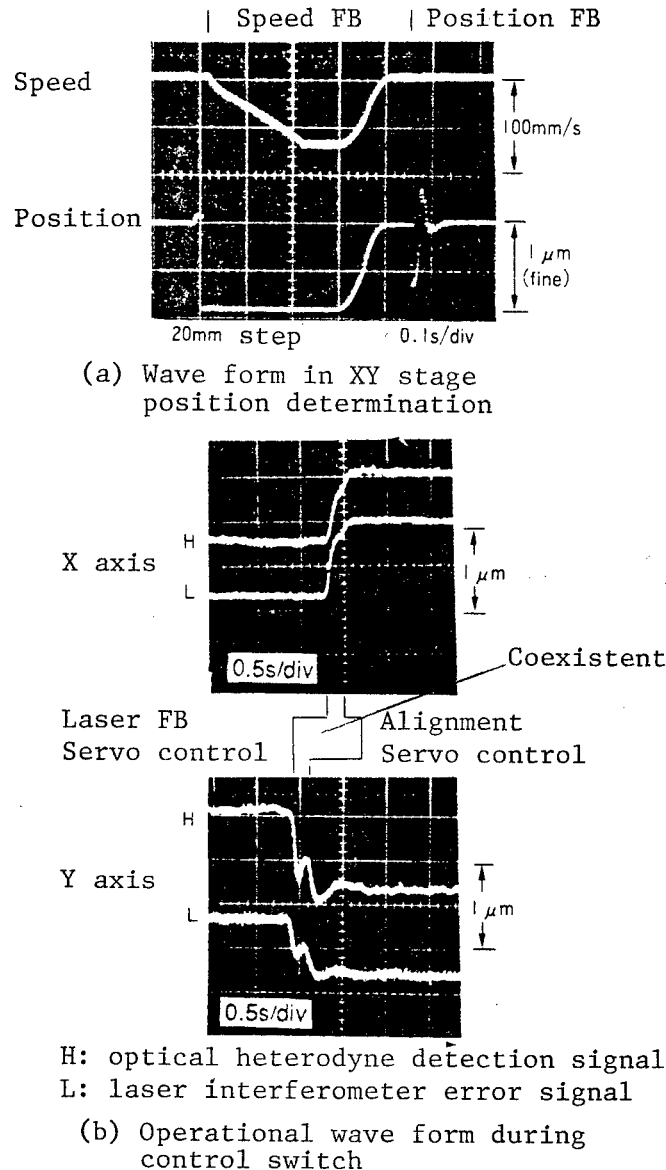


Figure 6. Operational Properties of a SOR-Use X-Ray Stepper

Figure 7 (b) shows the position alignment accuracy we sought by carrying out SOR exposure using the same mask through piling up two layers, wherein the position alignment points of diffraction lattice marks are shifted by one pitch, to remove the error factors except for the exposure equipment, such as the aforementioned mask errors, and by measuring the relative position of a replicated pattern. This shows the overlay accuracy between two SOR exposures, and clearly indicates the position alignment accuracy of the equipment itself. The illustration shows that the position alignment accuracy of the equipment is satisfactory, with the average value of position divergence being 50 nm or less and the dispersion being ± 80 nm (3σ value) or less. However, the results of these exposure experiments were obtained only in a state where resist was applied on a silicon wafer, so it

is necessary to promote accuracy evaluation in the future in the case of applying the experiments to an actual LSI manufacturing process.

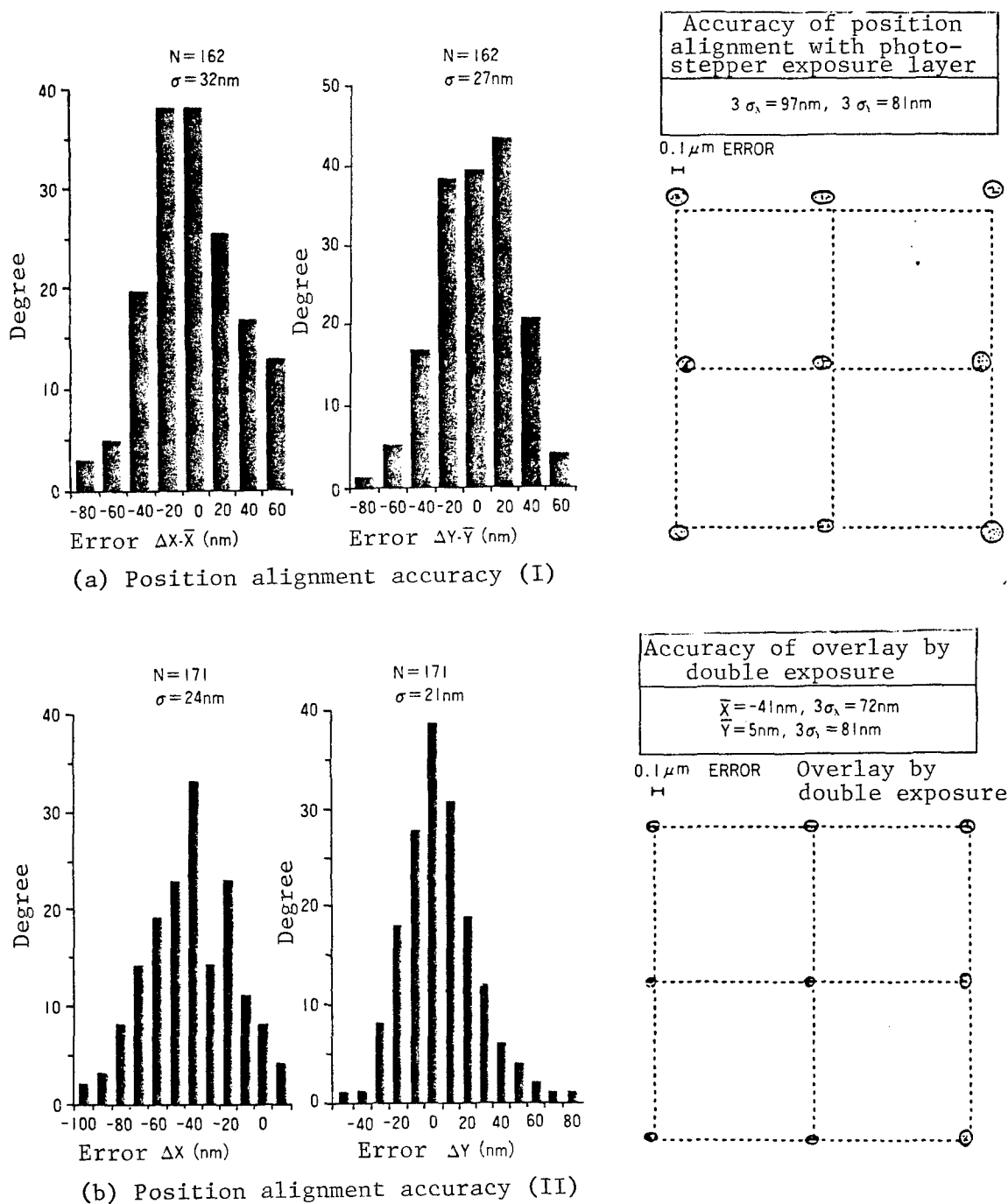


Figure 7. Position Alignment Accuracy of SOR-Use X-Ray Stepper

5. Conclusion

To make it possible to apply SOR exposure to superfine pattern replication in the future, we pursued the research and development of vertical X-ray exposure equipment having high-precision position alignment performance. The results obtained are as follows:

- (1) As the most important element technology to enhance the performance of exposure equipment, we have developed an optical-heterodyne interference position inspection method marked with air bearing lead screws to realize high-precision XY stages and with diffraction lattices.
- (2) We trial-manufactured a SOR-use X-ray stepper combining these element techniques, and evaluated its performance through exposure experiments; as a result, we obtained a position alignment accuracy of $\pm 0.1 \mu\text{m}$.
- (3) From these results it has become clear that the technology thus developed involves useful performance for the creation of SOR-use exposure equipment applicable to the quarter-micron region.

We are scheduled to promote the application of this technology to actual LSI manufacturing, evaluate its process applicability, and work to improve the reliability of the equipment.

Acknowledgement

We would like to express our thanks to Dr. Hisakazu Mukai, former director of the LSI Laboratories, and former chief researcher Toyoki Kitayama of the same laboratories, for giving us guidance and encouragement from beginning to end, and to chief researcher Fukuda and senior researcher Omata of the laboratories for taking charge of equipment tests and so forth together with us.

Profiles of the Authors

Sunao Ishihara, chief researcher of the LSI Laboratories, joined NTT in 1973 and engaged mainly in research on X-ray exposure. He is now engaged in the development of SOR-use exposure equipment.

He finished the precision engineering course of the Tokyo University engineering department in 1971, and in 1973 finished the master's course in the engineering study department of the same university.

He is a member of the Society of Precision Engineering, the Society of Applied Physics, and the Society of Electronic Communications.

He was awarded the 17th (fiscal 1982) prize of the Association for the Promotion of Machinery.

Atsunobu Une, chief researcher of the LSI Laboratories, joined NTT in 1971 and engaged in research on high-precision plane processing by isolated ground

grains research and practical use of an automatic programming system for NC machine tools, and development of X-ray exposure equipment. He is now engaged in research on position measurements of SOR-use aligners and so forth.

He finished the precision engineering course of Osaka University's engineering department in 1969, and finished the master's course of the same university's engineering research department in 1971. He received a doctorate in engineering (Osaka University) in 1985.

He is a member of the Society of Electronic Information and Communications, the Society of Applied Physics, and the Society of Precision Engineering.

He was awarded a thesis prize from the Society of Precision Engineering in 1983.

Munenori Kanai, chief researcher of the LSI Laboratories, joined NTT in 1963 and engaged mainly in mechanism designing. He is now engaged in the development of SOR-use position alignment mechanism.

He finished the second course of machine engineering of Kogakuin University in 1971.

He is a member of the Society of Precision Engineering.

He was awarded the 17th (fiscal 1982) prize of the Association for the Promotion of Machinery, and the fiscal 1987 thesis prize of the Society of Precision Engineering.

Masanori Suzuki, chief researcher of the LSI Laboratories, joined NTT in 1977 and engaged in research on fine patterning technologies by electron beam exposure, optical exposure, and X-ray exposure. Currently he is engaged in research and practical use of position alignment equipment for X-ray exposure.

He finished the electronic engineering course of Shizuoka University's engineering department in 1975, and finished the master's course in electronic engineering at the same university's graduate school in 1977.

He is a member of the Society of Applied Physics and the Society of Electronic Information and Communications.

References

1. S. Ishihara, T. Kitayama, and H. Yoshihara, X-Ray Lithography for Quarter-Micron Structures, Extended Abstract of 1st Micro Process Conf., Tokyo (1988) 72.
2. J. P. Silverman, et al., Fabrication of Fully Scaled 0.5- μm n-Type Metal-Oxide Semiconductor Test Devices Using Synchrotron X-Ray Lithography, J. Vac. Sci. Technol. B6(6), Nov/Dec (1988) 2147.

3. E. Kouno, Y. Tanaka, J. Iwata, Y. Tasai, and E. Kakimoto, An X-Ray Stepper for Synchrotron Radiation Lithography, J. Vac. Sci. Technol. B6(6), Nov/Dec (1988) 2135.
4. E. Cullmann and K. Cooper, Experimental Results With a Scanning Stepper for Synchrotron-Based X-Ray Lithography, J. Vac. Sci. Technol. B6(6), Nov/Dec (1988) 2132.
5. S. Ishihara, M. Kanai, A. Une, and M. Suzuki, A Vertical Stepper for Synchrotron X-Ray Lithography, J. Vac. Sci. Technol. B7(6), Nov/Dec (1989) 1652.
6. M. Suzuki, T. Kaneko, and Y. Saitoh, Replicated Resist Pattern Resolution With Synchrotron Orbital Radiation, J. Vac. Sci. Technol. B7(1), Jan/Feb (1989), 47.
7. T. Kaneko, M. Suzuki, A. Ozawa, and T. Ohkubo, Measurement of Mask Temperature Rise and Distortion in SR Lithography, Extended Abstract of the 17th Conf. on SSDM, Tokyo (1985) 353.
8. Kanai and Ishihara, Development of Ceramic Air Bearing Screws, (I), (II), and (III), a collection of theses for the fiscal 1987 autumn speech meeting of the Society of Precision Engineering, 595.
9. M. Suzuki and A. Une, An Optical-Heterodyne Alignment Technique for Quarter-Micron X-Ray Lithography, J. Vac. Sci. Technol. B7(6) 1971.

X-Ray Mask

916C3800F Tokyo NTT R&D in Japanese Vol 39 No 4, 10 Apr 90 pp 591-600

[Paper by Hideo Yoshihara, Shigehisa Oki, Masatoshi Oda, and Masami Kakuchi, NTT LSI Laboratories]

[Text] Preface

This paper describes processes to fabricate X-ray masks that have SiN as a membrane and Ta as an absorber, and the processing characteristics in each process. Noting that it is possible to mass-produce X-ray masks with a simple process using semiconductor manufacturing equipment, we adopted here the process of thinning a mask membrane after forming a Ta absorber pattern. Until now, it has been said that a high-precision mask is hard to obtain by this process because the Si frame is deformed. However, we have clarified that a high-precision mask can be produced by sufficiently controlling the stress of the Ta absorber and securing the hardness of the Si frame.

[English abstract reprinted from original] This paper describes the fabrication of a Ta/SiN structure x-mask. In this process, bulk Si etching is performed to produce a thin SiN membrane after Ta pattern fabrication. The process is very simple and can be performed using common LSI fabrication apparatus without many modifications. The X-ray masks have high pattern position accuracy due to the accurate stress control technology for the SiN and Ta films, and the use of thick Si wafers.

1. Introduction

Among the important techniques in X-ray exposure technology, there is an X-ray mask technique. The X-ray mask consists of a mask membrane (hereinafter referred to as a membrane) that efficiently transmits soft X-rays and an absorber that fully absorbs these rays. The membrane is made of a material consisting of light elements several microns thick, and therefore transmits soft X-rays having a wavelength of about 8 Å. For the absorber, it was necessary to use a heavy metal about 1 µm thick in order to fully intercept the transmission of soft X-rays. Thus, the fabrication of a comparatively thick, heavy metal pattern on a thin membrane required development of an entirely new technique, one that had not been used for conventional photomasks. Therefore, research on individual techniques for

the fabrication of absorbers was actively carried out, and reports on fabrication of membranes and absorbers were made. Recently, techniques for the manufacture of X-ray masks have made rapid progress, and energetic research on the accuracy and radiation resistance of X-ray masks and the rise in temperature during exposure have been carried out. IBM,¹ IMT,² and so forth have reported results predicting that high-precision masks for practical use will be mass-produced in the near future.

The items that should be met by a membrane include the following:

- (1) It must satisfactorily transmit soft X-rays and must not deteriorate.
- (2) It must have no warp, and its surface must be smooth.
- (3) It must have large mechanical strength.
- (4) To facilitate optical alignment, it must be highly transparent to visible light.

Transparent, large-caliber membranes can be easily obtained from high-polymer materials represented by polyimide³ and Mylar TM⁴ (trade mark for polyethylene terephthalate). However, they have such disadvantages as being inferior in X-ray resistance, resistivity to chemicals, and size stability. Therefore, their accuracy and so forth present a problem when they are to be used for submicron pattern replication. On the other hand, such inorganic materials as Si,⁵ SiC,⁶ and Si₃N₄⁷ are superior in size stability, resistivity to chemicals, and so forth. At the initial stage of research and development, however, it was difficult to produce masks using these materials because of great difficulties in fabrication.

The items that should be met by an absorber include the following:

- (1) It must have great X-ray absorbing power.
- (2) Its internal stress must be low enough to prevent distortion of a membrane.
- (3) It must make it possible to process submicron patterns with high accuracy.

Au,⁸ which can be used as an absorber material through an electroplating method, was explored earlier, but Ta^{9,10} and W,¹¹ which make it possible to form fine patterns by dry etching, have recently come to be studied energetically.

We proposed X-ray masks using SiN as a membrane material and Ta as an absorber material, and have been making constant studies to put them into practical use.^{9,12,13}

Here we will explain various processing conditions in manufacturing X-ray masks, and then describe membranes, the relationship between the stress of

an absorber and pattern accuracy, and the characteristics of pattern formation when a Ta absorber is used.

2. X-Ray Mask Manufacturing Process

Figure 1 shows the X-ray mask manufacturing process that we developed. A SiN film 2 μm thick that serves as a membrane is formed by a pressure-reduced CVD [chemical vapor deposition] method on a 3-inch Si wafer 1 mm thick. On this film, Ta films each measuring about 0.8 μm in thickness are piled up by a high-frequency sputtering method. Furthermore, SiO_2 , which forms a Ta etching mask, is accumulated on this pile by an ECR [electronic cyclotron resonance] plasma CVD method, and thus mask blanks are fabricated. A resist pattern is formed on the mask blanks through EB [electron beam] drawing and, with this resist pattern as a mask, the SiO_2 film is etched by the reactive ion etching process. As the next step, the Ta film is etched, using the SiO_2 pattern as an etching mask. A window is formed in the SiN in the rear of the Si wafer, and the Si is removed to turn the SiN on the surface into a membrane (this is hereinafter referred to as back etch). A glass frame is then bonded, and the mask is completed.

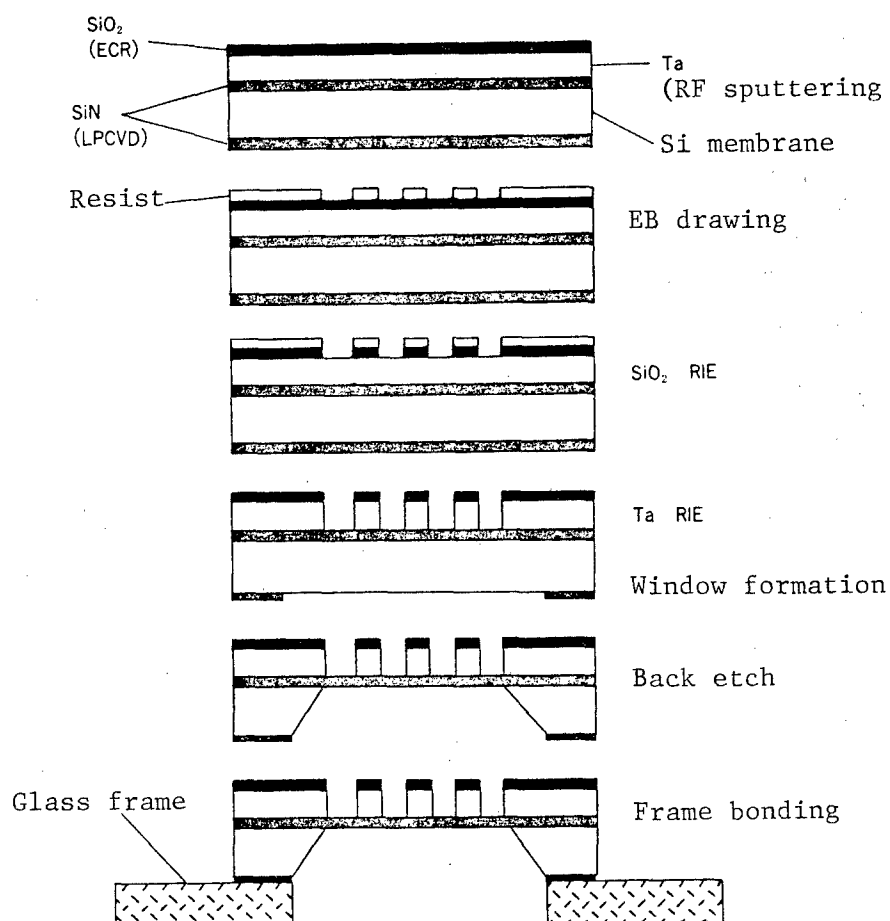


Figure 1. An X-Ray Mask Manufacturing Process

Figure 1 shows the process of back etch after formation of an absorber pattern is adopted. During back etch, however, there has been a case of a membrane's breaking or a Si frame's being deformed and bringing about a marked divergence of the pattern position. Therefore, a method has been studied to form absorber patterns after producing membranes. However, because of the long process in handling a test sample having a membrane region, this method has a strong possibility of the sample breaking during the process, thus requiring a special contrivance for the equipment. From the viewpoint of developing a technique for mass production of masks, we did the back etch after formation of an absorber pattern, attaching importance to the advantage that this process is simple and makes it possible to use semiconductor manufacturing equipment with only partial readjustment. To minimize the breakage and deformation of membranes and to ensure pattern accuracy, we developed a technique to control the stress on membranes and absorber films by such contrivances as increasing the Si thickness to make the Si frame harder.

The internal stress of a SiN film fabricated by the CVD method largely depends on gas composition and the temperature for film fabrication. Figure 2 shows the relationship between the stress and the gas ratio when the temperature for film fabrication is used as a parameter. The SiN film used for manufacturing integrated circuits is ordinarily formed with the $\text{SiH}_2\text{Cl}_2/\text{NH}_3$ ratio below 1. However, it cracks when a high tensile stress exists and causes the film to become thicker. The effective way to reduce the stress in the SiN film is by raising the SiH_2Cl_2 ratio and increasing the Si content in the film. However, raising the SiH_2Cl_2 ratio only will cause both an increase in the refractive index of the SiN and a drop in visible light transparency. On the other hand, when the temperature for film formation is raised, stress can be reduced without lowering the visible light transparency. We raised the film formation temperature within the limit wherein the equipment operated stably, and at the same time controlled the stress by increasing the SiH_2Cl_2 ratio. As a result, we were able to form a SiN film 2 μm thick with a transmissibility of 80 percent or higher, with the stress scope necessary for a membrane ranging over 5 to 10×10^8 dyn/cm^2 , for the 6,328 \AA wavelength of the He-Ne laser used for alignment. This membrane is very stable both chemically and thermally, and does not deteriorate even when it absorbs 2 MJ/cm^2 X-rays. For this reason, it can be regarded as an extremely superior membrane.

When Ta, a metal with a high melting point, is formed into a film by ordinary methods such as deposition or sputtering, it involves a high stress. Figure 3 shows the relationship between gas pressure during high-frequency sputtering and stress. In this illustration, the gas pressure that causes the internal stress of the film to become zero exists at two places--on the high gas pressure side and on the low gas pressure side. On the high gas pressure side, the density of the film is 10 to 20 percent lower than the bulk value, and its X-ray absorption coefficient is low; therefore it is not suitable as an absorber. On the low gas pressure side, on the other hand, the density of the film is high, and it is suitable as an absorber. To obtain a Ta film with low stress, it is necessary to control the gas pressure very precisely, as is clear from the illustration. Therefore, we developed a sputtering apparatus that can precisely control gas pressure during the

sputtering process. Figure 4 shows an example of the results of stress measurement. The average value of the measurement is 0.47×10^8 dyn/cm², and the standard deviation is 1.96×10^8 dyn/cm². Thus, it has become possible to consistently obtain low-stress Ta films with this equipment.

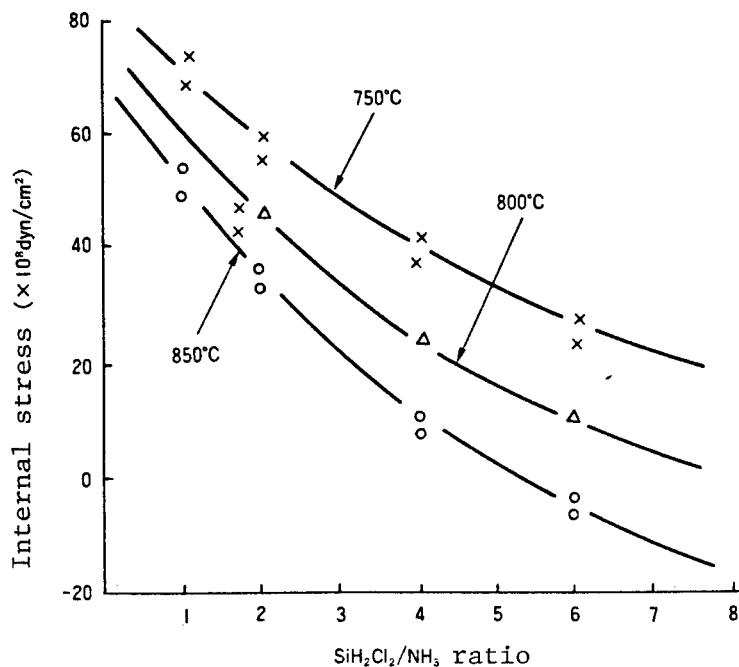


Figure 2. Relationship Between the Ratio of Gas Composition and Internal Stress During SiN Film Formation

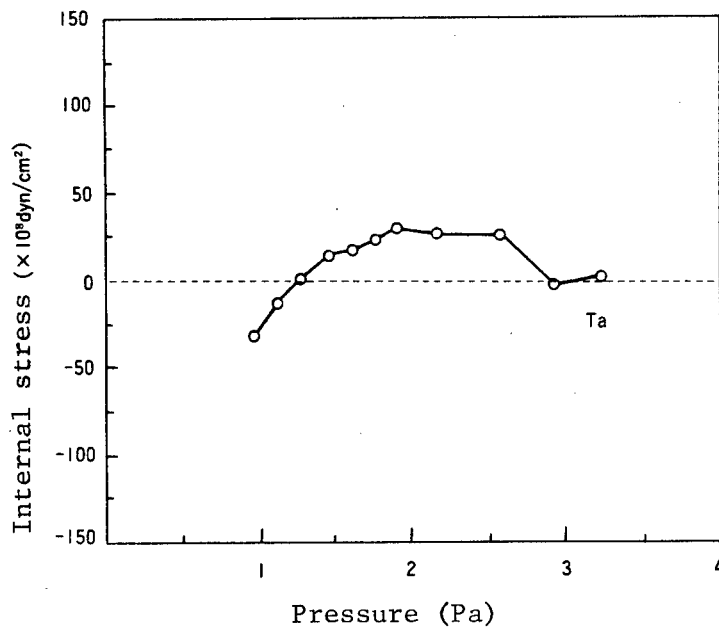


Figure 3. Relationship Between the Pressure and the Internal Stress During Film Fabrication

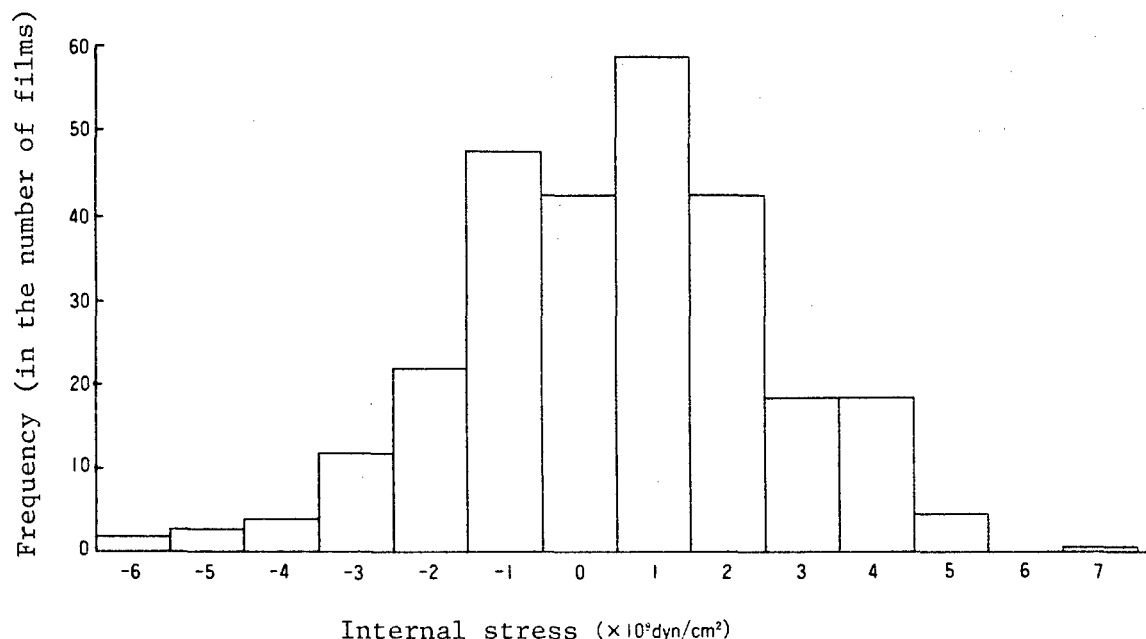


Figure 4. Reproducibility of Internal Stress of Ta

What is important next is the pattern formation process by electron beam drawing. In the case of an X-ray mask, it has the following characteristics:

- (1) Because X-ray exposure is accomplished through projection at the same ratio, the size and position of a pattern to be drawn on the mask need to be more accurate than in the case of a photomask.
- (2) Because Ta, a heavy metal, is present in the substrate, many reflection electrons are generated, which makes the proximity effect greater.
- (3) Because the substrate is uniform, the process can be easily made correspondent with theoretical analysis.
- (4) Compared with direct drawing on the wafer, the throughput can be more than 10 percent lower.

Therefore, this process requires a pattern generation technique different from photomask drawing or direct drawing on the wafer. Figure 5 shows the sensitivity curves of a resist in the case of employing a membrane that uses a Si substrate and a Ta absorber. The membrane with Ta attached is strongly influenced by the rear scattering of electrons in comparison with the Si substrate, and therefore the sensitivity of the resist is several times higher. Because the influence of the rear scattering is thus conspicuous, it is essential to revise the proximity effect in the case of drawing a complex, large-scale pattern. We are currently using a size of $0.1 \mu\text{m}$ as a minimum pattern width by adopting the proximity effect revising method that has been independently developed by NTT. We have also obtained a pattern position accuracy of $\pm 0.08 \mu\text{m}$ (three times the standard deviation) by

contriving a method of pattern generation in a state in which the fluctuation of beams is slight.

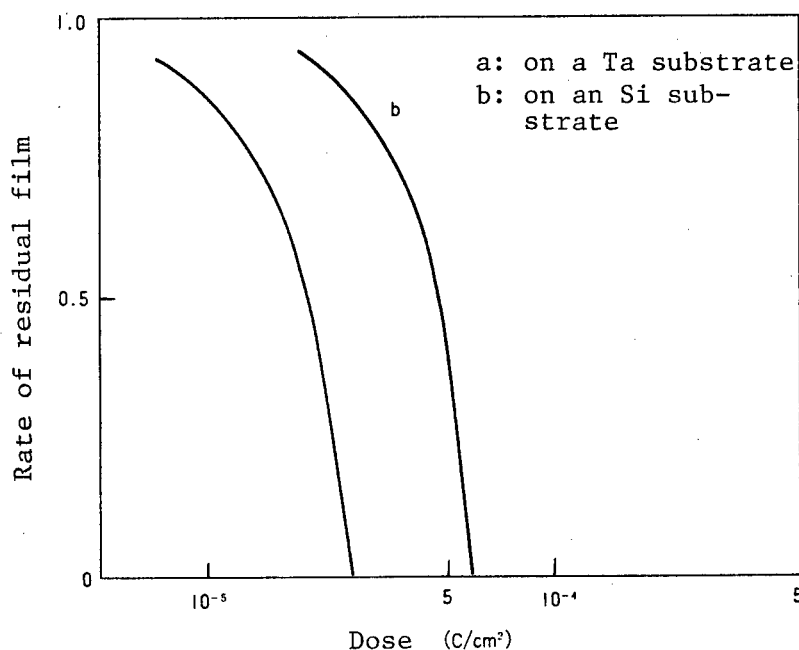


Figure 5. Sensitivity Curves of Electron Beam Resist

Next, a pattern is formed on the Ta film by dry etching using the EB-drawn resist pattern as a mask. We investigated various kinds of etching gas, and used CBrF_3 reactive ion etching which caused the least undercut. However, this Ta etching involved the problem that the etching selective rate between the Ta and the resist is not high. Figure 6 shows the relationship between the etching speed of various materials and power. The etching selective rate between the resist (PMMA) and Ta is as low as less than 2. Therefore, we provided a SiO_2 film as an intermediate etching layer. In the current situation, the reactive ion etching of a SiO_2 film can safely be regarded as the most stable technology. The etching selective rate at 50 W between Ta and SiO_2 , shown in Figure 6, is close to 7. Therefore, when a thin SiO_2 film is etched by using a resist pattern as a mask, and when Ta is etched by using the etched SiO_2 as a mask, it is possible to form a Ta submicron pattern having a steep side-wall.

After a Ta absorber pattern is formed, it is turned into a membrane by removing the Si in the needless part, and then bonding a glass frame to it. In the process of bonding the glass frame, care must be taken to prevent position distortion.

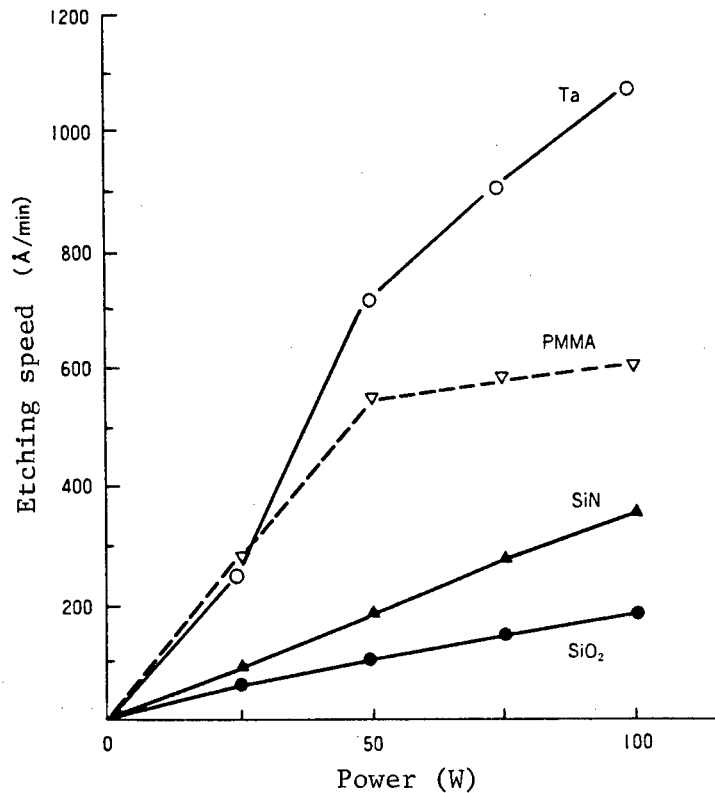


Figure 6. Characteristics of Reactive Ion Etch Using CBrF_3

3. Characteristics of the X-Ray Mask

In the process for our mask fabrication, back etch is done after patterning. Therefore, to ensure the accuracy of the pattern position, it is necessary to precisely control the stress of a Ta absorber. However, the relationship between the stress and pattern strain has hardly been analyzed correctly. Here we will describe the results¹³ of our studies using the boundary element method, concerning the following points:

- (1) Change in a pattern position resulting from a membrane stress' distorting a Si frame on the occasion of a Si back etch.
- (2) Change in a pattern position due to the stress of a Ta absorber.

The boundary element method divides the boundary or the surface of a structure into small elements and gives boundary conditions to each of them, thereby calculating the displacement and stress of each element. Here we regarded the membrane region as consisting of SiN and the Si frame region as forming a Ta/SiN/Si/SiN structure, and made calculations regarding the sum total of the stress of each film as a boundary condition at each boundary. Figure 7 shows the relationship between the product of stress and the thickness of the SiN membrane and the degree of position change. The solid line represents the result of the calculations and the black circles indicate the experimental results. The size of the window was fixed

at 19 mm x 19 mm, the thickness of the Ta absorber at 0.95 μm , and the stress at $3 \times 10^8 \text{ dyn/cm}^2$. For the position of the measurement point, we chose a place just inside the window, where the degree of change was considered the highest. The illustration shows that the results of the experiments agree comparatively well with those of the calculations. The dashed line shows the calculation result that there is no Ta on the surface of the Si frame. This corresponds with the membrane strain by the SiN stress. In the case of using a membrane 2 μm thick, the stress needs to be fixed at $5 \times 10^8 \text{ dyn/cm}^2$ or lower to limit the degree of pattern change to 0.04 μm or less. This calculation was made by estimating the thickness of the Si frame at 1 mm. If the thickness is 2 mm, the degree of the change will be 50 percent.

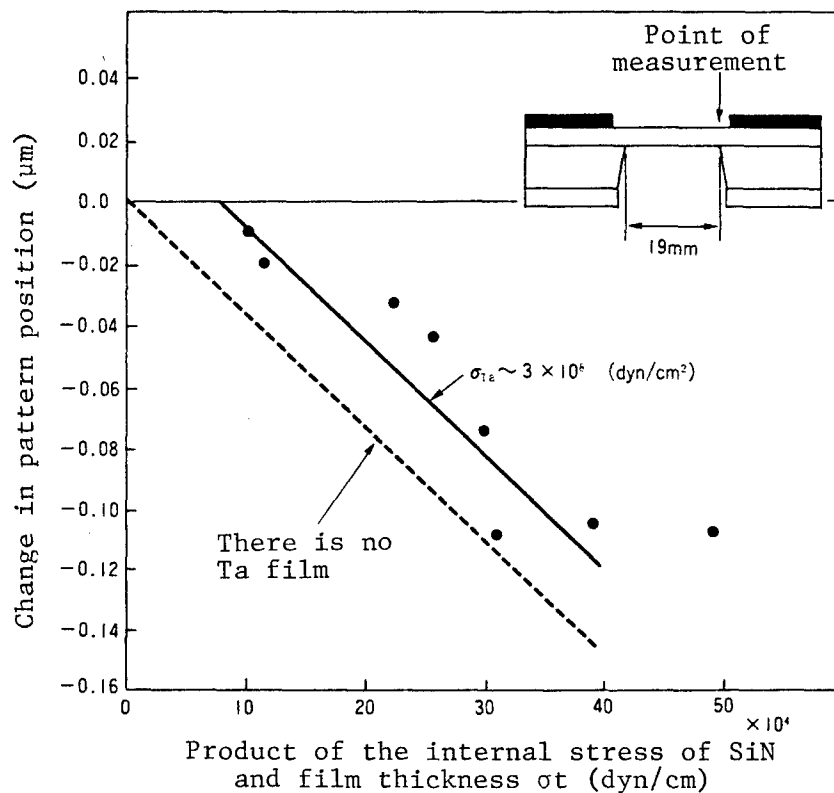


Figure 7. Relationship Between the Internal Stress of SiN and Change in Pattern Position

Figure 8 shows the relationship between the degree of position change when there is Ta to the extent of 1 mm inside the window and the Ta stress. Here the thickness and stress of the SiN membrane are fixed at 2 μm and $5 \times 10^8 \text{ dyn/cm}^2$, respectively, and the size of the window is fixed at 23 mm x 23 mm. The solid line represents the calculation result, and the black circles show the experimental results. The two agree with each other comparatively well. Even when there is no Ta stress, a position change due to the SiN stress amounts to about 0.07 μm , as seen in Figure 7. Therefore, a highly precise mask can be obtained when there is a Ta stress amounting to $3 \times 10^8 \text{ dyn/cm}^2$. Further, this suggests that an increase in Ta stress brings about a rapid, large change in pattern position.

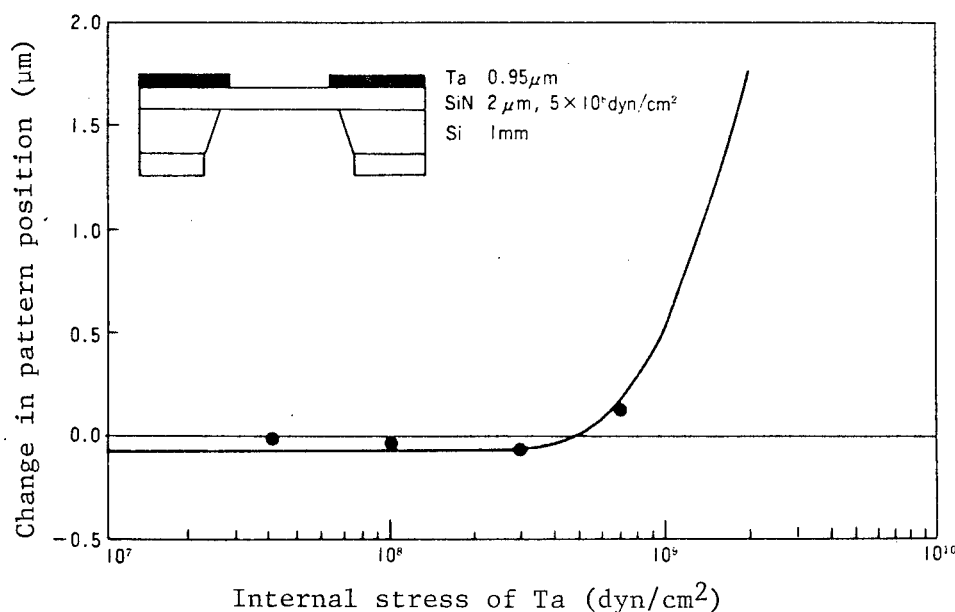


Figure 8. Relationship Between the Internal Stress of Ta and Change in Pattern Position

As mentioned above, high-precision masks can be obtained even in the process of back etch after pattern formation, if the stress of Ta and that of a SiN membrane are counterbalanced through consideration of the hardness of a Si frame.

Figure 9 shows a sectional SEM photo of a Ta absorber pattern, indicating that a 0.1 μm line and space pattern is obtainable. From this, it has become clear that this mask process makes it possible to obtain resolution to the extent of 0.1 μm .

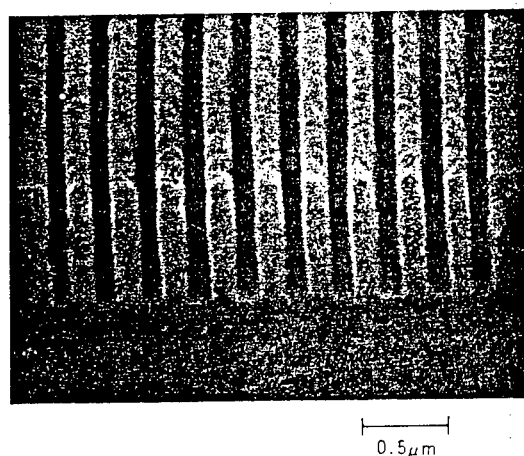


Figure 9. Absorber Pattern

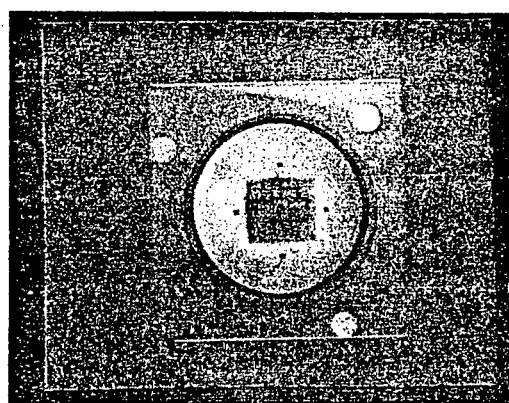


Figure 10. X-Ray Mask

Figure 10 shows the external appearance of a final form of the mask, with a glass frame attached. The size of the glass frame is 10 cm x 10 cm, and the thickness is 4 to 5 mm. Because of this glass frame, the operability of masks of this kind, including automatic conveyance, has improved greatly.

4. Conclusion

We chose SiN as a membrane material and Ta as an absorber material, and created a mask manufacturing process on the premise of this choice of materials. This process is characterized by etching after patterning, followed by the bonding of a glass frame. With this process, a problem has been pointed out that it is difficult to obtain a high-precision mask because the stress of the SiN membrane and the Ta absorber deforms the mask during back etch. In this report, however, we have clarified that a high-precision mask can be obtained if the stress of the SiN membrane and Ta absorber is appropriately controlled. We have also confirmed that a 0.1 μm Ta absorber pattern can be formed by using a SiO₂ pattern for the etching mask.

To apply the mask manufacturing process to a 0.2 μm -level device, for which the SOR lithography is thought to exert its influence most greatly, it is essential to develop EB equipment exclusively used for mask drawing, length measuring equipment, defects inspection equipment, and so forth, in parallel with improvement of the mask manufacturing process.

Acknowledgement

We deeply thank Dr. Hisakazu Mukai, former director of the LSI Laboratories, and Dr. Toyoki Kitayama, former chief researcher of the same Laboratories, for giving us guidance in carrying out this research. In addition, we thank Matsuda of the LSI Laboratories fine patterning research division and chief researcher Tamamura of the optoelectronics laboratory for promoting useful discussions on EB drawing, and chief researchers Okubo and Ozawa of the LSI Laboratories for taking charge of experiments in the formation of SiN membranes and Ta absorbers.

Profiles of the Authors

Hideo Yoshihara, chief researcher and the third project team leader of the LSI Laboratories, joined NTT in 1968 and engaged in research on surface treatment and on thin film formation using plasma. Since 1976 he has been carrying out research on X-ray exposure.

He finished the metal engineering course of the engineering department, Yokohama National University, in 1966, and finished the master's course in metal engineering at the same university in 1968. He received a doctorate in engineering from Hokkaido University in 1983.

He is a member of the Society of Applied Physics and the Society of Electronic Information and Communications.

In 1982 he was awarded the 17th prize by the Association for the Promotion of Machinery.

Shigehisa Oki, chief researcher of the LSI Laboratories, joined NTT in 1982 and engaged in research on the technology for superfine pattern fabrication by dry etching, and on the enhancement of the precision of X-ray masks. Currently he is carrying out research on the formation of high-precision X-ray mask patterns by electron beam drawing equipment.

He graduated from the electronic equipment engineering department of the Technological University of Nagaoka in 1980, and in 1982 finished the master's course in electronic equipment engineering at that same university's graduate school.

He is a member of the Society of Physics and the Society of Applied Physics.

Masatoshi Oda, chief researcher of the LSI Laboratories, joined NTT in 1976 and engaged chiefly in research on microprocessing in MOS device manufacture. He is currently carrying out research on X-ray mask manufacturing technology.

In 1974 he finished the electronic engineering course of the engineering department, Nagoya Institute of Technology, and in 1976 finished the master's course in electronic engineering at the same institute.

He is a member of the Society of Applied Physics.

Masami Kakuchi, chief researcher of the LSI Laboratories, joined NTT in 1972 and engaged in development of X-ray and electron beam resist materials and in research on nanometer processing and X-ray optical devices. He is currently engaged in development of techniques for EB drawing for X-ray masks.

He finished the course of applied physics of the Hokkaido University engineering department in 1970, and finished the master's course in applied physics of the same university's graduate school in 1972.

He is a member of the Society of Applied Physics and the Society of Radiation Optics.

References

1. R. Viswanathan, R. Acosta, D. Seeger, H. Voelker, A. D. Wilson, I. Babich, J. Maldonado, J. Warlaumont, O. Vlandirmirsky, F. Hohn, D. Crockkatt, and R. Fair, Fully Scaled 0.5 μm MOS Circuits by Synchrotron Radiation X-Ray Lithography: Mask Fabrication and Characterization, *Microelectric Engineering*, 9, 93 (1989).
2. S. Pongratz, U. Meschder, Ch. Ehrlich, H. L. Huber, K. Kohlmann, and W. Windbracks, State of the Art of Pattern Placement Accuracy of Silicon X-Ray Master Masks, *Microelectric Engineering*, 9, 117 (1989).

3. D. C. Flanders and H. I. Smith, Polyimide Membrane X-Ray Lithography Masks--Fabrication and Distortion Measurements, J. Vac. Sci. and Technol., 15, 995 (1978).
4. E. Spiller, R. Feder, J. Topalin, E. Castellani, L. Romankiw, and M. Heritage, X-Ray Lithography for Devices, Solid State Technol., 19, 62 (1976).
5. C. J. Schmidt, P. V. Lenzo, and E. G. Spencer, Preparation of Thin Windows in Silicon Masks for X-Ray Lithography, J. Appl. Phys., 46, 4080 (1975).
6. R. K. Watts, X-Ray Lithography, Solid State Technol., 22, 68 (1979).
7. E. Bassous, R. Feder, E. Spiller, and J. Topalian, High Transmission X-Ray Masks for Lithographic Applications, 19, 55 (1976).
8. D. Hofer, J. Powers, and W. D. Grobman, X-Ray Lithographic Patterning of Magnetic Bubble Circuits With Submicron Dimensions, J. Vac. Sci. Technol., 16, 1968 (1979).
9. M. Sekimoto, H. Yoshihara, and T. Ohkubo, Silicon Nitride Single-Layer X-Ray Mask, J. Vac. Sci. Technol., 21, 1017 (1982).
10. M. Yamada, M. Nakaishi, J. Kudou, T. Eshita, and Y. Furumura, An X-Ray Mask Using Ta and Heteroepitaxially Grown SiC, Microelectric Engineering, 9, 135 (1989).
11. H. Luthje, M. Harms, B. Matthiessen, and A. Bruns, X-Ray Lithography: Novel Fabrication Process for SiC/W Stepper-Masks, Jpn. J. Appl. Phys., 28, 2342 (1989).
12. M. Sekimoto, A. Ozawa, T. Ohkubo, and H. Yoshihara, A High Contrast Submicron X-Ray Mask With Ta Absorber Patterns, Extended Abstracts 16th Int. Conf. Solid State Device and Materials, Kobe, 1984, 23.
13. S. Ohki, M. Kakuchi, T. Matsuda, A. Ozawa, T. Ohkubo, M. Oda, and H. Yoshihara, Ta/SiN-Structure X-Ray Masks for Sub-Half-Micron LSIs, Jpn. J. Appl. Phys., 28, 2074 (1989).
14. K. Komatsu and S. Moriya, Pattern Data Processing Technology for Electron Beam Direct Writing, Proceedings of the 23rd Symposium on Semiconductors and Integrated Circuit, 1982, 84.

Resist Process for SOR Lithography

916C3800G Tokyo NTT R&D in Japanese Vol 39 No 4, 10 Apr 90 pp 601-608

[Paper by Kimiyoshi Deguchi, Toshiyuki Horiuchi, Akinobu Tanaka, and Akira Yoshikawa, NTT LSI Laboratories]

[Text] Preface

We attempted to apply SOR lithography to the exposure of all layers in trial-manufacturing a deep submicron MOSIC, and evaluated its applicability to device processes. As X-ray resists, we adopted high-sensitivity FBM-G and SPP, and carried out the formation of patterns of multilayer resist structure. The characteristics of pattern replication were satisfactory, and it was confirmed that the resolution was $0.2\ \mu\text{m}$. In addition, we showed quantitatively that the process margin for pattern size control was large. We also evaluated overlay accuracy through trial manufacture. However, the overall overlay error was about $0.1 \pm 0.6\ \mu\text{m}$ (3σ); therefore, the conditions for requirements for SOR lithography have not yet been satisfied. To improve the overlay accuracy, we analyzed error factors and have obtained improvement indices for the future.

[English abstract reprinted from original] The feasibility of SOR lithography for the fabrication of deep-submicrometer devices is investigated by test application to small-geometry MOS device processes at all exposure levels. Multi-layer resist systems are used to exploit the high sensitivity and high resolution features of both FBM-G and SPP resists. Patterns of $0.2\ \mu\text{m}$ are obtained with good accuracy. Excellent exposure latitude for linewidth control is confirmed. Overlay performance is also evaluated. The mean value and standard deviation of overall overlay errors are about $0.1 \pm 0.6\ \mu\text{m}$ (3σ). Since these values are not satisfactory, error factors are investigated to improve overlay accuracy.

1. Introduction

Electron beam lithography and X-ray lithography are most likely to replace optical lithography as the next-generation lithographic technologies. X-ray lithography can achieve a high degree of resolution, capable of easily replicating even a $0.2\ \mu\text{m}$ pattern. In addition, a package replication method using a mask is adopted for this lithography.¹ Therefore, it is

expected to become a lithography aimed at mass production in the next generation.

However, actual use of the X-ray lithography has so far been limited to the manufacture of small-scale test devices,²⁻⁶ and some problems are still left unresolved in introducing this lithography to the mass-production line for device manufacture. In particular, an insufficient processing capability (throughput) per unit hour is a strong factor obstructing the practical use of the X-ray lithography.

Use of SOR as an X-ray source with a high degree of brightness has so far been regarded as hopeful for improvement of throughput.⁷ However, introducing it into an LSI manufacturing line has hardly been practicable because of the overly large scale of the equipment. Recently, compact SOR equipment has been produced in various countries,⁸⁻¹² and the elimination of obstacles as to cost, floor space, and so forth, has also been making progress. Thus, use of SOR rays has become realistic, and it has become possible to anticipate the shortening of exposing time by one to two digits compared with conventional electron beam excitation type X-ray sources and plasma X-ray sources. Development of a resist for X-ray exposure has also become active, and high-sensitivity resists below the 50 mJ/cm² level are going to be marketed.^{13,14} With these trends put together, a throughput of tens of wafers per hour has come to be anticipated, and expectations for SOR lithography are growing. With this, applications of this lithography to LSI manufacture are also gradually being attempted.^{15,16}

We conducted basic studies on SOR lithography and trial-manufactured test devices, using the beam line of the photo factory of the High Energy Physical Research Institute, and thus confirmed their effectiveness.¹⁷ We applied SOR exposure to an Al wired layer for the trial manufacture of a deep submicron MOSIC, using the beam line¹⁹ that had been set up for an acceleration ring¹⁸ with the operation of the SOR ring of the NTT Atsugi Development Center, and obtained a favorable result.²⁰ On the basis of this result, we attempted to apply SOR lithography to five exposure layers. Through this trial manufacture, we evaluated the applicability of SOR lithography to a ULSI manufacturing line, and clarified the problems involved. In this paper we will describe the resist process and the characteristics of pattern formation. In addition, we will state the result of our evaluation of overlay accuracy, which is an important improvement item in SOR lithography, together with the problem of throughput.

2. Resist Process

The ideal point in choosing a resist is to use a single-layer resist that is superior in dry etching resistance, to give full play to its ability to replicate patterns to thick resists, which is a characteristic of X-ray exposure. However, because the stored current is low density due to the ring being in the course of a rise, and because a sufficient X-ray intensity was not obtainable, we gave top priority to high sensitivity as the standard for choosing the resist. Ensuring resolution and size controllability in a 0.2 μm region also are important standards for choice. Here we adopted a

high-sensitivity, high-resolution resist that was actually used for development by NTT, although it was inferior in tolerance to etching.

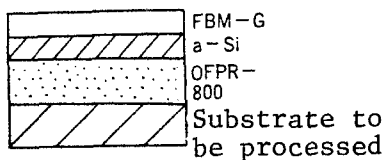
Structure of the exposure and resist layers are shown in Table 1. We applied FBM-G resist as the positive type and SPP resist as the negative type.^{21,22} To cope with the insufficient tolerance to etching, and to improve the characteristics of pattern formation on the step, we adopted a multilayer resist structure using the novolac resist OFPR-800 (Tokyo Ohka Kogyo Co., Ltd.) as the lower layer resist. The process for processing each kind of resist is given in Figure 1. The FBM-G resist was a three-layer resist structure, with a-Si as an intermediate layer. After etching the intermediate layer by the RIE [reactive ion etching] process using fluorine gas, with the FBM-G resist pattern as a mask, we formed the lower layer resist pattern by the RIE process using oxygen gas. The SPP resist was a two-layer structure because of its high tolerance to oxygen RIE. For the pattern replication we used an image reversal method to effect flat exposure by UV rays after X-ray exposure. With UV irradiation, the part not exposed to X-rays becomes highly soluble in an alkali development solution, whereas the solubility of the part exposed to X-rays becomes lower, and therefore this part shows the characteristics of the negative type. In both the resist processes, we cooled the substrate to -10°C to restrain the difference in pattern transformation to the utmost when etching the intermediate and lower layer resists.²³ Figure 2 shows a $0.4\text{ }\mu\text{m}$ contact hole layer using FBM-G and an example of forming the lower layer resist pattern for a $2\text{ }\mu\text{m}$ gate layer. In both cases, we obtained satisfactory pattern forms.

Table 1. Exposure Layer and Resist Structures

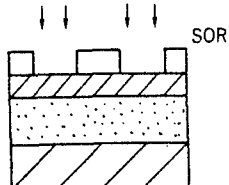
LOCOS classification	SPP 2-layer resist
Gate	SPP 2-layer resist
Source and drain contacts	FBM-G 3-layer resist
Gate contact	FMB-G 3-layer resist
Wiring	SPP 2-layer resist

Curves showing the exposure sensitivity of FBM-G and SPP resists are shown in Figure 3. Their sensitivity to X-rays is 80 mJ/cm^2 and 360 mJ/cm^2 , respectively. For the positive resist, exposure sensitivity was defined with the extent of exposure (D_0) that caused the residual resist film after development to become zero in the X-ray irradiation region; for the negative resist, it was defined with the extent of exposure (D_{50}) that caused the residual film to account for 50 percent of the coated film thickness. FBM-G has the highest exposure sensitivity among the current X-ray resists. The sensitivity of the SPP resist is one-fourth that of the FBM-G, but it is superior in resolution.

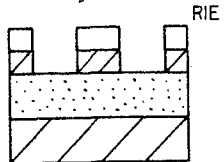
1) Three-layer resist structure



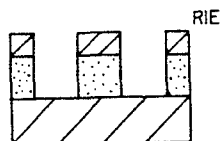
2) Exposure and development



3) Intermediate layer etching

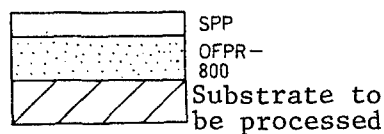


4) Lower-layer resist etching

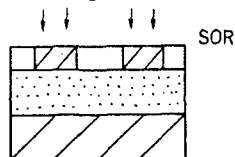


(a) FBM-G

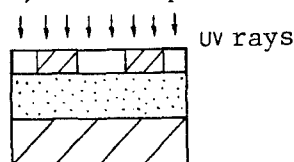
1) Two-layer resist structure



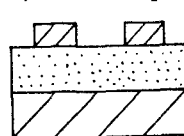
2) Exposure



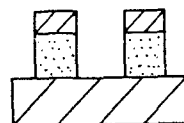
3) Flat exposure



4) Development

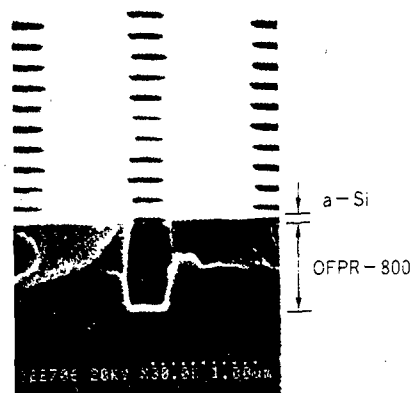


5) Lower-layer resist etching

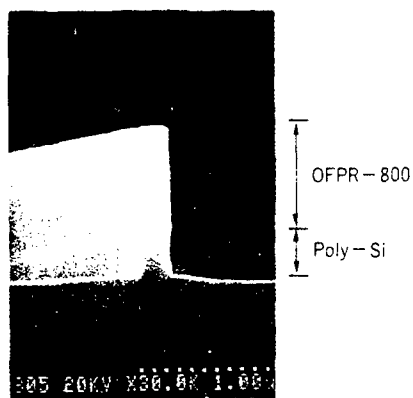


(b) SPP

Figure 1. Course of Resist Processing



a) Contact hole



b) Gate

Figure 2. Example of Pattern Formation

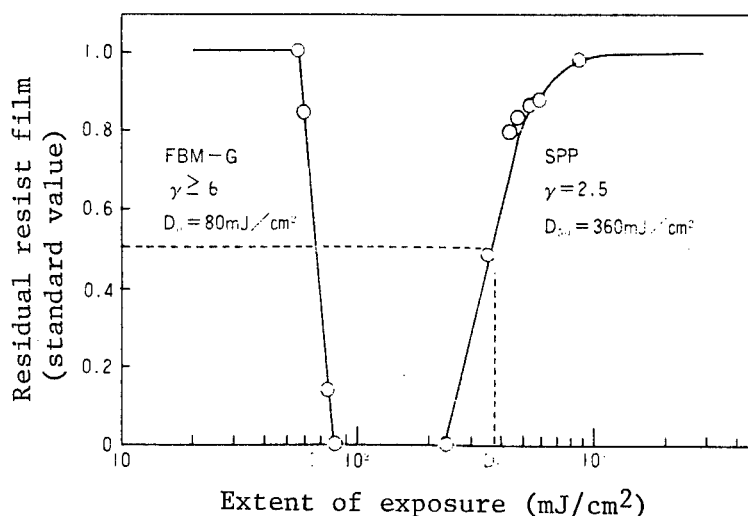


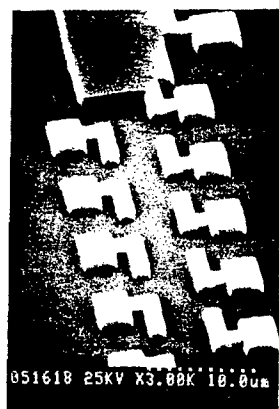
Figure 3. Curves Showing Exposure Sensitivity

3. Characteristics of Pattern Formation

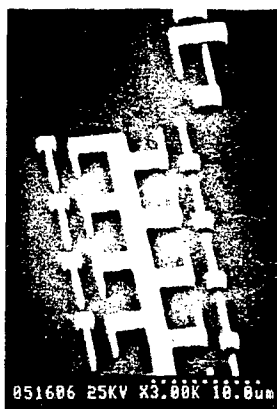
For SOR exposure we used a vertical X-ray stepper having the function of optical-heterodyne alignment.²⁴ The exposure was made so that the proximity gap was about 40 μm in atmosphere. The peak wavelength of X-rays was 0.85 nm, and their intensity was 0.09 mW/cm²/mA (stored current) on the wafer surface after mask transmission. The X-ray mask was made up of a SiN membrane 2 μm thick, a Ta absorber 0.65 μm thick, an Si substrate 1 mm thick, and a frame.²⁵

An example of resist pattern formation in all five exposure layers is given in Figure 4. The smallest pattern size is 0.2 μm in gate length, 0.4 μm in contact hole diameter, and 0.4 μm in wiring width. The pattern resolution was satisfactory in all cases, and the effectiveness of pattern formation in the deep submicron region was confirmed. The relationship between the extent of exposure and the size of the replicated pattern is shown in Figure 5. In light of the small change in pattern size due to the change in the extent of exposure, it is understood that the process margin for a change in the extent of exposure is large in the case of SOR exposure. The change in resist pattern size involved in the change in the extent of exposure is chiefly due to the horizontal spread of the light or Auger electrons released in the resist by X-ray irradiation, as well as to the dullness of the X-ray intensity profile at the pattern edge, arising from Fresnel diffraction. Detailed replication characteristics, such as linearity for mask size, are subjects for future study.

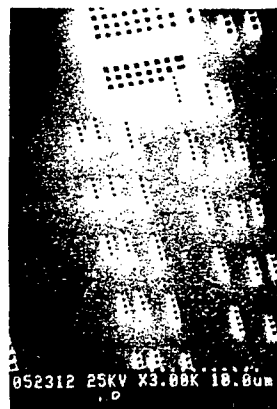
The size controllability in an independent pattern is shown in Figure 6. We evaluated it during formation of the gate layer pattern. The vertical axis is the tolerance limit of change in the extent of exposure to restrict the change in the replicated pattern size to less than ± 10 percent. The characteristics of an i-ray stepper, with the NA for optical lithography standing at 0.42, are also shown by way of comparison. In both cases of SOR



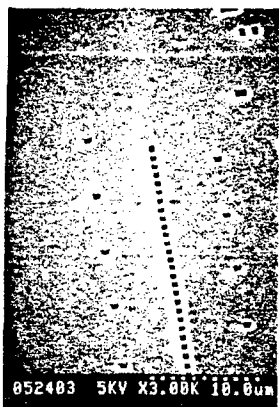
Separation



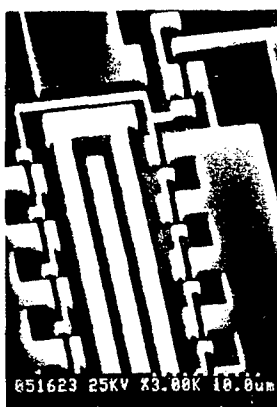
Gate



Source/drain contact



Gate contact



Al wiring

Figure 4. Example of Resist Pattern Formation

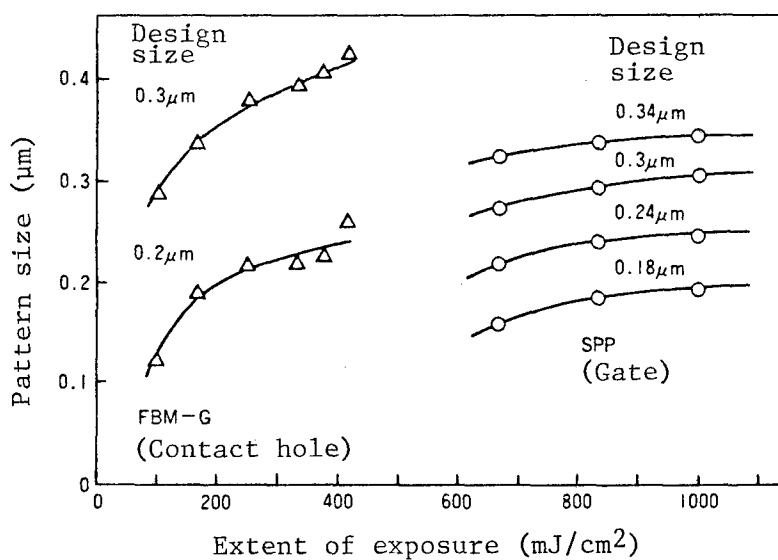


Figure 5. Dependence of Pattern Size on Extent of Exposure

and i-ray exposure, the tolerable limit of change in the extent of exposure tends to become narrower as the pattern size comes closer to the resolution limit. In the case of SOR exposure, however, resolution is evidently higher than that in the case of i-ray exposure. Therefore, the pattern replication region where the pattern size can be controlled shifts to a very fine region. In the case of i-ray exposure, for example, a $0.5\text{ }\mu\text{m}$ pattern has an approximately 20 percent tolerable limit of change in the extent of exposure, while in the case of SOR exposure, even a $0.2\text{ }\mu\text{m}$ pattern has a tolerable limit of 20 percent. This means that the margin for process change in the intensity of exposure, development conditions and so forth is large, and serves as a datum substantiating the charm of the SOR exposure.

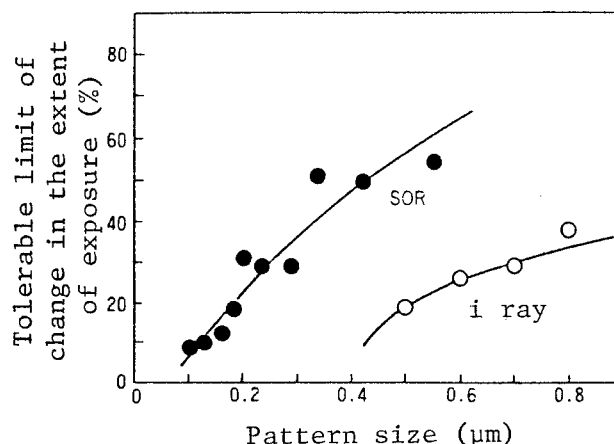


Figure 6. Size Controllability

4. Overlay Accuracy

Among the technological tasks for SOR lithography, the most important item is to improve overlay accuracy, together with the improvement of throughput. Unlike optical lithography by mask-reduced projection, SOR lithography entails a 1:1 equimultiple exposure. Therefore, it is handicapped because an error in the X-ray mask used and an error in alignment are reflected intact in an overlay error. In addition, an error in the establishment of a proximity gap is also a factor causing an overlay error, making alignment difficult to that extent. In the trial manufacture attempted this time, we used an X-ray mask for which the accuracy of a pattern position was enhanced by controlling the stress of the membrane and the absorber.²⁶ For position alignment, we used a stepper to which an optical-heterodyne alignment method was applied with high position detecting power.²⁷

We evaluated the overlay accuracy of all five layers that had been revealed at the time of trial manufacture. In measuring overlay errors, we measured the positions of evaluation patterns arranged at nine places in an 8 mm square chip at a 4 mm pitch, using laser interference type coordinate measurement equipment (Nikon-21). The mean value and standard deviation of overall overlay errors in the four other layers, based on the separated

layer, were $0.111\text{ }\mu\text{m}$ and $0.245\text{ }\mu\text{m}$, respectively, in the x-axis direction, and $0.072\text{ }\mu\text{m}$ and $0.185\text{ }\mu\text{m}$ in the y-axis direction. The number of evaluation points was 1,300. As a result, we even confirmed the action of a ring oscillator designed with an alignment margin of $0.3\text{ }\mu\text{m}$, but did not go to the point of satisfying the overlay accuracy of $0.1\text{ }\mu\text{m}$ or less (3σ) that would naturally be required of the lithography in the quarter-micron region.

We analyzed the error factors in order to improve the overlay accuracy. The standard deviation was as large as $0.2\text{ }\mu\text{m}$, but it became clear that this was mostly due to the imperfection of aligner adjustment. In particular, the aligner was in the course of a rise, and it was impossible to adjust it until the removal of the drift in the heterodyne-optical system. This resulted in a revolution error and was reflected in the alignment error. However, this problem is not vital, and can be resolved. The alignment accuracy of the aligner itself is being improved to the extent that $0.1\text{ }\mu\text{m}$ (3σ) can be anticipated. For details, refer to another paper in this special edition.

Figure 7 shows the position errors among the five mask patterns. The solid lines show the separated layers, and the other layers are shown by the divergence from the pattern positions of the separated layers. The standard deviation of the position divergence in all the points of evaluation is $0.047\text{ }\mu\text{m}$ (σ) in the x-axis direction and $0.068\text{ }\mu\text{m}$ (σ) in the y-axis direction. The five masks used here were arbitrarily selected from several masks fabricated for each layer. Therefore, we think that the alignment will be improved further if the combination is sorted. At any rate, the values have been improved to about one-half in comparison with the mask pattern position accuracy shown several years ago. Thus, steady progress is recognizable. Another investigation result shows that a mask below the $0.1\text{ }\mu\text{m}$ level with 3σ has been fabricated.²⁶ Therefore, we think that the values can be improved still further. The overlay accuracy ascertained in this research is not at all satisfactory, but we believe that the causes of this will become clear and that accuracy will be improved further, along with repeated applications of SOR lithography to this kind of tentative device manufacture and so forth.

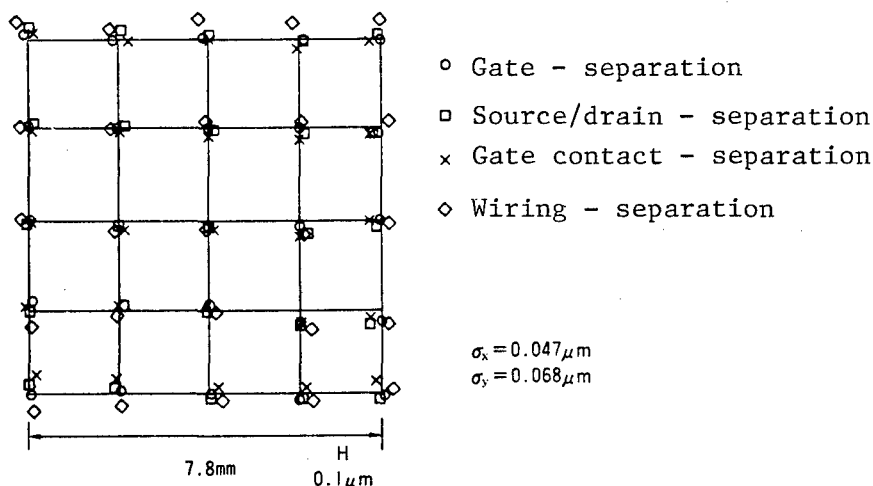


Figure 7. Position Errors of Mask Patterns

5. Conclusion

Through our MOSIC trial-manufacture with SOR exposure applied to five-layer exposure equipment, we evaluated the resist process, the characteristics of pattern formation, and overlay accuracy. In addition, we clarified the problems involved.

- (1) We obtained good patterning properties through pattern replication using FBM-G and SPP resists, and confirmed a pattern resolution of $0.2\ \mu\text{m}$.
- (2) We showed quantitatively that SOR exposure gives a large process margin even in the $0.2\ \mu\text{m}$ region, as can be seen from the high degree of tolerance for fluctuations in the degree of exposure, which tolerance is provided for control of pattern size.
- (3) The overall overlay accuracy was about $0.1 \pm 0.6\ \mu\text{m}$ (3σ). We confirmed the action as far as the ring oscillator designed with an alignment margin of $0.3\ \mu\text{m}$, but it has not yet reached the point of realizing an alignment accuracy matching the resolution. To improve the overlay accuracy, we analyzed the error factors and obtained indices for future improvement.

In the future, we will attempt to use single-layer resists, and will work for improvement of overlay accuracy.

Acknowledgement

We thank manager Sakai of the microprocessing technology research department and Dr. Toyoki Kitayama, former chief researcher of the LSI Laboratories, for giving us guidance in pursuing this research. In addition, we thank the persons concerned for lending us their cooperation.

Profiles of the Authors

Kimiyoshi Deguchi, chief researcher of the LSI Laboratories, joined NTT in 1977 and engaged mainly in development of an X-ray exposure system and research on its applications. He is currently engaged in research and development on process technology for SOR lithography.

In 1975 he finished the electrical engineering course of the department of engineering, Kumamoto University, and in 1977 finished the master's course in electrical engineering in the department of engineering study of the same university's graduate school.

He is a member of the Society of Applied Physics, the Society of Precision Engineering, the Society of Automatic Measurement Control, and the Society of Electronic Information and Communications.

He was awarded a thesis prize by the Society of Precision Engineering in 1986.

Toshiyuki Horiuchi, chief researcher of the LSI Laboratories, joined NTT in 1970 and engaged in the stress analysis of a sea bottom relay core line introduction region and in research on the measurement of small-section shield positions. From 1976 he engaged in research and development on exposure equipment for lithography and lithographic process technology. He is now engaged in the study of SOR lithographic technology.

He finished the machine engineering course of Tokyo University's engineering department in 1970.

He is a member of the Society of Applied Physics, the Society of Electronic Information and Communications, and the Institute of Electrical Engineers.

Akinobu Tanaka, chief researcher of the LSI Laboratories, joined NTT in 1970 and engaged in research on print wiring plate materials and in development of iron plate core print plate for automatic switchboards. Currently he is engaged in the study of resist materials used for 0.2 μm rule LSI processing.

In 1968 he finished the applied chemistry course in the engineering department of Nagoya University, and in 1970 finished the master's course in applied chemistry in the engineering department of the same university's graduate school.

He is a member of the Chemical Society of Japan, the Society of High Polymers, the Society of Applied Physics, and the Society of Electronic Information and Communications.

He was commended by the NTT president in 1979.

Akira Yoshikawa, chief researcher of the LSI Laboratories, joined NTT in 1968 and engaged mainly in research on the physical properties of semiconductor materials and various applications. He is now engaged in research and development on lithographic techniques.

In 1966 he finished the applied physics course of Waseda University's department of science and engineering, and in 1968 finished the master's course in applied physics at the same university's graduate school.

He is a member of the Society of Applied Physics, the Physical Society of Japan, and the Institute of Electrical Engineers.

References

1. H. I. Smith, J. Vac. Sci. & Technol., B4, p 148, 1986.
2. S. E. Bernacki and H. I. Smith, IEEE Trans. Electron Devices, ED-22, p 421, 1975.
3. H. L. Stover, F. L. Hause, and D. McGreivy, J. Vac. Sci. & Technol., 16, p 1635, 1979.

4. D. Hofer, J. Powers, and W. D. Grobman, J. Vac. Sci. & Technol., 16, p 1965, 1979.
5. P. I. Suci, E. N. Fuls, and H. J. Boll, IEEE Trans. Electron Device Lett., EDL-1, p 10, 1980.
6. K. Deguchi, K. Komatsu, H. Namatsu, M. Sekimoto, M. Miyake, and K. Hirata, IEEE Trans. Electron Devices, ED-34, p 759, 1987.
7. E. Spiller, D. E. Eastman, R. Feder, W. D. Grobman, W. Gudat, and J. Topalian, J. Appl. Phys., 47, p 5450, 1976.
8. H. Betz, F. K. Fey, A. Heuberger, and P. Tischer, IEEE Trans. Electron Devices, ED-26, p 693, 1979.
9. M. N. Wilson, A. I. C. Smith, V. C. Kempson, A. L. Purvis, M. C. Townsend, A. R. Jorden, R. J. Anderson, R. C. Lobel, A. S. Bhutta, and D. E. Andrews, Digest Papers, 1989 2nd Micro Process Conf. (Kobe, Japan), p 98, 1989.
10. T. Hori, and SHI Accelerator Research Group, Digest Papers, 1989 2nd Micro Process Conf. (Kobe, Japan), p 100, 1989.
11. S. Mandai, Y. Hoshi, and Y. Kohno, Rev. Sci. Instr., 60, p 1795, 1989.
12. T. Hosokawa, T. Kitayama, T. Hayasaka, S. Ido, Y. Uno, A. Shibayama, J. Nakata, K. Nishimura, and M. Nakajima, Rev. Sci. Instr., 60, p 1783, 1989.
13. W. E. Feely, J. C. Imhof, and C. M. Stein, Polym. Eng. Sci., 26, p 1101, 1986.
14. R. Dammel, K. F. Dossel, J. Lingnau, and J. Theis, Proceedings of the Int. Conf. on Microlithography (Vienna, Austria, 1988), Microelectronic Engineering, 9, p 575, 1989.
15. J. P. Silverman, V. Dimilia, D. Katcoff, L. K. Wang, J. M. Warlaumont, A. D. Wilson, R. Devenuto, B. Hill, L. C. Hsia, and R. Rippstein, Proceedings of the Int. Conf. on Microlithography (Vienna, Austria, 1988), Microelectronic Engineering, 9, p 101, 1989.
16. U. Mackens, U. Mescheder, F. Mund, H. Luthje, H. Lifka, C. A. H. Juffermans, P. H. Woerlee, and A. J. Walker, Proceedings of the Int. Conf. on Microlithography (Vienna, Austria, 1988), Microelectronic Engineering, 9, p 89, 1989.
17. Toshiyuki Horiuchi, Kohkichi Deguchi, Yohsuke Yamamoto and Akira Yoshikawa, Optical Application and Eyesight Study Conference of the Institute of Electrical Engineers of Japan, AV-89-11, p 49, 1989.

18. A. Shibayama, T. Kitayama, T. Hayasaka, K. Nishimura, and M. Nakajima, *Rev. Sci. Instr.*, 60, p 1779, 1989.
19. T. Kaneko, S. Itabashi, Y. Saito, H. Yoshihara, and T. Kitayama, *Digest Papers, 1989 2nd Micro Process Conf. (Kobe, Japan)*, p 104, 1989.
20. T. Kobayashi, M. Miyake, Y. Okazaki, T. Matsuda, M. Sato, K. Deguchi, S. Ohki, and M. Oda, *IEDM Tech. Digest*, p 881, 1988.
21. H. Asakawa and O. Kogure, *Digest of the 1982 Symposium on VLSI Technology (Oiso, Japan)*, p 88, 1988.
22. A. Tanaka, H. Ban, and S. Imamura, *ACS Symposium Series 412*, p 175, 1989.
23. H. Namatsu and A. Yoshikawa, *J. Electrochem. Soc.*, 133, p 2118, 1986.
24. S. Ishihara, M. Kanai, A. Une, and M. Suzuki, *J. Vac. Sci. & Technol.*, B7, p 1652, 1989.
25. M. Sekimoto, A. Ozawa, T. Ohkubo, and H. Yoshihara, *Extended Abstracts 16th Int. Conf. on Solid State Device Materials (Kobe, Japan)*, p 23, 1984.
26. S. Ohki, M. Kakuchi, T. Matsuda, A. Ozawa, T. Ohkubo, M. Oda, and H. Yoshihara, *Jpn. J. Appl. Phys.*, 28, p 2074, 1989.
27. M. Suzuki and A. Une, *J. Vac. Sci. & Technol.*, B7, p 1971, 1989.

Deep Submicrometer MOSICs Fabricated Using SOR Lithography for All Levels

916C3800H Tokyo NTT R&D in Japanese Vol 39 No 4, 10 Apr 90 pp 609-618

[Paper by Masayasu Miyake, Yukio Okazaki, and Toshio Kobayashi, NTT Laboratories]

[Text] Preface

We have fabricated deep submicrometer MOSICs consisting of 0.2- μm gate-length MOSFETs using SOR lithography for all levels. Extremely thin gate oxide (3.5 nm) and extremely shallow source-drain junctions (80 nm) were used to fabricate the deep submicrometer MOSFETs. We clarified that the 0.2- μm n-channel and p-channel MOSFETs trial-manufactured by using SOR lithography for all levels (five layers) exhibit the same high-performance characteristics as those fabricated by using EB [electron beam] lithography. Thus we showed that they have no effects such as SOR damage on device characteristics, at least at the stage of initial property evaluation. In addition, we have fabricated superfine n-channel ring oscillators with a gate length of 0.2 μm and with a minimum size of other elements measuring 0.3 μm , showing that the gate delay time is as short as 23 ps/stage. Thus, we have clarified the potential of SOR lithography for future ULSIs.

[English abstract reprinted from original] Deep submicrometer MOSICs which consist of 0.2- μm gate-length MOSFETs, have been fabricated using SOR lithography for all levels. Ultra thin gate oxide (3.5 nm) and extremely shallow source-drain junctions (80 nm) are used to fabricate 0.2- μm gate-length MOSFETs. It is found that 0.2- μm n-channel and p-channel MOSFETs fabricated using SOR lithography exhibit the same high-performance characteristics as MOSFETs fabricated using EB lithography, which indicates that the characteristics are not adversely affected by SOR damage. 0.2- μm gate-length n-channel ring oscillators based on a 0.3- μm rule are successfully fabricated, and a gate delay of 23 ps/stage is achieved. These results show that SOR lithography is a promising technique for future ULSIs.

1. Introduction

With the remarkable progress in silicon IC technology, research is being pursued with a view to achieving a still greater extent of micronization and higher integration from the level of VLSIs to that of ULSIs.^{1,2} To fabricate

ULSIs in which deep submicron elements are integrated, it is essential to establish techniques to process very fine patterns in a deep submicron range, as well as device and process techniques to create such infinitesimal elements.

SOR lithography is being noted as a lithographic technology in the deep submicron range, exceeding the limit of conventional UV exposure technology. Therefore, its application to ULSIs is being looked forward to.³⁻⁵ We have already trial-manufactured a superfine MOSIC for which SOR lithography, using the SOR ring of the NTT LSI Laboratories, is applied only to Al-wired layers.⁶ When SOR lithography is to be actually applied to ULSIs, it needs to be used for all lithographic layers. However, there has been no instance of applying all-layer SOR exposure for the fabrication of superfine MOSICs in the so-called sub-half-micron or quarter-micron range, wherein the minimum size with which SOR exposure technology is thought to be used on a full scale is 0.5 μm or smaller. To clarify the possibility of applying it to ULSIs, therefore, we trial-manufactured a superfine MOSIC with a 0.2 μm gate length by using the SOR exposure process for all layers. The superfine MOS process technology to realize such MOS devices has so far been developed by electron beam drawing. In this paper we will give an outline of the superfine MOS process technology to create superfine MOS devices, and will describe the results of our evaluation of the properties of devices produced by SOR lithographic technology and the superfine MOS process technology.

2. Trial-Manufactured Devices

The devices we trial-manufactured are 5l-stage E/E type ring oscillators and discrete MOSFETs. The n-channel and p-channel devices were fabricated on separate wafers respectively. The gate length, which is a size directly related to MOSFET performance, was extremely small, down to the 0.2 μm range, and we fabricated three kinds of ring oscillators with minimum sizes other than the gate length (size of the contact hole, minimum wiring width, margin of alignment between the contact hole and the wiring metal, and so forth) ranging over 0.3 μm , 0.4 μm , and 0.6 μm .

3. Device and Process Technologies To Create Superfine MOS Devices

3.1. Tasks on MOSFET Micronization

MOSFET is characterized by its performance improvement when the channel is shortened, and it can be expected that the performance of MOSLSIs will be improved rapidly by micronizing them. As is well known, however, a reduction in channel length brings about deterioration in device properties due to the short-channel effect, such as a drop in punch through breakdown voltage and a change in threshold voltage due to channel length.⁷ To create very fine MOSFETs, therefore, it is essential to develop device and process techniques to restrain short-channel effects, as well as to develop a technology to form very small patterns. The effective way to restrain short-channel effects is to reduce the thickness of the gate oxide film and the source-drain junction film.⁸ In the trial manufacture conducted this time, we restrained short-channel effects by using an extremely thin gate oxide

film, 3.5 nm thick, and an extremely shallow source-drain junction, measuring 80 nm in depth.

3.2. Techniques To Form Extremely Shallow Source-Drain Junctions

A source-drain junction is ordinarily formed by subjecting arsenic (As) to an ion implantation process for n+p junctions and boron (B) for p+n junctions, and annealing them in an electric furnace. To make the junctions shallow, the energy of ion implantation is lowered, but in the case of B in particular, the junctions cannot be made very shallow even when the energy is lowered, because of channeling during the low-energy ion implantation.^{9,10} In addition, impurities are diffused during the annealing and the form of distribution expands, too. Therefore, it is difficult to form by conventional methods an extremely shallow junction measuring less than 100 nm or so in depth. For this reason, we made studies on the formation of extremely shallow junctions for microscopic MOSLSIs. We will describe the results of our studies.

One of the causes of a junction becoming deep is the diffusion occurring with annealing. To minimize this diffusion, we used a rapid annealing process (ramp annealing) by ramp heating, which makes short-time annealing possible.^{11,12} By optimizing the conditions for ion implantation and ramp annealing, we were able to form extremely shallow n+p junctions, less than 100 nm deep. With regard to the p+n junctions using B, on the other hand, it became clear that the layer could not be thinned appropriately only by ramp annealing, because of channeling during ion implantation. Therefore, we sought to restrain channeling by making the neighborhood of the substrate surface noncrystalline through Si ion implantation before carrying out B ion implantation.^{13,14} The distribution of B density in the direction of depth, measured by SIMS, is shown in Figure 1. Figure 1 (a) shows the distribution immediately after the injection, and Figure 1 (b) the distribution after ramp annealing for 15 seconds at 950°C. Furthermore, we carried out BF₂ ion implantation at 15 keV in order to perform B ion implantation with very low energy. Figure 1 (a) shows that channeling takes place in the substrate that was not made noncrystalline, causing the distribution form to expand, and that channeling is restrained in the substrate that was made noncrystalline, bringing about a form of extremely shallow distribution. As shown in Figure 1 (b), the distribution form does not expand so markedly even after annealing, because the ramp annealing process is adopted, and very shallow p+n junctions are obtained, with the depth for a 10¹⁶ cm⁻³ density being 100 nm and the depth for a 10¹⁸ cm⁻³ density being 80 nm. For the noncrystalline junctions, their diode characteristics might pose a problem. As a result of investigation, however, we found that favorable diode characteristics could be obtained by making the depth of the noncrystalline layers smaller than that of the junctions.¹⁵ Thus, we have established a technique for forming extremely shallow source-drain junctions for superfine MOSLSIs.

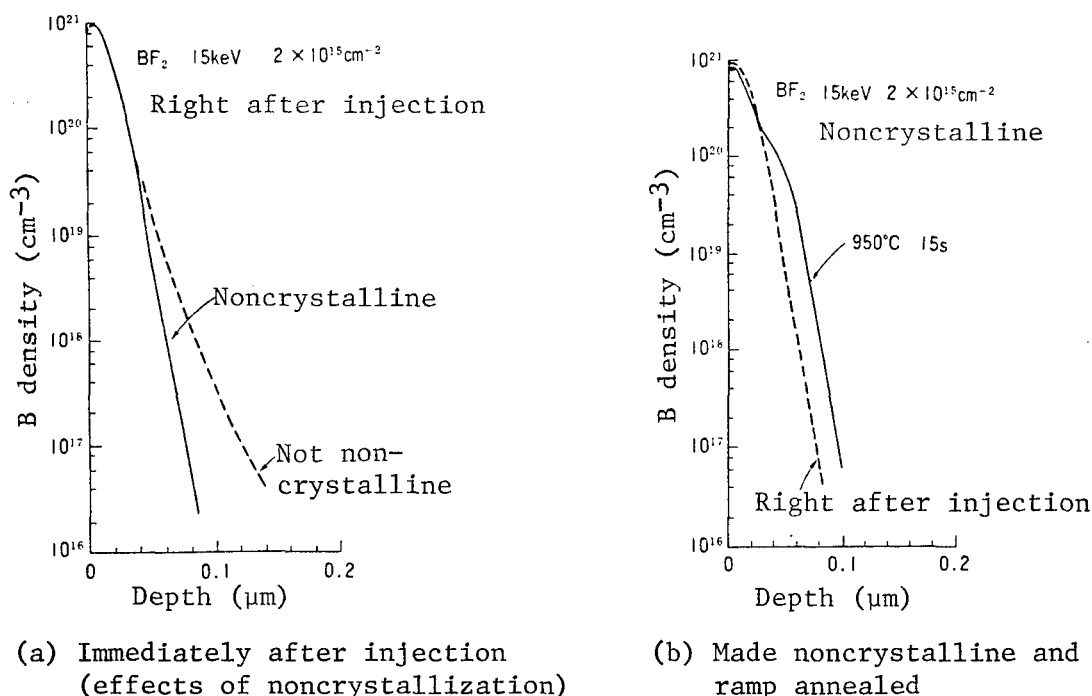


Figure 1. Distribution of B Density in the Direction of Depth, Measured by SIMS

4. Superfine MOSIC Trial-Manufacturing Process Using All-Layer SOR Exposure

The plane orientation of the Si substrates was (100). We used a p-type substrate for the n channel and an n-type substrate for the p channel. As for gate electrode materials, phosphor-doped silicon was used for both the n and p channels. Therefore, a surface channel type was formed in the case of the nMOSFET, and a buried channel type was formed for the pMOSFET because of the need for adjusting the threshold voltage. The process for the trial manufacture is described below. For the resist process in each layer, refer to another paper in this special edition. We carried out SOR exposure five times, as mentioned below, but we also fabricated wafers on which patterns were formed by direct electron beam drawing instead of SOR exposure, by way of comparison.

(1) Alignment Mark Formation

A trench $1 \mu\text{m}$ deep was formed on a Si wafer and was designated as an alignment mark. Lithography was used for the formation of an alignment mark pattern, and the five layers formed after that were aligned with this mark as the standard.

(2) Element Isolation (first SOR exposure)

For isolation of elements, the ordinary LOCOS method was used. The SOR exposure process was used for silicon nitride film patterning that determines the active region wherein elements are to be formed.

(3) Channel Doping and Gate Oxidation

Impurities were introduced into the active region by means of low-density ion implantation, and thus the density of the impurities in the channel part was adjusted. B ions were implanted into the n-channel elements, and phosphor (P), As, BF_2 ions were implanted into the p-channel elements. Figure 2 shows the doping profile in the channel section. As shown in the illustration, a shallow, B counter-doped layer is formed on the surface in the case of the pMOSFET in order to control the threshold voltage, and n-type impurities with a comparatively high density are introduced to a somewhat deep place in order to prevent punch through. To activate these impurities, ramp annealing was carried out for 15 seconds at 950°C , followed by the formation of a gate oxide film. We oxidized the gates in a dry oxygen atmosphere at 800°C , and formed extremely thin (3.5 nm) gate oxide films.

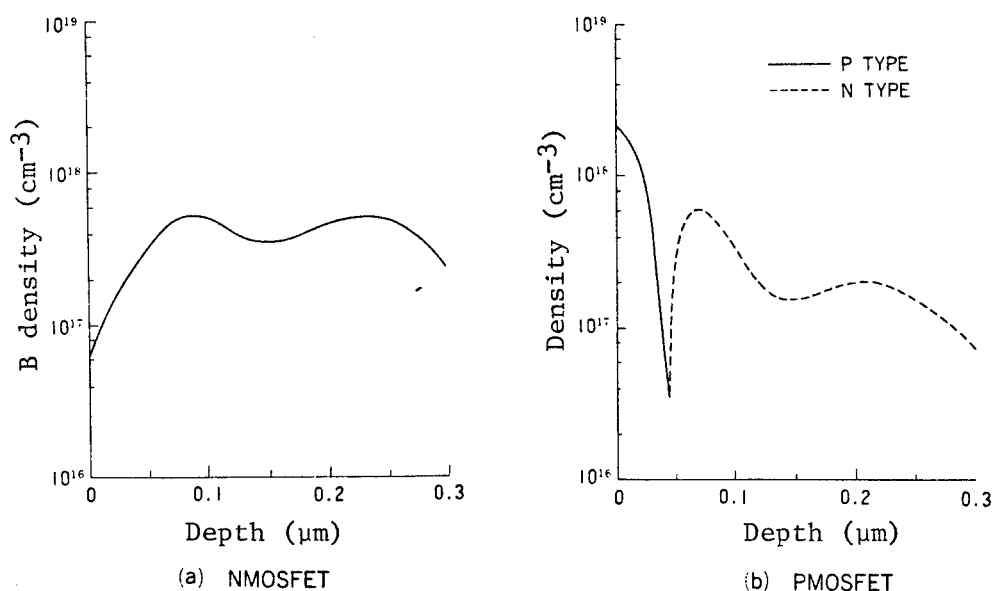


Figure 2. Doping Profile of the Channel Section

(4) Formation of Gate Electrodes (second SOR exposure)

For gate electrodes, we formed gate patterns through SOR exposure after accumulation of phosphor-doped polysilicon. Because the gate oxide film was extremely thin, measuring 3.5 nm, for the processing of the gate polysilicon we used the ECR etching process with a high etching selective ratio between Si and SiO_2 .¹⁶ If the selective ratio is low, the Si substrate would be etched in the region where the source and the drain are to be formed; this would cause deterioration of junction characteristics or an increase in the depth of junctions, making it impossible to produce the fine devices initially aimed at.

(5) Source and Drain Formation

We thinly oxidized the gate polysilicon through thermal oxidation. Thereafter, we carried out As ion implantation (10 keV , $4 \times 10^{15}\text{ cm}^{-2}$) into the n-channel elements on the basis of the research results mentioned in paragraph 3.2. We then made the p-channel elements noncrystalline through Si ion implantation and carried out BF_2 ion injection into it (15 keV , $2 \times 10^{15}\text{ cm}^{-2}$). After that, we thinly introduced impurities for the source and the drain.

(6) Formation of Interlayer Insulation Films and Contact Holes for Diffusion Layers (Source and Drain) (third SOR exposure)

After accumulating interlayer insulation films, we made SOR exposures and formed contact hole patterns for the source and the drain. The diffusion layer contact and the gate contact were exposed on different layers to prevent the ion-implanted impurities for contact compensation from entering the gate polysilicon. In other words, the source-drain impurities and the impurities in the gate polysilicon are different in type in the case of p-channel elements and, therefore, exposing the contact holes on the same layer may bring about such problems as an increase in the resistance of the gate polysilicon due to the ion implantation for contact compensation. After opening the contact holes for the source and the drain, we carried out the ion implantation for contact compensation, and formed a comparatively deep junction (200 nm) only for the contact section. After the ion implantation, we carried out ramp annealing to activate the impurities that had been ion-implanted into the source and the drain and those ion-implanted for contact compensation. The conditions for the ramp annealing were $1,000^\circ\text{C}$ at 10 seconds for the n channel and 950°C at 15 seconds for the p channel. This ramp annealing is available only for the high-temperature annealing of source-drain impurities. As a result, the source-drain junctions formed were extremely shallow-- 80 nm deep--for both the n-channel and p-channel elements. The sheet resistance is $120\Omega/\square$ (n channel) and $200\Omega/\square$ (p channel).

(7) Formation of Gate Contact Holes (fourth SOR exposure)

We formed the contact hole pattern for a gate electrode by the SOR exposure process and opened the gate contact hole.

(8) Formation of Al Wiring (fifth SOR exposure)

We piled up Al (2 percent Si) as a wiring metal, and formed a wiring pattern with a minimum width of $0.3\text{ }\mu\text{m}$ by using the SOR exposure process. Finally, we heat-treated it at 400°C in an oxygen-nitrogen mixed gas atmosphere to reduce the interface level density. In the part of contact between the diffusion layer and Al, the junction depth was increased by contact compensation; we were therefore able to form a source and a drain having good junction properties even when Al was used. However, when the problem of reliability, involving electromigration and so forth, is taken into consideration, it cannot necessarily be said that Al is suitable for superfine wiring, so the adoption of new wiring materials needs to be considered.

5. Results of Trial Manufacture

5.1. MOSFET Characteristics

Figure 3 shows the characteristics of the drain currents and voltage of the trial-manufactured MOSFET.

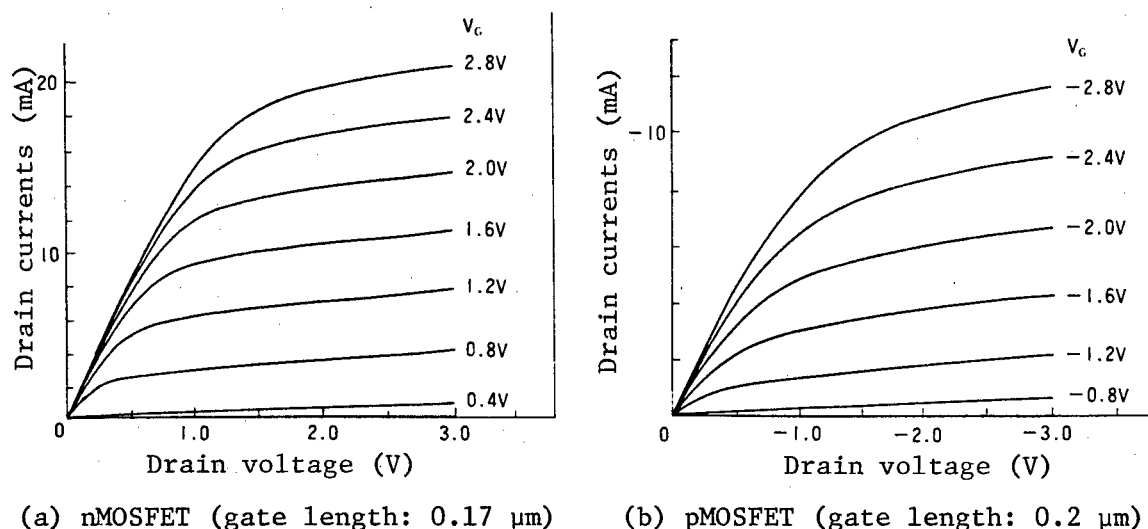
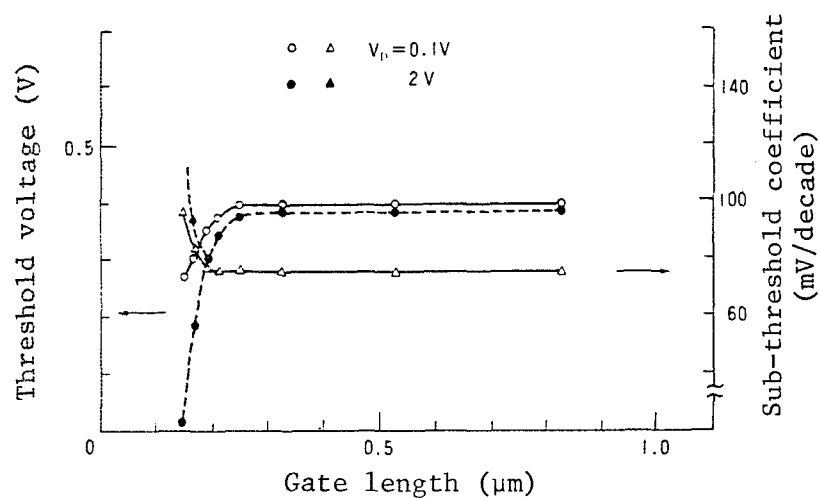


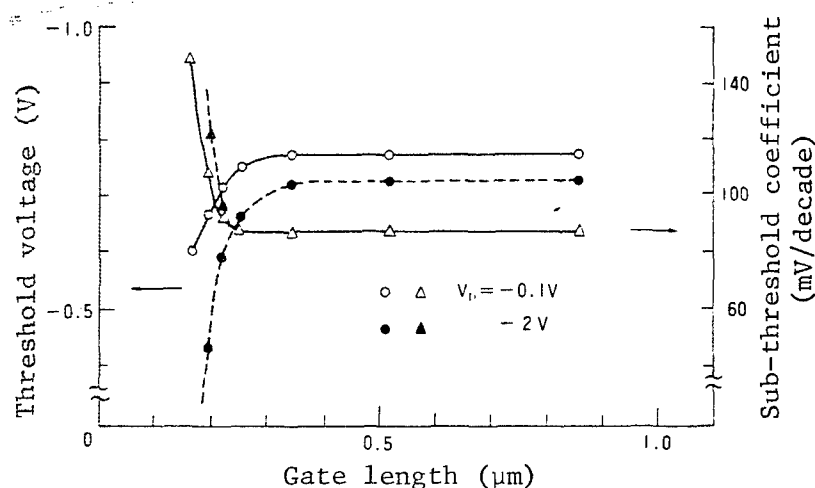
Figure 3. Characteristics of Drain Currents and Voltage of MOSFET (gate width: $20 \mu\text{m}$)

Figure 3 (a) shows nMOSFET with a $0.17 \mu\text{m}$ gate length; Figure 3 (b) shows a pMOSFET with a $0.2 \mu\text{m}$ gate length. The gate width is $20 \mu\text{m}$, and the absolute value of the gate voltage (V_G) is changed from 0 V to 2.8 V at an interval of 0.4 V. As shown here, the superfine MOSFET with a $0.2 \mu\text{m}$ gate length, trial-manufactured through all-layer SOR exposure, operates normally. Figure 4 shows the dependence of the threshold voltage and the sub-threshold coefficient on the gate length in the cases of the nMOSFET shown in Figure 4 (a) and the pMOSFET shown in Figure 4 (b). The absolute value of drain voltage (V_D) is shown in terms of 0.1 V and 2 V. In the superfine MOS device manufacturing process described in this paper, extremely thin gate oxide films and extremely shallow source-drain junctions were used. Therefore, the short-channel effect is restrained, and a superfine MOSFET in the range of $0.2 \mu\text{m}$ in gate length is realized. However, the pMOSFET, which is a buried channel type, tends to bring about short channel effects compared with the nMOSFET that is a surface channel type; further studies on devices and processes are therefore necessary. Consequently, we will explore such matters as making the counter-doped layers extremely shallow or turning them into a surface channel type.

Figure 5 shows the gate length dependence of the maximum value of mutual conductance in the case of $|V_D| = 2\text{V}$. The value of mutual conductance is 442 mS/mm in the case of nMOSFETs with a $0.17 \mu\text{m}$ gate length, and 291 mS/mm in the case of pMOSFETs with a $0.2 \mu\text{m}$ gate length. Thus high-performance, superfine MOSFETs have been realized.



(a) NMOSFET



(b) PMOSFET

Figure 4. Gate Length Dependence of Threshold Voltage and Sub-Threshold Coefficient

To examine whether or not there is any problem peculiar to SOR exposure, we compared it with the properties of a MOSFET trial-manufactured by using the electron beam drawing process. The effects conceivably exerted by SOR damage on its initial properties include a change in threshold voltage, an increase in sub-threshold coefficient, and a drop in mutual conductance. However, the properties of the MOSFET manufactured through electron beam drawing were found to be equal to the properties shown in Figures 3, 4, and 5. Thus, no difference is recognized between MOSFETs using SOR exposure and those using electron beam drawing. As far as evaluation of initial properties is concerned, therefore, there is no problem peculiar to SOR exposure, such as SOR damage. We are scheduled to clarify matters concerning long-term reliability, such as tolerance to hot carriers, which will become important in the case of applying SOR exposure to LSIs.

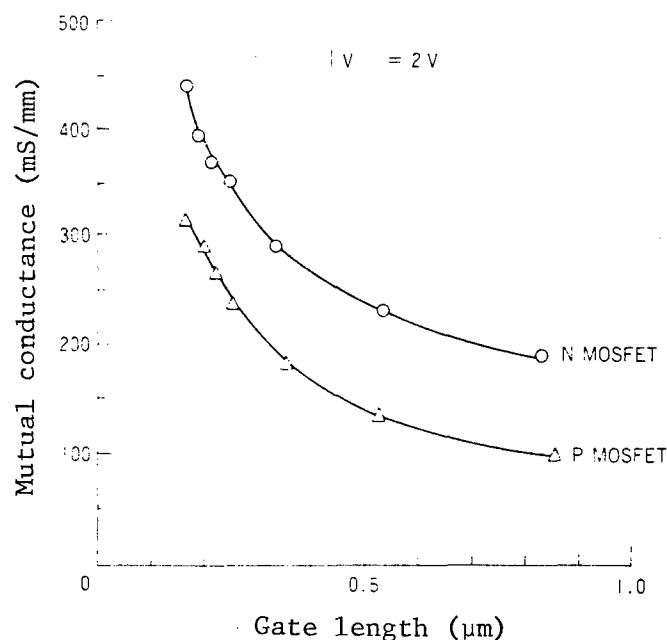


Figure 5. Dependence of the Maximum Value of Mutual Conductance on Gate Length

5.2. Properties of Ring Oscillators

Figure 6 is a SEM photo of a trial-manufactured ring oscillator, an n channel superfine MOSIC measuring $0.2\ \mu\text{m}$ in gate length and a minimum $3\ \mu\text{m}$ in other size. The minimum contact hole is $0.3\ \mu\text{m}$ square, and the minimum wiring width is $0.3\ \mu\text{m}$. In the trial manufacture attempted this time, we were able to fabricate a very fine MOSIC through all-layer SOR exposure, as shown in the illustration. Figure 7 shows the oscillation wave form of the ring oscillator shown in Figure 6. Thus, an extremely fine ring oscillator with the aforesaid size operates normally, with the gate delay time exhibiting a high value of $23\ \text{ps}/\text{stage}$ (power source voltage: $3\ \text{V}$; gate voltage of load MOSFET: $3\ \text{V}$). Figure 8 shows the change in gate delay time of the ring oscillator when a gate length of $0.2\ \mu\text{m}$ is kept constant and other minimum size and alignment margins are changed. As shown in the illustration, size reduction brings about a drop in parasitic capacity and an increase in speed. As stated in another paper in this special edition, titled "Resist Process for SOR Lithography," the overlay accuracy of the SOR exposure for this trial manufacture is about $0.1\ \mu\text{m} \pm 0.6\ \mu\text{m}$ (3σ), which cannot be regarded as sufficient for the fabrication of a superfine MOSIC. For the application of this lithography to ULSIs, improving this overlay accuracy is an important task.

As mentioned above, we fabricated superfine, high-speed MOSICs by adopting the SOR exposure process for all layers, and clarified the potential of SOR exposure as a lithographic technology for LSIs.



Figure 6. SEM Photo of a Trial-Manufactured 51-Stage n Channel Ring Oscillator

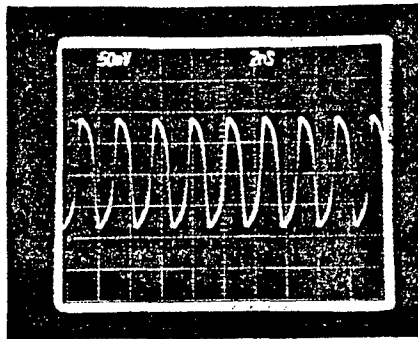


Figure 7. Oscillation Wave Form of a Trial-Manufactured 51-Stage n Channel Ring Oscillator (power source voltage: 3 V; gate voltage of load MOSFET: 3 V)

6. Conclusion

To verify the possibility of SOR exposure application to ULSIs, we trial-manufactured superfine MOSICs using SOR exposure for all layers. To produce a MOSFET with a gate length of $0.2\ \mu\text{m}$, we used an extremely thin gate oxide film (3.5 nm) and an extremely shallow source-drain junction (80 nm). This junction was created by change to an amorphous structure by Si ion implantation and by ramp annealing. The results obtained are summarized as follows.

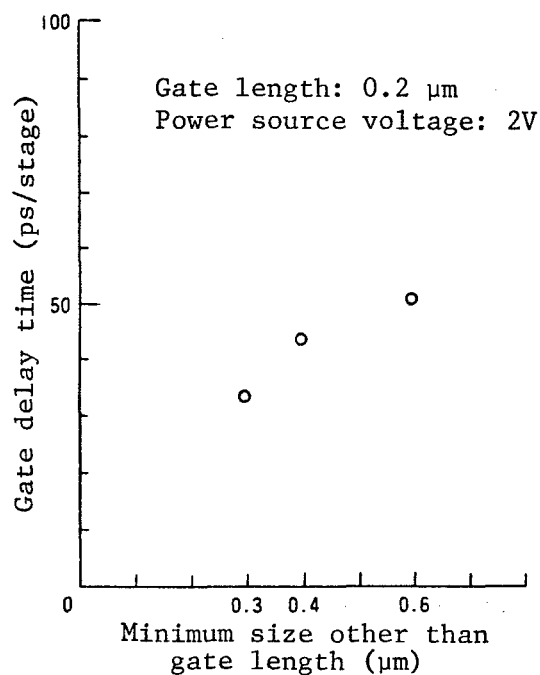


Figure 8. Change in Gate Delay Time of a Ring Oscillator, Due to Change in Minimum Size Other Than the Gate Length (gate length: $0.2 \mu\text{m}$; power source voltage: 2 V; gate voltage of load MOSFET: 2 V)

(1) The superfine nMOSFET and pMOSFET with a gate length of $0.2 \mu\text{m}$, trial-manufactured by the SOR exposure process for all layers (for element isolation, gate electrode, diffusion layer contact, gate contact, and Al wiring) exhibit high performance equal to that of MOSFETs produced by electron beam direct drawing. Within the scope of initial property evaluation, there is no effect on device properties, such as SOR damage.

(2) By a superfine MOS process using the SOR exposure process for all layers, we produced a superfine n-channel ring oscillator measuring $0.2 \mu\text{m}$ in gate length and $0.3 \mu\text{m}$ in other minimum size. Its gate delay time was as short as 23 ps/stage.

(3) From the aforesaid results, we clarified the potential of SOR exposure as a lithographic technology for LSIs. In this paper, we described the results of our evaluation, paying attention only to the initial properties of devices. From the viewpoint of applying this technology to ULSIs, long-term reliability of devices, such as their tolerance to hot carriers, is important. Therefore, we are scheduled to clarify the relationship between SOR exposure and long-term reliability of devices.

Acknowledgement

We would like to express our thanks to department manager Tetsushi Sakai of the LSI Laboratories, chief researcher Kazuo Imai, and Dr. Toyoki Kitayama, former chief researcher of the LSI Laboratories, for giving us guidance in

the pursuit of our research, and to the persons concerned for lending us their cooperation.

Profiles of the Authors

Masayasu Miyake, chief researcher of the LSI Laboratories, joined NTT in 1975 and engaged in research on the distribution control of ion-implanted impurities. At present he is engaged in research on the formation of shallow junctions and a superfine device manufacturing process using this formation.

In 1973 he finished the electronic engineering course of Kyoto University's engineering department, and in 1975 finished the master's course in electronic engineering in the engineering research department of that same university's graduate school. He received a doctorate in engineering (Kyoto University) in 1989.

He is a member of the Society of Applied Physics and the Society of Electronic Information and Communications.

Yukio Okazaki, chief researcher of the microprocessing research department of the LSI Laboratories, joined NTT in 1986 and engaged in the study of structural design for fine MOS devices. He is currently engaged in research and development on the structure of fine CMOS devices.

In 1984 he finished the physical course of Tohoku University's department of science, and in 1986 finished the master's course in physics in that same university's department of physical study.

He is a member of the Society of Electronic Communications and the Society of Applied Physics.

Toshio Kobayashi, chief researcher of the LSI Laboratories, joined NTT in 1974 and engaged in research chiefly on the structure of and the process for fine MOS devices. He is currently engaged in research and development on a 0.2 μm CMOS LSI.

In 1972 he finished the physical course of Sophia University's department of science and engineering, and in 1974 finished the master's course in applied physics in Waseda University's graduate school.

He is a member of the Society of Electronic Information and Communications, the Society of Applied Physics, the Physical Society of Japan, and the IEEE.

References

1. M. Miyake, T. Kobayashi, and Y. Okazaki, IEEE Trans. Electron Devices, 36, 392, 1989.
2. G. A. Sai-Halasz, M. R. Wordeman, D. P. Kern, E. Ganin, S. Rishton, D. S. Zicherman, H. Schmid, M. R. Polcari, H. Y. Ng, P. J. Restle, T. H. P. Chang, and R. H. Dennard, IEEE Electron Device Lett., EDL-8, 463, 1987.

3. J. P. Silverman, V. DiMilia, D. Katcoff, K. Kwietniak, D. Seeger, L. K. Wang, J. M. Warlaumont, A. D. Wilson, D. Crockatt, R. Devenuto, B. Hill, L. C. Hsia, and R. Rippstein, *J. Vac. Sci. Technol.*, B6(6), 2147, 1988.
4. U. Mackens, U. Mescheder, F. Mund, H. Luthje, H. Lifka, C. A. H. Juffermans, P. H. Woerlee, and A. J. Walker, *Proc. International Conference on Microlithography*, 1988, p 89.
5. J. P. Silverman, V. DiMilia, D. Katcoff, L. K. Wang, J. M. Warlaumont, A. D. Wilson, R. Devenuto, B. Hill, L. C. Hsia, and R. Rippstein, *Proc. International Conference on Microlithography*, 1988, p 101.
6. T. Kobayashi, M. Miyake, Y. Okazaki, T. Matsuda, M. Sato, K. Deguchi, S. Ohki, and M. Oda, in *IEDM Tech. Dig.*, 1988, p 881.
7. S. M. Sze, "Physics of Semiconductor Devices," 2nd ed., p 469 (John Wiley & Sons, New York, 1981).
8. J. R. Brews, W. Fichtner, E. H. Nicollian, and S. M. Sze, *IEEE Electron Device Lett.*, EDL-1, 2, 1980.
9. T. M. Liu and W. G. Oldham, *IEEE Electron Device Lett.*, EDL-4, 59, 1983.
10. A. E. Michel, R. H. Kastl, S. R. Mader, B. J. Masters, and J. A. Gardner, *Appl. Phys. Lett.*, 44, 404, 1984.
11. J. B. Lasky, *J. Appl. Phys.*, 54, 6009, 1983.
12. J. Narayan, O. W. Holland, R. E. Eby, J. J. Wortman, V. Ozguz, and G. A. Rozgonyi, *Appl. Phys. Lett.*, 43, 957, 1983.
13. T. E. Seidel, R. Knoell, F. A. Stevie, G. Poli, and B. Schwartz, in "VLSI Science and Technology/1984," Vol 84-7, K. E. Bean and G. A. Rozgonyi, Editors, p 201, The Electrochemical Society Softbound Proceedings Series, Pennington, NJ, 1984.
14. M. E. Lunnon, J. T. Chen, and J. E. Baker, *J. Electrochem. Soc.*, 132, 2473, 1985.
15. M. Miyake, S. Aoyama, S. Hirota, and T. Kobayashi, *J. Electrochem. Soc.*, 135, 2872, 1988.
16. T. Ono, C. Takahashi, M. Oda, and S. Matsuo, in *Symp. VLSI Technol. Dig. Tech. Papers*, 1985, p 84.

- END -

22161

SPRINGFIELD, VA
5285 PORT ROYAL RD
ATTN: PROCESS 103
NTIS

17
22161

This is a U.S. Government publication. Its contents in no way represent the policies, views, or attitudes of the U.S. Government. Users of this publication may cite FBIS or JPRS provided they do so in a manner clearly identifying them as the secondary source.

Foreign Broadcast Information Service (FBIS) and Joint Publications Research Service (JPRS) publications contain political, military, economic, environmental, and sociological news, commentary, and other information, as well as scientific and technical data and reports. All information has been obtained from foreign radio and television broadcasts, news agency transmissions, newspapers, books, and periodicals. Items generally are processed from the first or best available sources. It should not be inferred that they have been disseminated only in the medium, in the language, or to the area indicated. Items from foreign language sources are translated; those from English-language sources are transcribed. Except for excluding certain diacritics, FBIS renders personal and place-names in accordance with the romanization systems approved for U.S. Government publications by the U.S. Board of Geographic Names.

Headlines, editorial reports, and material enclosed in brackets [] are supplied by FBIS/JPRS. Processing indicators such as [Text] or [Excerpts] in the first line of each item indicate how the information was processed from the original. Unfamiliar names rendered phonetically are enclosed in parentheses. Words or names preceded by a question mark and enclosed in parentheses were not clear from the original source but have been supplied as appropriate to the context. Other unattributed parenthetical notes within the body of an item originate with the source. Times within items are as given by the source. Passages in boldface or italics are as published.

SUBSCRIPTION/PROCUREMENT INFORMATION

The FBIS DAILY REPORT contains current news and information and is published Monday through Friday in eight volumes: China, East Europe, Soviet Union, East Asia, Near East & South Asia, Sub-Saharan Africa, Latin America, and West Europe. Supplements to the DAILY REPORTs may also be available periodically and will be distributed to regular DAILY REPORT subscribers. JPRS publications, which include approximately 50 regional, worldwide, and topical reports, generally contain less time-sensitive information and are published periodically.

Current DAILY REPORTs and JPRS publications are listed in *Government Reports Announcements* issued semimonthly by the National Technical Information Service (NTIS), 5285 Port Royal Road, Springfield, Virginia 22161 and the *Monthly Catalog of U.S. Government Publications* issued by the Superintendent of Documents, U.S. Government Printing Office, Washington, D.C. 20402.

The public may subscribe to either hardcover or microfiche versions of the DAILY REPORTs and JPRS publications through NTIS at the above address or by calling (703) 487-4630. Subscription rates will be

provided by NTIS upon request. Subscriptions are available outside the United States from NTIS or appointed foreign dealers. New subscribers should expect a 30-day delay in receipt of the first issue.

U.S. Government offices may obtain subscriptions to the DAILY REPORTs or JPRS publications (hardcover or microfiche) at no charge through their sponsoring organizations. For additional information or assistance, call FBIS, (202) 338-6735, or write to P.O. Box 2604, Washington, D.C. 20013. Department of Defense consumers are required to submit requests through appropriate command validation channels to DIA, RTS-2C, Washington, D.C. 20301. (Telephone: (202) 373-3771, Autovon: 243-3771.)

Back issues or single copies of the DAILY REPORTs and JPRS publications are not available. Both the DAILY REPORTs and the JPRS publications are on file for public reference at the Library of Congress and at many Federal Depository Libraries. Reference copies may also be seen at many public and university libraries throughout the United States.